



Australia's National
Science Agency

Advancing new fracture sealing materials to assist mitigating fugitive gas emission from well casings

Bailin Wu, David Down, Wendy Tian, Buu Dao, Shiqin Yan,
and Elaheh Arjomand

EP211394

18 May 2021

ISBN Print: 978-1-4863-1588-8

ISBN Online: 978-1-4863-1589-5

Citation

Wu B, Down D, Tian W, Dao B, Yan S and Arjomand E (2021) Advancing new fracture sealing materials to assist mitigating fugitive gas emission from well casings. CSIRO, Australia.

Copyright

© Commonwealth Scientific and Industrial Research Organisation 2021. To the extent permitted by law, all rights are reserved and no part of this publication covered by copyright may be reproduced or copied in any form or by any means except with the written permission of CSIRO.

Important disclaimer

CSIRO advises that the information contained in this publication comprises general statements based on scientific research. The reader is advised and needs to be aware that such information may be incomplete or unable to be used in any specific situation. No reliance or actions must therefore be made on that information without seeking prior expert professional, scientific and technical advice. To the extent permitted by law, CSIRO (including its employees and consultants) excludes all liability to any person for any consequences, including but not limited to all losses, damages, costs, expenses and any other compensation, arising directly or indirectly from using this publication (in part or in whole) and any information or material contained in it.

CSIRO is committed to providing web accessible content wherever possible. If you are having difficulties with accessing this document please contact csiroyenquiries@csiro.au.

Contents

Acknowledgments.....	v
Executive summary	vi
1 INTRODUCTION.....	1
2 CHARACTERIZATING NEW FRACTURE SEALING MATERIALS	3
2.1 Specially formulated thermal activated polymer resin systems.....	3
2.2 Geopolymer system.....	6
2.3 Class G well cement.....	7
3 INJECTIVITY PERFORMANCE EVALUATION.....	9
3.1 Sand pack injection tests	9
3.2 Planar fracture sealing experiments	15
4 FRACTURE SEALING PERFORMANCE EVALUATION	28
4.1 Testing apparatus	28
4.2 Gas flow in planar fractures	28
4.3 Results and analyses.....	29
5 BONDING STRENGTH PERFORMANCE EVALUATION.....	36
5.1 Direct shear strength testing apparatus and testing procedure.....	36
5.2 Results and analyses.....	37
5.3 Fracture sealing – observations on fracture surfaces	43
5.4 SEM and FIR studies on primer enhanced bonding strength mechanisms.....	47
6 SUMMARY, CONCLUSIONS AND SUGGESTIONS FOR FURTHER STUDIES.....	52
Appendix A Chemical Structure and DSC Spectra for Polymer Resins	54
Appendix B Mechanical Properties of Cured Fracture Sealing Materials.....	58
Appendix C Results of Injectivity Tests and Photos of Tested Fracture Samples.....	61
Appendix D Ardex P51 Primer Datasheet	105
References	110

Figures

Figure 2-1 Viscosities of the selected polymer resin systems (a) at room temperature (RT), and (b) at elevated temperature.	5
Figure 3-1 Ingress of sealant materials into sand packs (a) Resin polymer, (b) Geopolymer 2 and (c) Class G cement. The numbers at bottom of the photos show the date.month.year and time when the photos were taken.	10
Figure 3-2 Injection force, rate and volume vs time, (a) polymer resin (720-3), (b) geopolymer (GP2) and (c) Class G. Note that the volume measurements geopolymer and Class G slurries are considered unreliable due to plunger buckling.	13
Figure 3-3 Photos of slurry injection at different injection times, (a) polymer resin (720-3), (b) geopolymer (GP2) and (c) Class G cement. The numbers at bottom of the photos show the date.month.year and time when the photos were taken.	14
Figure 3-4 Synthetic fracture sample, a) schematics and dimensions, b) transparent fracture sample assembly, and c) non-transparent fracture sample assembly.	15
Figure 3-5 Slurry injection system comprising fracture sample assembly, slurry injection pump, control box and a laptop for data acquisition and control.	16
Figure 3-6 Measured parameters vs time for a typical water injection test. The fracture aperture is 25µm based on shim thickness, the hydraulic aperture is estimated to be 68µm.	19
Figure 3-7. Summary of cement slurry injection. Injection pressure vs volume.	20
Figure 3-8 Summary of GP1 slurry injection. Injection pressure vs injection volume.	21
Figure 3-9 Summary of GP2 slurry injection. Injection pressure vs injection volume.	22
Figure 3-10. Summary of polymer resin 620-1 injection tests. Injection pressure vs injection volume.	24
Figure 3-11 Summary of polymer resin 620-5 injection tests. Injection pressure vs injection volume.	24
Figure 3-12 Photo of a fracture sample set up in hot water bath.	26
Figure 3-13 Summary of polymer resin 720-3 injection tests. Injection pressure and injection volume.	27
Figure 4-1 Testing apparatus for assessing fracture sealing performance, a). Photo of the testing set up, and b). Schematic of the apparatus.	29
Figure 4-2 Gas pressure vs time for planar fractures sealed with Class G cement slurries.	30
Figure 4-3. Gas pressure vs time for planar fractures sealed with geopolymer 1 slurries.	31
Figure 4-4. Gas pressure vs time for planar fractures sealed with geopolymer 2 slurries.	31
Figure 4-5. Gas pressure vs time for planar fractures sealed with polymer resin 620-1.	32
Figure 4-6. Gas pressure vs time for planar fractures sealed with polymer resin 620-5.	32
Figure 4-7. Gas pressure vs time for planar fractures sealed with polymer resin 720-3.	33

Figure 5-1 Shear bonding strength testing apparatus, a). Schematic of the shear strength testing jig, b). Photo of the testing jig installed in an Instron loading frame.	37
Figure 5-2 Shear force vs shear displacement curves for direct shear bonding strength tests for fractures sealed with Class G cement.....	38
Figure 5-3 Shear force vs shear displacement curves for direct shear bonding strength tests on fractures sealed with GP1.....	39
Figure 5-4 Shear force vs shear displacement curves for direct shear bonding strength tests for fractures sealed with GP2.....	39
Figure 5-5 Shear force vs shear displacement curves for direct shear bonding strength tests for fractures sealed with Polymer Resin 620-1.....	40
Figure 5-6 Shear force vs shear displacement curves for direct shear bonding strength tests for fractures sealed with Polymer Resin 620-5.....	40
Figure 5-7 Shear force vs shear displacement curves for direct shear bonding strength tests for fractures sealed with Polymer Resin 720-3.....	41
Figure 5-8. Photos for fracture samples PMMA_SS_CG_350 and ST_CG_CG_650 sealed with Class G cement slurry, a). Cement slurry flow blocked close to injection point for the 350µm aperture fracture, b). Cement slurry flowed through entire length of the 650µm aperture fracture.....	44
Figure 5-9 Photos for fracture samples ST_CG_GP2_25 and ST_CG_GP2_130 sealed with GP2 slurry, a). GP2 slurry flow blocked close to injection point for the 25µm aperture fracture, b). GP2 slurry flowed through entire length for the 130µm aperture fracture.....	45
Figure 5-10 Photos for fracture samples ST_CG_620-1_230 and ST_CG_720-3_5_T=70C sealed with polymer resins, a). 620-1 with a fracture aperture of 230um injected at room temperature, b). 720-3 with a fracture aperture of 25um injected at 70°C.....	46
Figure 5-11 SEM images of polymer resin film bonding with carbon steel for the fracture samples, a) ST_CG_720-3_25_T=70C without application of the primer solution and b) ST_CG_720-3+Primer_25_T=70C with application of the primer solution.....	48
Figure 5-12 SEM images of polymer resin surface. Images a (no primer treatment) and b (primer treatment) in contact with siltstone, Image c (no primer treatment) and d (primer treatment) in contact with cement.....	49
Figure 5-13 Chemical structures of Acrylic Copolymer.....	50
Figure 5-14. FTIR Spectra of polymer resin film samples, a) bonding to carbon steel surface, b) bonding to cement surface, and c) bonding to siltstone surface.....	51

Tables

Table 2-1 Compositions of selected polymer resins (by weight).....	4
Table 2-2 Rheological properties of the polymer resin systems	5
Table 2-3 Curing and glass transition temperature for the selected polymer resin systems	5
Table 2-4 Summary of compressional mechanical properties for the selected resin systems	6
Table 2-5 Composition of geopolymer systems	7
Table 2-6 Summary of compressional mechanical properties for geopolymer systems	7
Table 2-7 Summary of compressional mechanical properties for Class G cement	8
Table 3-1 Experimental program for planar fracture injection tests.....	17
Table 3-2. Summary of observations on cement slurry injection.....	20
Table 3-3. Summary of observations on GP1 slurry injection	22
Table 3-4. Summary of observations on GP2 slurry injection	22
Table 3-5. Summary of observations on polymer resin 620-1 injection	25
Table 3-6. Summary of observations on polymer resin 620-5 injection	25
Table 3-7. Summary of observations on polymer resin 720-3 injection	27
Table 4-1 Summary of observations on sealability for Class G cement.....	33
Table 4-2 Summary of observations on sealability for GP1.....	33
Table 4-3 Summary of observations on sealability for GP2.....	34
Table 4-4 Summary of observations on sealability for polymer resin 620-1.....	34
Table 4-5 Summary of observations on sealability for polymer resin 620-5.....	34
Table 4-6 Summary of observations on sealability for polymer resin 720-3.....	34
Table 5-1 Summary of direct shear bonding strength for Class G cement.....	41
Table 5-2 Summary of direct shear bonding strength for GP1.....	41
Table 5-3 Summary of direct shear bonding strength for GP2.....	42
Table 5-4 Summary of direct shear bonding strength for polymer resin 620-1.....	42
Table 5-5 Summary of direct shear bonding strength for polymer resin 620-5.....	42
Table 5-6 Summary of direct shear bonding strength for polymer resin 720-3.....	42

Acknowledgments

This research has been funded through CSIRO's Gas Industry Social and Environmental Research Alliance (GISERA) with contributions from the Australian Government's Department of Industry, Science, Energy and Resources. GISERA is a collaboration between CSIRO, Commonwealth, state and territory governments and industry established to undertake publicly reported independent research. For information about GISERA's governance structure, projects and research findings visit <https://gisera.csiro.au>

The authors are grateful to Dr Colin Wood, Dr Cameron Huddleston-Holmes of CSIRO, and Dr Kwesi Sagoe-Crentsil of Monash University for various discussions during the project.

Executive summary

Fugitive gas emission from well casings is a potential risk in developing unconventional gas resources. The objective of the project is to identify and evaluate new fracture sealing materials that may be applied to seal gas leaks behind well casings where conventional well cement slurry may fail to mitigate.

A comprehensive experimental study has been conducted to evaluate the performance of five potential fracture sealing materials, including two geopolymers and three thermal-activated polymer resins. They were firstly evaluated for their injectivity into sand packs, and then for their performance in sealing planar fractures with apertures ranging from 25 μm to 650 μm with majority less than 400 μm . The major findings from the study are:

- Both the geopolymers and thermal-activated polymer resins were able to be injected into the sand pack to form a solid sand plug upon curing, while it was not possible to inject the conventional Class G cement slurry into the sand pack. The particle sizes of the sand packs were between 250 μm and 425 μm ;
- The thermal-activated polymer resins were able to penetrate a planar fracture with an aperture as narrow as 25 μm , whilst the minimum fracture aperture that could be injected through was approximately 50 μm for the geopolymer and 350 μm for the conventional Class G cement slurry;
- The seal to gas generated in the planar fractures by Class G cement and geopolymer slurries was poor in general ranging from almost no seal to partial seal. Partial to complete seal was achieved with one of the thermal-activated polymer resins when the injection was conducted at 70°C. The seal could be improved further by applying a water-based primer solution prior to the polymer resin injection; and
- The shear bonding strength of the fracture was, in general, very weak for the Class G cement and geopolymer slurries. In comparison, the shear bonding strength generated from one of the thermal-activated polymer resins was more than ten times higher. The bonding strength could be improved further by applying the water-based primer solution prior to the polymer resin injection.

The experimental study so far demonstrated that the thermal-activated polymer resin (code name 720-3) is a promising sealant material in sealing small fractures where conventional oil well cement would likely fail to seal. Further laboratory experimental studies are recommended to evaluate its performance in sealing small/micro fractures, and the longevity and effectiveness of the seal under simulated downhole pressure, temperature, and other adverse conditions, prior to field trials.

1 INTRODUCTION

The GISERA Project G. 6 project, titled “Advancing new materials to assist mitigating fugitive gas emission from well casings”, consists of three project phases:

- Phase 1 – Material selection and performance criteria;
- Phase 2 – Bench top screening and evaluation; and
- Phase 3 – Performance evaluation under downhole condition

The outcomes from Project Phase 1 were summarised in a comprehensive literature review report on sealant technologies applied for mitigating and remediating cement-related well leakage in oil and gas industry (Wu et al. 2020). Some of the technologies and their limitations are summarised below:

- Conventional oilfield cements have been the option of choice for majority of oil and gas well remediation treatments. Squeeze cementing has been applied to remediating leaking wells related to poor primary cement jobs and has been mostly successful. However, due to their particle sizes, the conventional oilfield cement cannot penetrate and seal small fractures or defects with an aperture less than approximately 400 μm (micron);
- Micro fine cements have been developed and applied to seal small well leaks, where the conventional oilfield cements failed. However, laboratory and field case studies have demonstrated that the micro fine cement systems cannot penetrate and seal a micro fracture with an aperture less than approximately 120 μm ; and
- Polymer resins have a number of advantages over cementitious sealants including the perceived ability to penetrate deeper into smaller fractures due to its solid free nature. In addition, with proper formulation the polymer resin can be fine-tuned in terms of curing time and viscosity to suit downhole conditions.

Despite the progress in sealant technologies made over the years, significant technology gaps remain in meeting industry needs. In particular, sealing small/micro fractures with an aperture less than approximately 120 μm is a significant challenge. Solid free polymer resins are perceived to be able to penetrate deeper and seal narrow fractures. However, the commercial products of the polymer resins have high viscosities which would make them difficult to be injected into small leaking pathways behind well casings.

CSIRO has developed novel materials for civil and oil and gas applications for many years. These include geopolymer systems and related formulations deployed in the building and construction sectors and polymer composite materials for oil and gas infrastructure rehabilitation in the oil and gas industry. A number of candidate materials with potential for fracture sealing were identified and formulated in Project Phase 1. This report summarises the findings from Project Phase 2 and part of Phase 3, i.e., Bench top screening and evaluation for the selected candidate fracture sealing materials. The objective is to conduct bench top screening experiments to evaluate the performance of the candidate materials, in terms of their injectivity, sealability and mechanical

shear bonding strength, and to identify the most promising ones for further evaluation under simulated downhole pressure and temperature conditions.

The rest of the report is organised as follows:

Section 2 provides background information of the candidate materials, including their physical, rheological and mechanical properties.

Section 3 describes injectivity performance of the candidate materials. This includes sand pack injectivity tests and planar fracture injection tests.

Section 4 documents the performance of the candidate materials in sealing planar fractures, evaluated with compressed air.

Section 5 describes evaluation of shear bonding strength of the fractures sealed with the candidate sealant materials, including the testing apparatus and the results.

The major results and conclusions are summarised in Section 6, which also includes suggestions for further studies.

Figure 1 depicts the workflow adopted in this project.

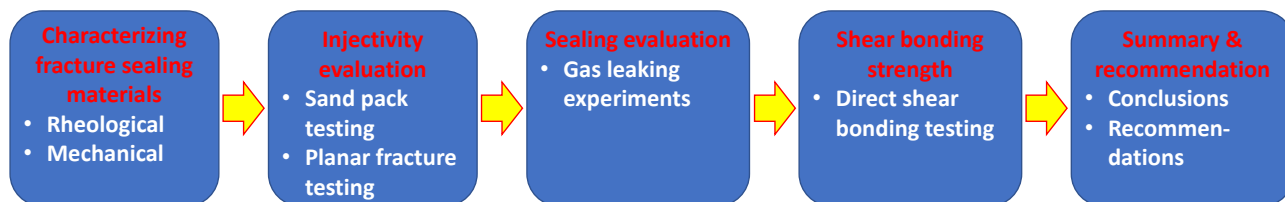


Figure 1. Project workflow

2 CHARACTERIZATING NEW FRACTURE SEALING MATERIALS

A number of fracture sealing materials alternative to conventional oil well cement was identified following a brainstorm workshop in the early stage of the project. Several new fracture sealing materials were selected for bench top screen tests based on the expertise of the project team members in material science and well sealing material selection criteria (Wu, et al 2020). The selected fracture sealing materials include geopolymers and thermal activated polymer resins. This section documents rheological, physical, and mechanical properties of the selected new fracture sealing materials. Furthermore, the properties of the conventional Class G well cement was also evaluated as a reference material.

2.1 Specially formulated thermal activated polymer resin systems

The polymer resins identified as potential fracture sealing materials are solid free polymer resin systems which consist a single, double or multiple components. They can be formulated purposely to have desired viscosity range, curing temperature, and curing time to facilitate a sealing operation for a leaking gas well.

A number of resin formulations were screened at the initial stage of the project in terms of viscosity, glass transition temperature and the degree of curing for a given period of time. The target curing temperature is 70°C representing an underground temperature condition at approximately 2000 m deep. Three resin systems were eventually selected as candidates for fracture sealing materials. These systems consisted of a blend of di-functional aromatic (DGEBA) and di-functional aliphatic (PPGDGE or ECHO or D4) polymer resins and an aromatic diamine (ET100) as a hardener. Their chemical structures are given in Appendix A.

The selected polymer resin systems were designed to provide a low viscosity at room temperature and continue to maintain low viscosity (say less than 400 mPa s or cP) at downhole temperature (~70°C) for at least 5 to 6 hours before the gel formation. This would allow sufficient time for field operation to deliver the resin system into the leaking well section and penetrate deep into the leaking pathways. The selected polymer resin systems can be cured under fresh water as well as sea water (brine) and can tolerate some degree of contamination environment such as sands or other wellbore fluids.

In the selected resin systems, di-functional aliphatic polymer resin (PPGDGE or ECHO or D4) was used as a reactive diluent to reduce the viscosity of the blended polymer resin at room temperature or downhole temperature. It is expected that the low viscosity feature of the selected polymer resin system will likely help the mixing, pumping and injection process. In addition to their main role as a reactive diluent, PPGDGE (or ECHO or D4) also imparts the flexibility therefore enhance cured resin's resistance to fracturing.

All the components of the resin system, except D4-polymer, can be obtained locally and they were used without further purification. The D4-polymer was prepared in the laboratory in 0.5kg to 1kg batch.

The compositions of each polymer resin system are given in Table 2-1.

Table 2-1 Compositions of selected polymer resins (by weight)

BND #	DGEBA	ECHO POLYMER	D4- POLYMER	PPGDGE	ET100
010620-0*	1.0g				0.226g
010620-1	0.9 g	0.1 g			0.273 g
010620-5	0.8 g		0.2 g		0.229 g
020720-3	0.8 g			0.2 g	0.217 g

*: BND010620-0 contains no diluent as a reference

2.1.1 Rheological properties

The viscosities of the resin systems were measured by using HAAK Rheostress 600 with constant rotation (CR=418.9 1/s equivalent to 200rpm) and gap setting at 0.5mm at both ambient and elevated temperatures (70°C) over the period of 6 hours. Figure 2-1 shows viscosity vs time curve for the selected resin systems, whilst the ranges of viscosity and density prior to cure are summarised in Table 2-2.

2.1.2 Curing and glass transition temperature

The glass transition temperature (Tg) is one of the key parameters for polymer resin. Tg is the onset temperature when a solid polymer transits from a rigid glassy stage to a soft (not melted) material stage. Therefore, the Tg is used to set the upper limit service temperature when used in structure application. However, the Tg may not be as important for sealing fractures behind well casings as for structure application, since a less rigid sealing material would be more resistant to fracturing, hence provide a better seal. Another key performance indicator is the degree of curing of the resin, this is determined by comparing the energy released from the pre-cured and cured samples. The degree of curing relates to the mechanical properties and resin's integrity. In general, the higher the %curing associates with the better mechanical performance.

In this study, Tg and degree of curing were determined by DSC (Differential Scanning Calorimeter). Each pre-cured polymer resin sample was run by DSC under thermal dynamic condition from 30°C to 350°C at a rate of 10°C/min. and cured polymer resin sample was run by the same condition. The Tg of cured resin sample was obtained from the DSC of cured sample. The DSC Spectra is presented in Appendix A. The degree of curing and Tg determined are summarised in Table 2-3 for all the four polymer resins.

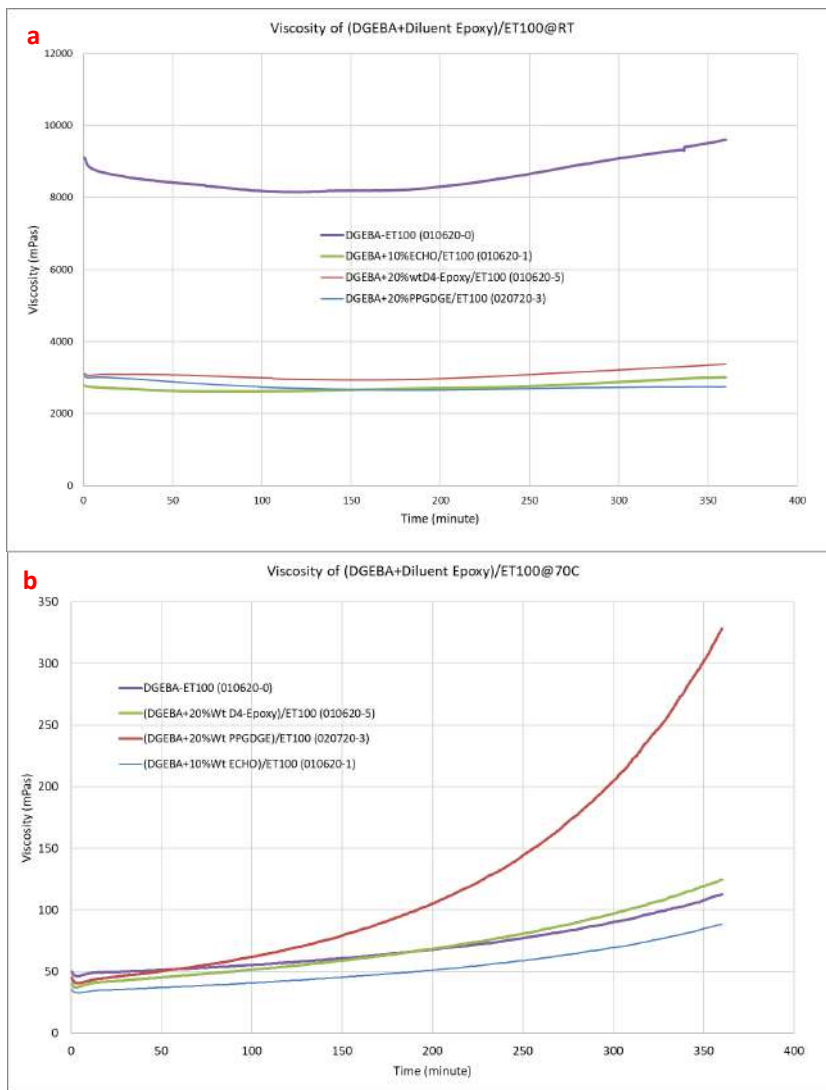


Figure 2-1 Viscosities of the selected polymer resin systems (a) at room temperature (RT), and (b) at elevated temperature.

Table 2-2 Rheological properties of the polymer resin systems

BND#	VISCOSITY RANGE AT RT (CP)	VISCOSITY RANGE AT 70° C (CP)	DENSITY(G/CM ³)
010620-0	9100-9600	50-113	1.11
010620-1	2750-3000	35-80	1.11
010620-5	3070-3370	40-125	1.12
020720-3	3000-2740	45-330	1.10

Table 2-3 Curing and glass transition temperature for the selected polymer resin systems

BND#	CURE CONDITION	% CURING	TG (DEG C)
010620-0	24hrs@70C under water	85.0	80.6
020620-1	24hrs@70C under water	90.5	90.3
010620-5	24hrs@70C under water	87.9	92.8
020720-3	24hrs@70C under water	80.7	65 - 80

2.1.3 Mechanical properties

Mixed polymer resin systems contained in syringes were cured underwater at 70°C for 24 hours and continued to cure at ambient condition for further about one week. The cured resin plugs were then released from the syringes with the end surfaces grinded flat and parallel to each other. The finished plugs were then installed in an INSTRON loading frame. Unconfined compressive strength tests were conducted at a nominal axial strain rate of approximately 15%/hour. The stress vs strain curves and the photos of the tested samples are presented in Appendix B. The plugs were deformed (compressed) by over 20% of their original lengths and no fractures/failure were observed in the plugs.

The key mechanical properties and the density of the sample plugs are summarised in Table 2-4.

Table 2-4 Summary of compressional mechanical properties for the selected resin systems

SAMPLE NAME	DENSITY (G/CM ³)	YOUNGS MODULUS (GPA)	PEAK STRENGTH (MPA)
010620-1	1.17	1.74	87.90
010620-5	1.16	1.91	99.15
020720-3	1.17	1.95	111.98

2.2 Geopolymer system

Geopolymers are alumino-silicate-based inorganic polymers that exhibit excellent physical and chemical properties. In general, geopolymers have been synthesized by alkali activation of mineral compounds rich in SiO₂ and Al₂O₃, such as metakaolin, fly ash and bottom ash. The base reaction mechanism involves the dissolution of Al and Si in the alkali medium, followed by a polycondensation forming a 3D network of silico-aluminate structure.

Some potential benefits expected from the use of geopolymer technology in sealing small fractures may include:

- Water based, non-toxic durable material that has low curing temperature;
- Greater chemical resistance to acid and sulphate attack;
- Good adhesion and durability;
- Thermal stability- provided by alumino-silicate matrix;
- Improved mechanical and thermal performance;
- More flexible structure network than pure inorganic polymer when incorporating organic functional groups; and
- Low cost;

The geopolymer system identified as potential candidates for fracture sealing consists of three components, i.e., potassium silicate solution (Kasil 226), potassium hydroxide (KOH) and MetaStar 501 (calcined kaolin). Two compositions were considered, i.e., geopolymer 1 (GP1) and

geopolymer 2 (GP2). The amount of KOH was increased by 5% for GP2 to accelerate curing process and increase early strength development.

The mixing ratios between the components by weight are summarised in Table 2-5.

Table 2-5 Composition of geopolymer systems

NAME	KASIL2236 (G)	KOH (G)	METASTAR 501 (G)
GP-1	1	0.10	0.58
GP-2	1	0.15	0.61

The key parameters of particle size distribution for the solid component Metastar 501 are D10=0.473µm, D50=3.2µm and D90=10.4µm.

All the components of the geopolymer systems can be acquired locally and they are used without further processing.

The viscosity of the geopolymer 2 was measured using a Brookfield viscometer. Two spindle speeds were used (60rpm and 200rpm). The measurements were made for 30 minutes and the results showed that the viscosity of GP2 ranges from 900mPas to 1300mPas. No direct measurements were made for the viscosity of GP1, however, the liquid to solid ratio by weight was kept the same for both compositions, and it was expected that both GP1 and GP2 would have a similar viscosity range.

The mixed geopolymer slurry was poured into a plastic syringe and cured in a hot water bath at 70°C for 24 hour and continue to cure for a further 28 days underwater at room temperature. The cured geopolymer plugs released from the syringe were cut to length with both ends grinded flat and smooth. The prepared samples were then tested for unconfined compressive strength using the INSTRON loading frame. The stress vs strain curves are presented Appendix B with the key mechanical properties summarised in Table 2-6

Table 2-6 Summary of compressional mechanical properties for geopolymer systems

NAME	DENSITY (G/CM ³)	YOUNGS MODULUS (GPA)	PEAK STRENGTH (MPA)
GP-1	1.14	1.91	15.99
GP-2	1.17	2.09	19.22

2.3 Class G well cement

Class G cements are sulfate-resistant Portland cements and widely applied to oil and gas well cementing. As a reference material, commercially available Class G well cement was evaluated for its fracture sealing performance.

The neat Class G component was mixed with fresh water with a water to cement ratio of 0.45 by weight. No additives were added to the slurry. Viscosity of Class G cement slurry was measured using a HAAK RheoStress 600 rheology metre. Continuous measurements in 15 minutes showed that the viscosity of the cement slurry ranged from 250 mPas to 500 mPas.

Mechanical properties were measured on the cured Class G cement. The fully mixed Class G slurry was poured into a syringe and cured in a hot water bath at 70°C for 24 hours and continued to cure under water at room temperature for a further 28 days. Two test samples were obtained by cutting a long cylindrical plug cast inside the syringe into two halves. Unconfined compressive strength tests were conducted using the Instron loading frame. The key mechanical properties of the Class G cement are summarised in Table 2-7 whilst the stress vs strain curves are presented in Appendix B.

Table 2-7 Summary of compressional mechanical properties for Class G cement

NAME	DENSITY (G/CM ³)	YOUNGS MODULUS (GPA)	PEAK STRENGTH (MPA)
CG-1	1.58	3.05	31.11
CG-2	1.63	3.42	42.34

3 INJECTIVITY PERFORMANCE EVALUATION

Injectivity performance of the selected fracture sealing materials as described in Section 2 was evaluated in two types of injection test, i.e., sand pack injection tests and planar fracture injection tests.

3.1 Sand pack injection tests

Mineral sands with particle size ranged between 250 μ m and 425 μ m was packed in plastic syringes with an internal diameter approximately 29mm. To prevent sand particles from falling out of the syringes from the nozzle, a mesh disk was placed to cover the nozzle at the bottom of the sand pack. The sand packs were then fully saturated with fresh water. The sand packs had a porosity approximately 38% based on the packed amount of sands, the sand pack volume and sand particle grain density. Permeability of the sand packs was measured to be between 12 Darcy and 17 Darcy by water falling head method (Head 1982). Two types of sand pack injection tests were then carried out, i.e., sealant ingress due to gravity and sealant injection by force, as detailed in the following sub-sections.

3.1.1 Sealant ingress by gravity

The top of the fully water saturated sand pack was at proximately 20ml mark of the syringe. The sealant materials, be it geopolymers or Class G cement slurries, or the mixed polymer resins, were poured into the syringe on top of the sand pack until the height of the sealant material reached the 50ml mark. The slurries and polymer resins were mixed based on the compositions given in Table 2-1 and Table 2-5. The syringe was held vertical and the test started by open the nozzle to atmospheric condition to allow ingress of the slurry or polymer resin into the sand pack and water to drain out from the nozzle. Photos were taken at different times to record ingress of the slurry or polymer resin into the sand pack, as shown in Figure 3-1. Note that the polymer resin (BND020720-3, or 720-3 for short) was heated and maintained at 70°C in an oven, whilst the Class G and Geopolymer slurries were tested at room temperature.

As can be observed from Figure 3-1, the polymer resin (720-3) was able to ingress into the sand pack under gravity. It displaced the free water in the sand pack and reached the nozzle at the bottom of the sand pack in approximately 40 minutes. However, no movement of the slurry front into the sand pack was observed for the geopolymers (GP2) and Class G cement slurries. It was indeed observed that water was drained from the syringe nozzle for the two sand packs. This may indicate that the liquid phase in the slurry may have entered the sand pack to displace water, whilst the solid phase was filtered out on the slurry and sand pack interface. The loss of liquid phase would lead to an increase in slurry viscosity and slurry thickening, which in turn would prevent the ingress of the slurry into the sand pack.

Following the sand pack tests, the syringes containing the sand packs and slurries, or polymer resin were immersed in hot water bath at 70°C to allow the contents in the syringes to cure for at least

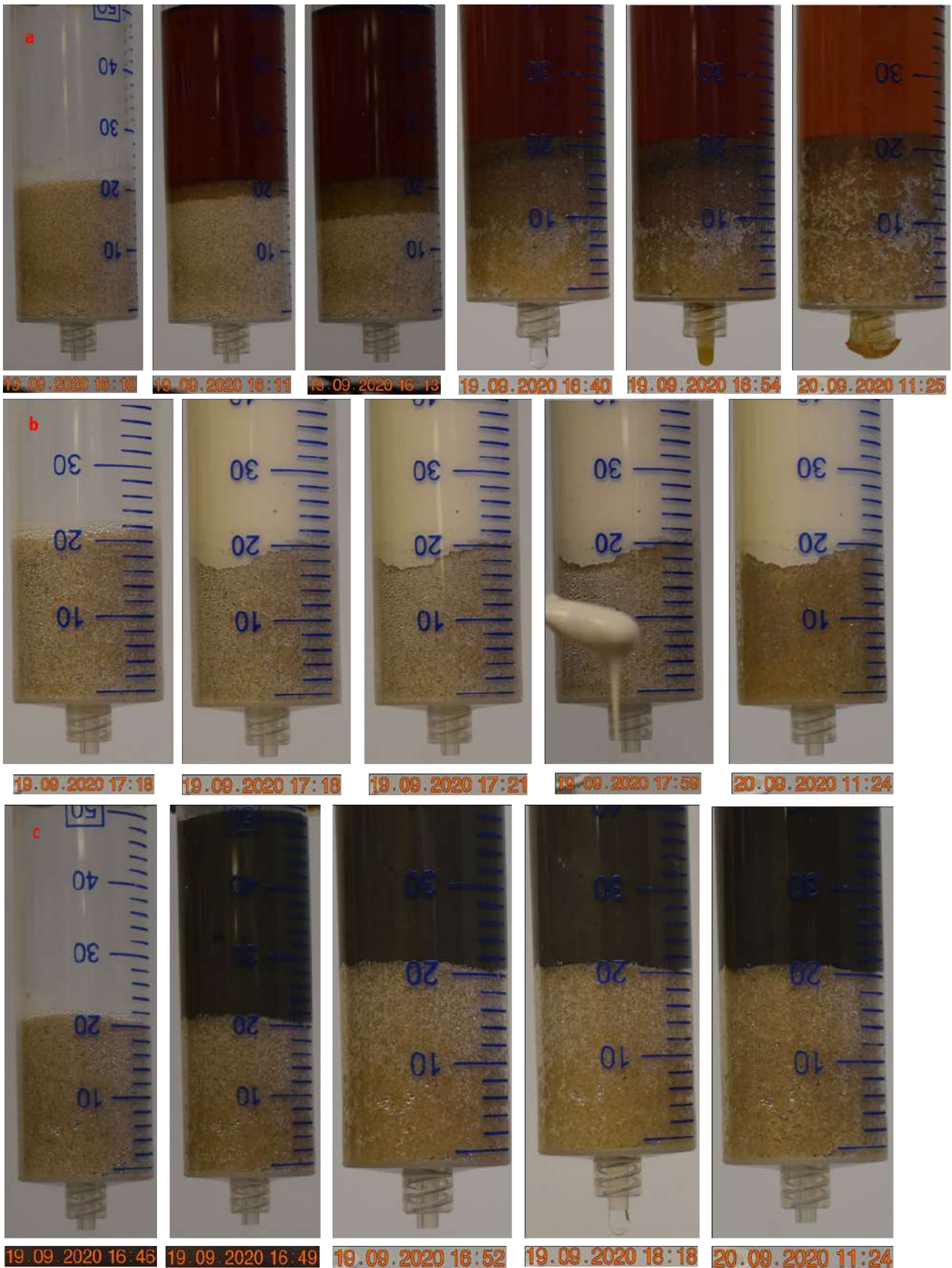


Figure 3-1 Ingress of sealant materials into sand packs (a) Resin polymer, (b) Geopolymer 2 and (c) Class G cement. The numbers at bottom of the photos show the date.month.year and time when the photos were taken.

24 hours. Upon curing, the sand pack tested with the polymer resin (720-3) was able to form a firm sand plug. However, the sand pack tested with geopolymer and Class G cement slurries

remained loose sand, which confirms further that no or insignificant amount of geopolymer and Class G cement slurries were able to ingress into the sand packs.

3.1.2 Sand pack injection tests by force

The sand packs were prepared using the same method as described in Section 3.1.1, whilst the sand pack height was at approximately 32ml mark on the syringe. The slurry, be it geopolymer or Class G cement or polymer resin, was poured into the syringe. This was followed by inserting the plunger into the syringe. The slurry compositions were the same as that used in Section 3.1.1. The initial start position of the plunger was at approximately 54 ml mark. The slurry injection was conducted using a specially designed and manufactured injection rig. Injection force and volume were measured by using a loadcell and a displacement meter measuring the distance the syringe plunger moved. The injection was conducted at a constant flow rate. All the data acquired from the rig were recorded using a laptop. More details of the injection system will be given in Section 3.2.

The slurry injection started at a nominal injection rate of 5ml/min with the fluids drained out at atmospheric condition from the nozzle. Figure 3-2 presents the curves of injection force, injection rate and injection volume vs time for the three fracture sealing materials and Figure 3-3 are the photos taken at different injection times. The time when the photos was taken are approximately marked in Figure 3-2.

The injectivity of the fracture sealing materials may be evaluated based the force required to inject the slurry into the sand pack. The injection force is proportional to the injection pressure on the syringe plunger since the cross-section area of the syringe was the same for all the slurry injection tests. Figure 3-2 (a) showed that the maximum injection force for polymer resin was approximately 9.5 kg before it rapidly increased to over 16 kg. This increase in the injection force was caused by the restriction of the nozzle to the polymer resin (720-3) flow. The diameter of the nozzle was 1mm. The injection force rapid increase indicated that the polymer resin flow had reached the nozzle. Because the viscosity of the polymer resin was significantly higher than the fresh water, the force required to inject at the same injection rate was increased significantly. When the injection rate was reduced to 1ml/min, the injection force required was around 6.5 kg. Note that the liquid resin polymer was heated to 70°C before the injection test.

For the geopolymer slurry injection, at an injection of 5 ml/min, the injection force increased to approximately 23 kg, Figure 3-2 (b). It was observed that the plunger started buckling when the injection force was over approximately 20 kg. The injection rate was then reduced to 1 ml/min. However, the injection force continued to increase to over 16 kg. The injection rate was again reduced to 0.5 ml/min with an approximate injection force of 12 kg. Due to the buckling of the plunger, the travel distance measurement of the plunger is considered unreliable. However, from the photos taken during the injection, Figure 3-3 (b), a total of approximately 14 ml of the slurry was injected into the sand pack.

For the injection of Class G cement slurry, the injection force increased rapidly at an injection rate of 5 ml/min and reached approximately 40 kg, Figure 3-2 (c). The plunger started buckling with the injection force being over 20 kg with a very small slurry volume being injected into the sand pack. Only the water phase of the slurry was able to be squeezed into the sand pack and to displace the free water in the sand pack.

Following the slurry injection tests, the syringes containing the sand packs and the fracture sealing materials were immersed in the hot water bath at 70°C at for least 24 hours. Upon curing, the sand pack tested with polymer resin and geopolymer formed firm sand plugs. However, the one

with Class G cement remained the loose sands, confirming further that no or insignificant Class G cement slurry was injected into the sand pack.

The injectivity behaviour observed above could be understood based on the size distribution of the sands forming the sand packs. As the sand particle sizes ranged between 250 μm to 425 μm , and the pore size could be one fourth of the particle size, i.e., between 60 μm to 105 μm , the particle size in the slurry without bridging the pore size would be one fifth of the pore size using the rule of thumb (Nelson and Guillot 2006), i.e., the particle size in the slurry that could penetrate the sand pack would be in the range of 12 μm to 22 μm . As discussed in Section 2.1, the D50 and D90 of the solid phase of the geopolymer are 3.2 μm and 10.4 μm respectively, hence, injection of geopolymer slurry into the sand pack would be possible, and the solid particles are unlikely to be filtered out when entering the sand pack. However, for the Class G cement slurry (assuming a typical Portland cement particle size distribution), the D50 and D90 of the solid particles are 19.34 μm and 48.75 μm respectively (Nelson and Guillot 2006). Consequently, the cement particles would be filtered out at the sand pack surface and prevented from ingress into the sand pack, which is confirmed from the sand pack tests both by gravity and by injection. The polymer resin is solid free, hence, it would be expected that the polymer resin would be able to be injected into the sand pack. The observation of no or insignificant ingress of geopolymer slurry into the sand pack under gravity in Figure 3-1 was likely due to insufficient injection force because of the high viscosity of the geopolymer slurry, rather than particle size.

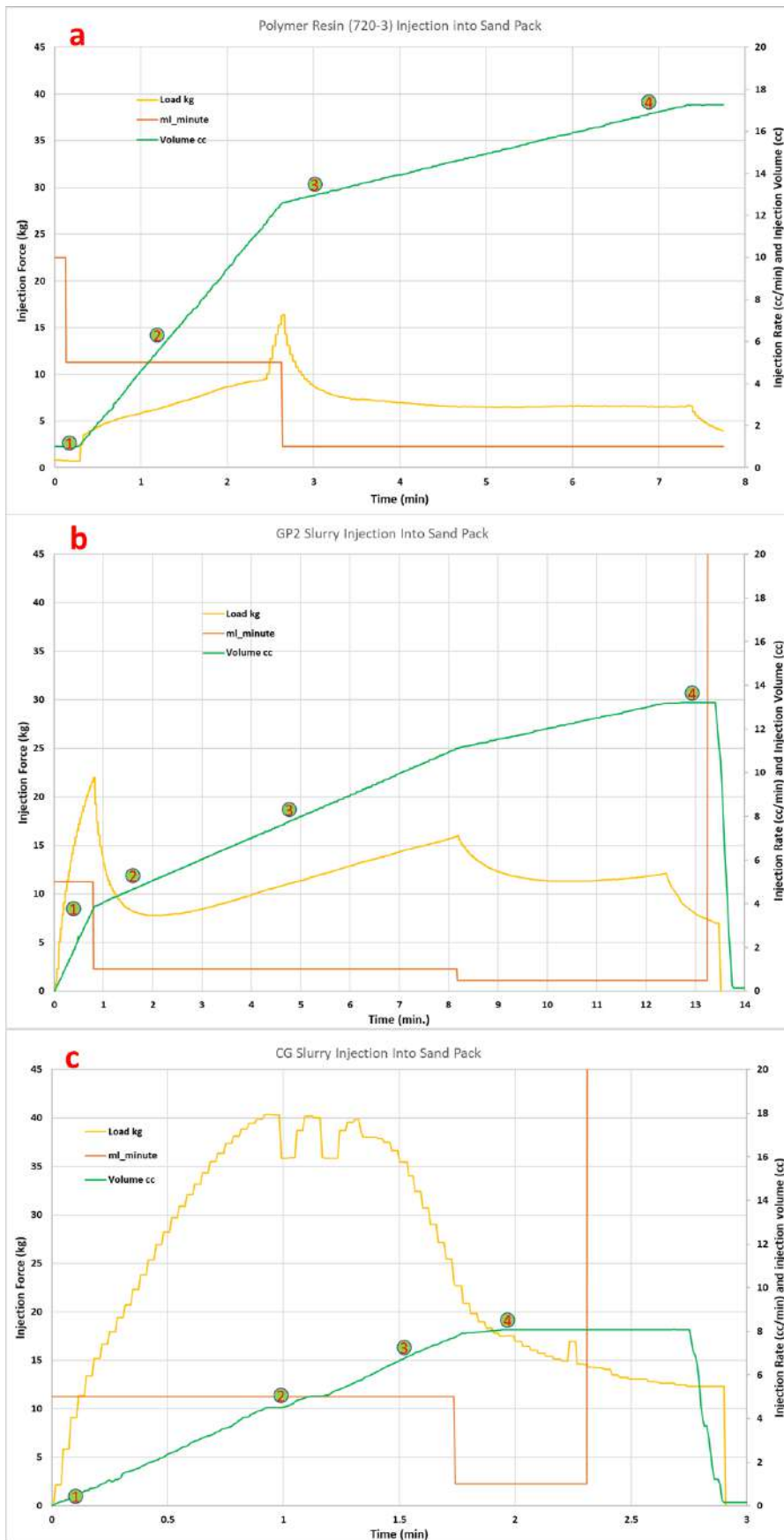


Figure 3-2 Injection force, rate and volume vs time, (a) polymer resin (720-3), (b) geopolymer (GP2) and (c) Class G. Note that the volume measurements geopolymer and Class G slurries are considered unreliable due to plunger buckling.

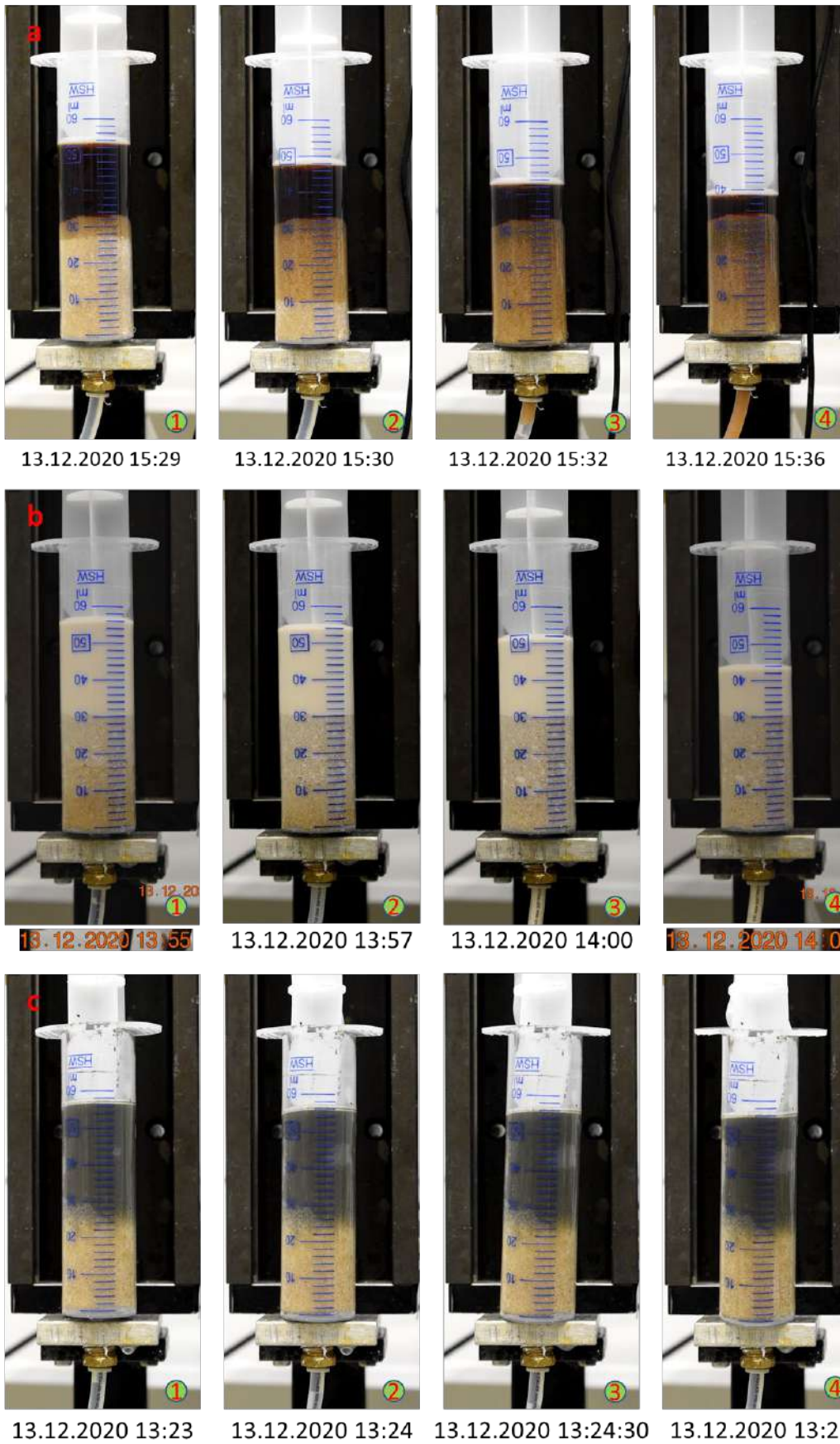


Figure 3-3 Photos of slurry injection at different injection times, (a) polymer resin (720-3), (b) geopolymer (GP2) and (c) Class G cement. The numbers at bottom of the photos show the date.month.year and time when the photos were taken.

3.2 Planar fracture sealing experiments

3.2.1 Synthetic planar fracture and liquid injection system

To further assess injectivity of the fracture sealing materials selected, synthetic planar fractures were created by inserting a pre-cut shim between two test slabs, so that the precise aperture of the fracture is known. The test slabs were carbon steel, cured Class G cement or formation rock, to simulate fractures induced on the interfaces between casing and cement sheath or between cement sheath and formation or the fracture within the cement sheath. Figure 3-4 shows a schematic of the synthetic planar fracture and the photo of a synthetic fracture sample.

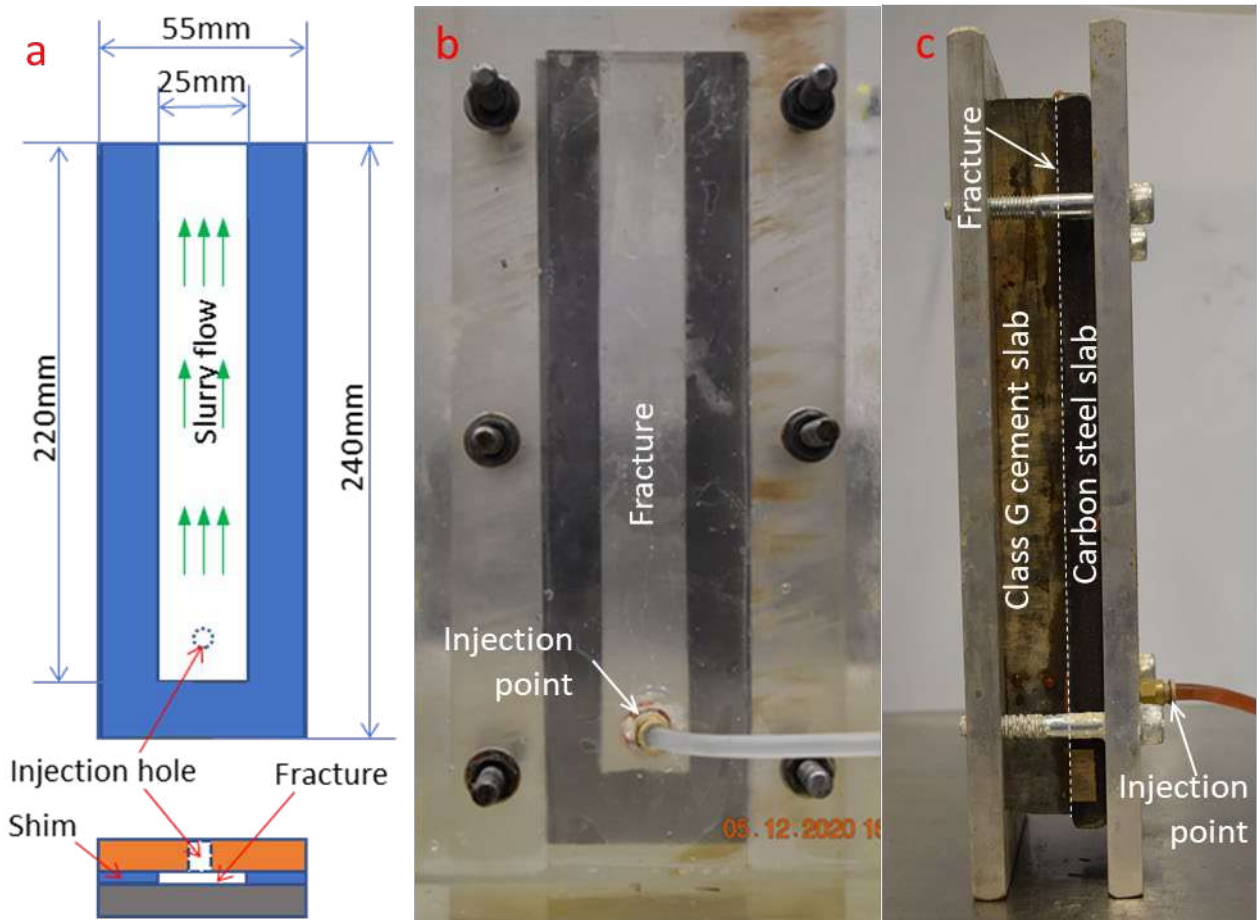


Figure 3-4 Synthetic fracture sample, a) schematics and dimensions, b) transparent fracture sample assembly, and c) non-transparent fracture sample assembly.

As illustrated in Figure 3-4a, a 6mm hole was drilled through one of the test slabs close to the sealed end of the planar fracture, so that slurry could be injected into the planar fracture and flow along the fracture towards the open end which was kept at atmospheric pressure condition. The two test slabs with the inserted shim was then placed between two stiff aluminium plates (Figure 3-4c) or two thick PMMA plates (Figure 3-4b), and cramped together by bolting the two aluminium plates or PMMA plates to form a fracture sample for injection tests. The PMMA set up was used for visual observation of the sealant flow within a planar fracture for some of the tests.

Figure 3-5 is a photo of the sealant injection system, purposely designed and manufactured for the project. It comprises the fracture sample, sealant injection pump, control box and a laptop for data acquisition and control. The measurements include sealant injection rate, injection pressure

at the injection point, injection force and injection distance from which the injected sealant volume could be derived. To improve the mechanical strength of the injection plunger, a new solid plunger was machined from PTFE material. The fracture sample was setup vertically with expectation that the injected slurry would completely displace the fluid (water) existing inside the fracture.

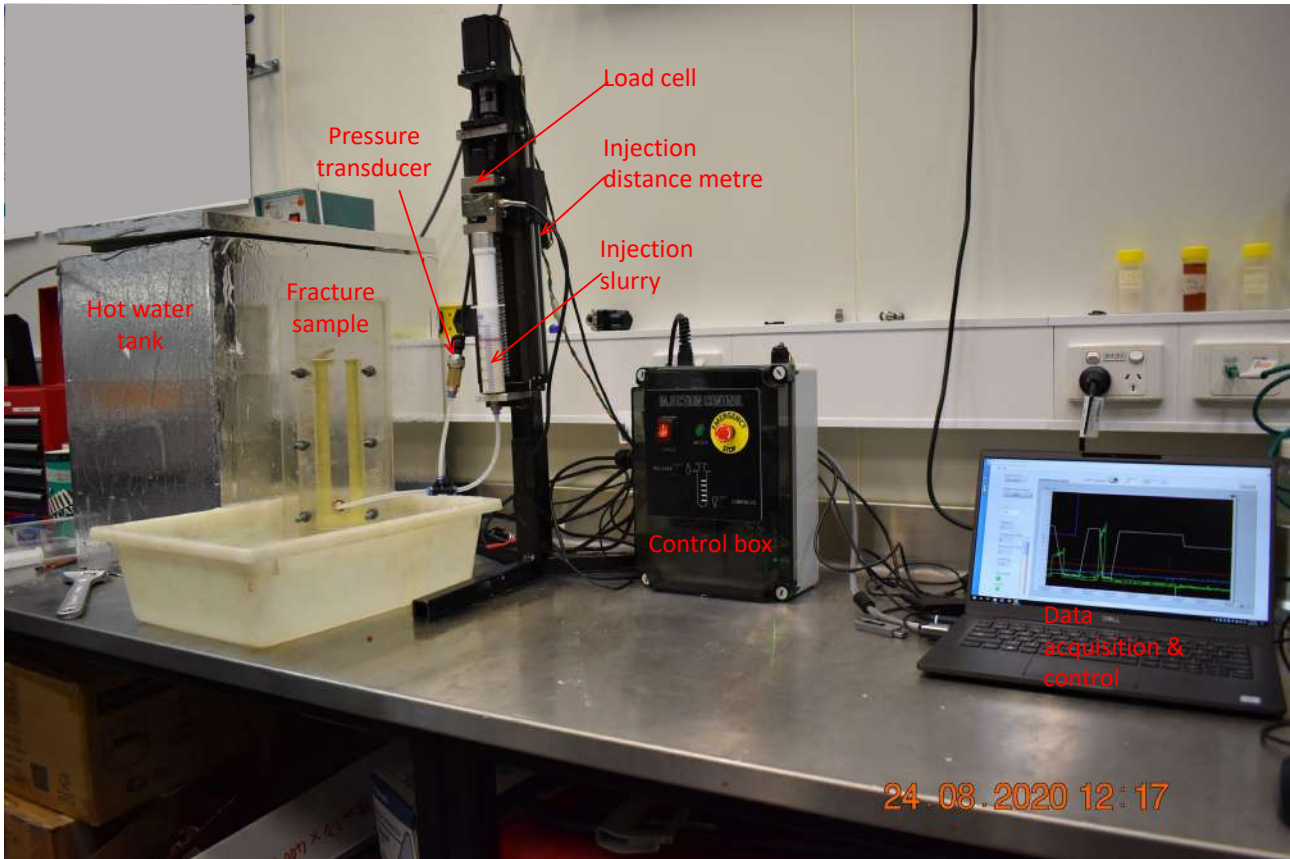


Figure 3-5 Slurry injection system comprising fracture sample assembly, slurry injection pump, control box and a laptop for data acquisition and control.

3.2.2 Test program and procedure

The planned test program for the selected fracture sealing materials are summarized in Table 3-1 together with the aperture size (shim thickness) of planar fractures. All the six fracture sealing materials characterized in Section 2 were evaluated for three different combinations of the test slabs, i.e., carbon steel and Class G cement, Class G cement and Class G cement, and Class G cement and Siltstone. Limited number of tests was also conducted using transparent PMMA slabs to gain a better understanding on the flow process of the sealant material in the planar fractures.

The thickness of the test slabs was 10mm for carbon steel, approximately 20mm for cured Class G cement and siltstone, and 11mm for PMMA. The other dimensions of the slabs are given in Figure 3-4a. The surface of the carbon steel slab was wet cleaned without other treatments and the skin on the carbon steel surface was intact. The cement and siltstone slabs were grinded to parallel, flat, and smooth on both sides. The cement slabs were sampled from a large cured Class G cement block which had been cured under water at 70°C in an oven for 28 days. The water to cement ratio used was 0.45 by weight. The siltstone slabs were prepared from large blocks sourced from a quarry in Queensland. The siltstone has a porosity of 12.8%. The 11mm thick PMMA slabs were

prepared from commercially available product. All the test slabs (except PMMA) were kept in fresh water before sealant injection tests.

Table 3-1 Experimental program for planar fracture injection tests

SEALANT	STEEL&CLASS G	CLASS G&CLASS G	CLASS G&SILTSTONE	PMMA&PMMA	PMMA&SILTSTONE
CLASS G	650@		650	350, 250	350
GP1	125, 150, 230, 350				
GP2	25, 125, 130			50, 125	
Polymer Resin 620-1	125, 230		125, 230	125	
Polymer Resin 620-5	125, 230, 350	125, 230	125, 230, 350		
Polymer Resin 720-3	25, 25+primer*, 125, 225, 330, 650	25+primer,	25, 25+primer, 125	150, 350	

@: the number in the table is shim thickness in μm (assumed to be fracture aperture size).

*: A pre-flush solution to enhance seal and shear bonding strength and will be discussed further in Section 5

Around 40 sealant injection tests were planned. The sealant injection procedure was as follows:

- Fracture sample assembly. A sealant injection test started with constructing the fracture sample using the desired test slabs and metal shim thickness;
- Fracture sample installation. The fracture sample was placed vertically in a plastic container or in a hot water bath and connected to the syringe injection system with flexible Nylon tube via quick fittings;
- Water injection. Water injection was conducted at several injection rates to determine the hydraulic aperture of the synthetic planar fracture; and
- Sealant injection. The test sealant was mixed based on the compositions presented Section 2 and transferred to the injection syringe which was then installed in the injection rig. The sealant was injected at a relatively fast flow rate to fill up the dead volume in the nylon tube between the injection syringe and the injection point on the fracture sample. The injection rate was then reduced to a lower injection rate. The injection rate might change during a test due to the limits on injection pressure or injection force of the injection rig. The sealant injection was terminated after the required sealant volume had been injected, which was many times of the fracture volume.

Note that when assembling fracture sample for testing, a nominal constant torque was applied to each bolt for all the fracture samples. It was observed that whilst the hydraulic aperture for the PMMA test fracture sample was not sensitive to the torque applied, for fracture samples assembled from other slabs, such Class G cement slabs and siltstone slabs, their hydraulic apertures could be affected by how much torque was applied when tightening the bolts.

Furthermore, it was not always possible to derive hydraulic aperture by conducting water injection tests due to limited flow rate that could be achieved with the injection system. When the aperture of the fracture assembly was large, say $250\mu\text{m}$, the pressure generated with the maximum

injection rate at 200 ml/min was very low, within the resolution of the pressure transducer, which made the evaluation of the hydraulic aperture unreliable.

3.2.3 Injection test results and analyses

Water injection

A typical plot for a water injection test is presented in Figure 3-6. Water injection was conducted at 10, 20 and 30 ml/min and repeated once. The injection rate was increased to a next (higher) rate after the injection pressure was approximately constant.

The model for steady state fluid flow in a parallel plate sample is used to interpret the water injection results. The so-called “cubic law” can be written as (Zimmerman & Bodvarsson 1996),

$$Q = \frac{-|\nabla P|wh^3}{12\mu} \quad (1)$$

where Q is fluid flow rate with a unit of m^3/s , $|\nabla P|$ is pressure gradient over the fracture length with a unit of Pa/m , w and h are fracture height and width (or aperture) respectively with a unit of m , and μ is viscosity of the fluid with a unit of $Pa.s$.

Using Equation 1, the hydraulic aperture of the fracture can be evaluated from the measured injection rate and the stable injection pressure, together with other parameters that are considered constants for different fractures and the fluid (water). Typically, the hydraulic aperture was greater than the shim thickness (or mechanical aperture). There are several reasons for this. Some of them are the unevenness of the slab surfaces forming the two walls of the fracture, the seal on the surfaces of the shim between the slabs and tightness of the bolts cramping the two slabs, although the bolts were tightened with a nominal constant torque for different fracture samples.

The hydraulic aperture derived based on Equation 1 will be presented together with the sealant injection results.

Sealant injection

Class G slurry injection

A total of 5 Class G cement slurry injection tests was carried out with fracture aperture (shim thickness) ranged from approximately $250\mu m$ to $650\mu m$. Only one meaningful water injection result with a hydraulic aperture of $281\mu m$ was obtained for a fracture with an aperture of $250\mu m$. To prevent potential nozzle blockage of the injection syringe by cement particles, the nozzle diameter was enlarged to approximately 3mm in diameter from the original hole of approximately 1mm in diameter.

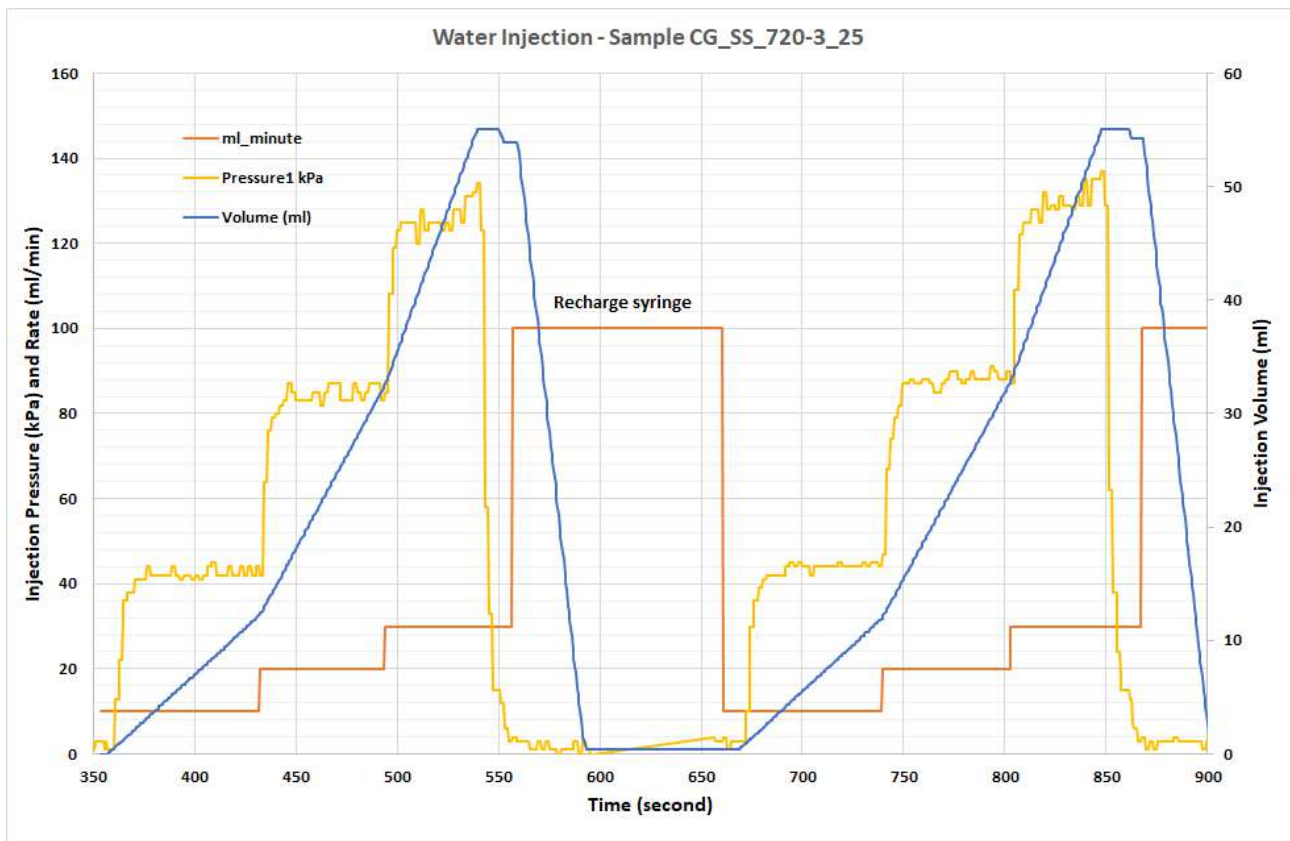


Figure 3-6 Measured parameters vs time for a typical water injection test. The fracture aperture is $25\mu\text{m}$ based on shim thickness, the hydraulic aperture is estimated to be $68\mu\text{m}$.

Slurry injection results are presented as curves of injection pressure vs injection volume as shown in Figure 3-7. The hydraulic apertures and observation from the injection tests are presented in Table 3-2. The complete results, including injection pressure, rate, force, and volume for individual injection tests are given in Appendix C. Major observations from the Class G cement slurry injection tests are

- The Class G cement slurry with a water cement ratio of 0.45 was unable to be injected into a fracture with a $250\mu\text{m}$ aperture formed by PMMA slabs. The blockage started from the slurry injection point into the fracture;
- The slurry flow was also blocked at the injection point into a fracture with an aperture of $350\mu\text{m}$. The fracture was formed by PMMA and siltstone slabs. However, if the fracture was formed by two PMMA slabs, the slurry was able to be injected into and flow through the fracture with the same aperture size. The reason is probably due to the filtrate loss of the slurry through the porous siltstone slab, such that the slurry became thicker within the fracture. Furthermore, the unevenness on the siltstone slab surface may also promote blockage to the slurry flow;
- Injection pressure fluctuation was observed when the injection rate was high or the slabs forming the fracture had a less smooth surface in comparison with PMMA. The injection pressure fluctuation indicated the process of blockage formation and breakdown in the slurry injection system, most likely within the fracture since it was the narrowest flow path of the entire slurry injection system.

Furthermore, unlike the water injection tests, all the cement slurry injection tests did not reach a steady state, i.e., a constant injection pressure for a constant injection rate.

It may be concluded from the observation above that the minimum fracture aperture into which the conventional Class G cement slurry can penetrate is approximately 350µm, consistent with that reported in literature (Wu et al, 2020).

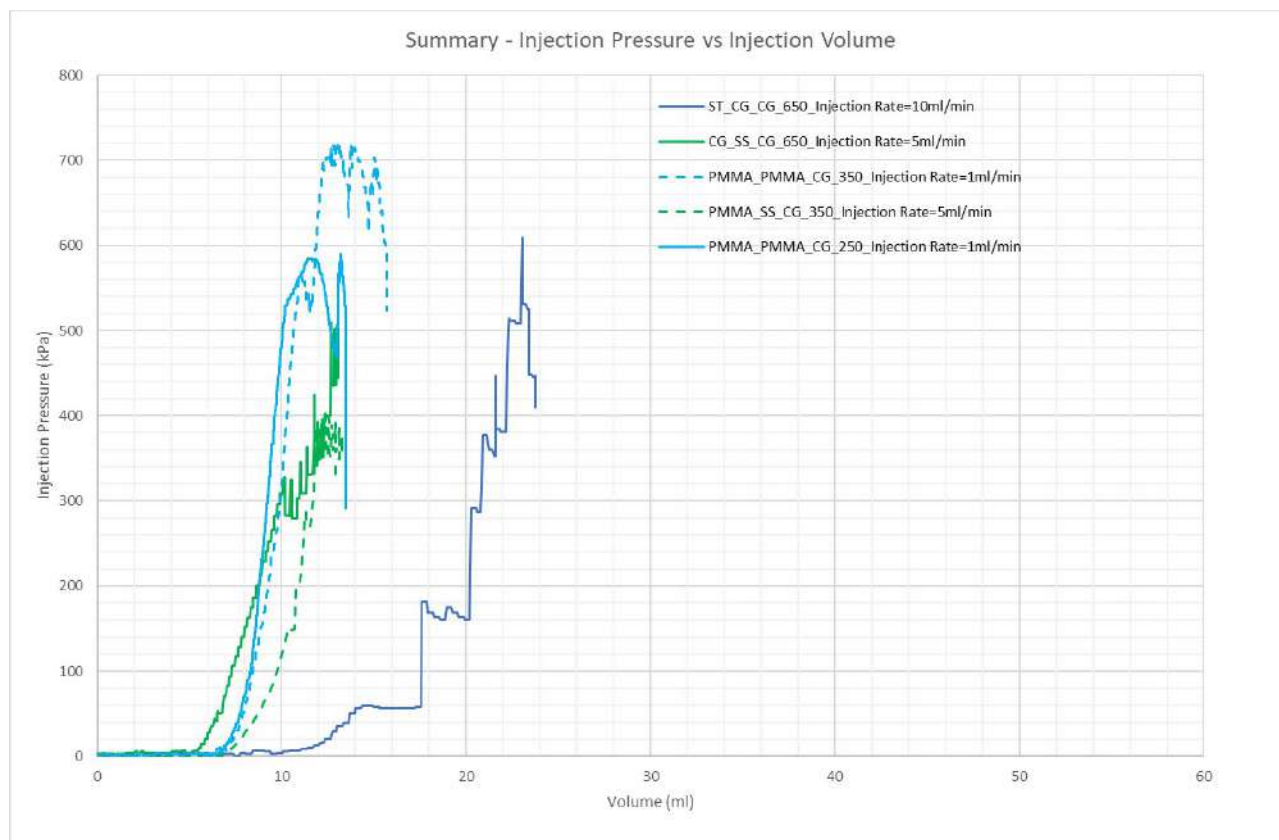


Figure 3-7. Summary of cement slurry injection. Injection pressure vs volume.

Table 3-2. Summary of observations on cement slurry injection

SAMPLE NAME*	FRACTURE APERTURE (MICRON)	HYDRAULIC APERTURE (MICRON)	INJECTION RATE (ML/MIN)	OBSERVATION
ST_CG_CG_650	650		10	Flow through
CG_SS_CG_650	650		5	Flow through
PMMA_SS_CG_350	350		5	Blocked at fracture mouth
PMMA_PMMA_CG_350	350		1	Flow through
PMMA_PMMA_CG_250	250	281	1	Blocked at fracture mouth

*- the sample name is coded as “fracture wall1_fracture wall2_sealant_fracture aperture”; ST – Steel, CG – Class G, SS - Siltstone

Geopolymer slurry injection

As discussed in Section 2.1, two compositions of geopolymer slurry were tested in this project, namely, GP1 (Geopolymer 1) and GP2 (Geopolymer 2). A total of 9 geopolymer slurry injection

tests were carried out, 4 for GP1 and 5 for GP2. For both compositions, the liquid (mixture of KOH and Kasil226) to solid (Metastar501) ratio was kept to 1.9. The fracture apertures ranged from approximately 25 μm to 350 μm . Hydraulic apertures were derived from water injection tests prior to slurry injection for the fractures with a shim thickness less than 150 μm . A constant slurry injection rate of 1ml/min was adopted for majority of the slurry injection tests.

The slurry injection test results are presented as injection pressure vs injection volume curves for GP1 and GP2 in Figure 3-8 and Figure 3-9 respectively, and the observations summarised in Table 3-3 and Table 3-4 respectively. The complete results, including injection pressure, rate, force, and volume for each injection tests are presented in Appendix C.

Major observations from the geopolymer slurry injection tests are

- The geopolymer slurry with a liquid to solid ratio of 1.9 by weight (GP2) was unable to be injected into a planar fracture with an aperture of 25 μm . The blockage started from the slurry injection point into the fracture;
- The injection into the fracture with an aperture of 50 μm was also difficult with a rapid increase in injection pressure at a constant injection rate, as evidenced from the injection pressure vs injection slurry volume plot in Figure 3-9;
- Similar to the cement slurry injection tests, all the geopolymer slurry injection tests did not reach a steady state, i.e., a constant injection pressure for a constant injection rate.

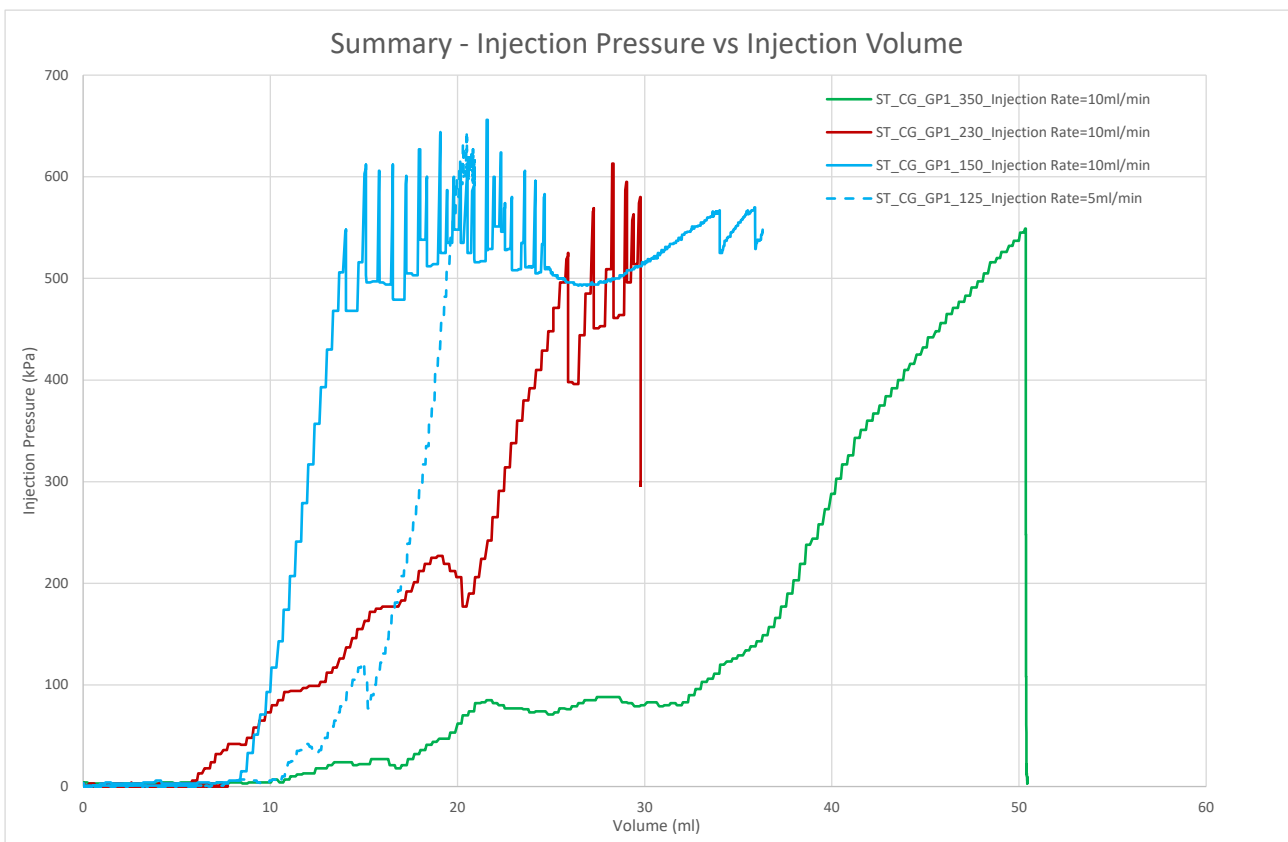


Figure 3-8 Summary of GP1 slurry injection. Injection pressure vs injection volume.

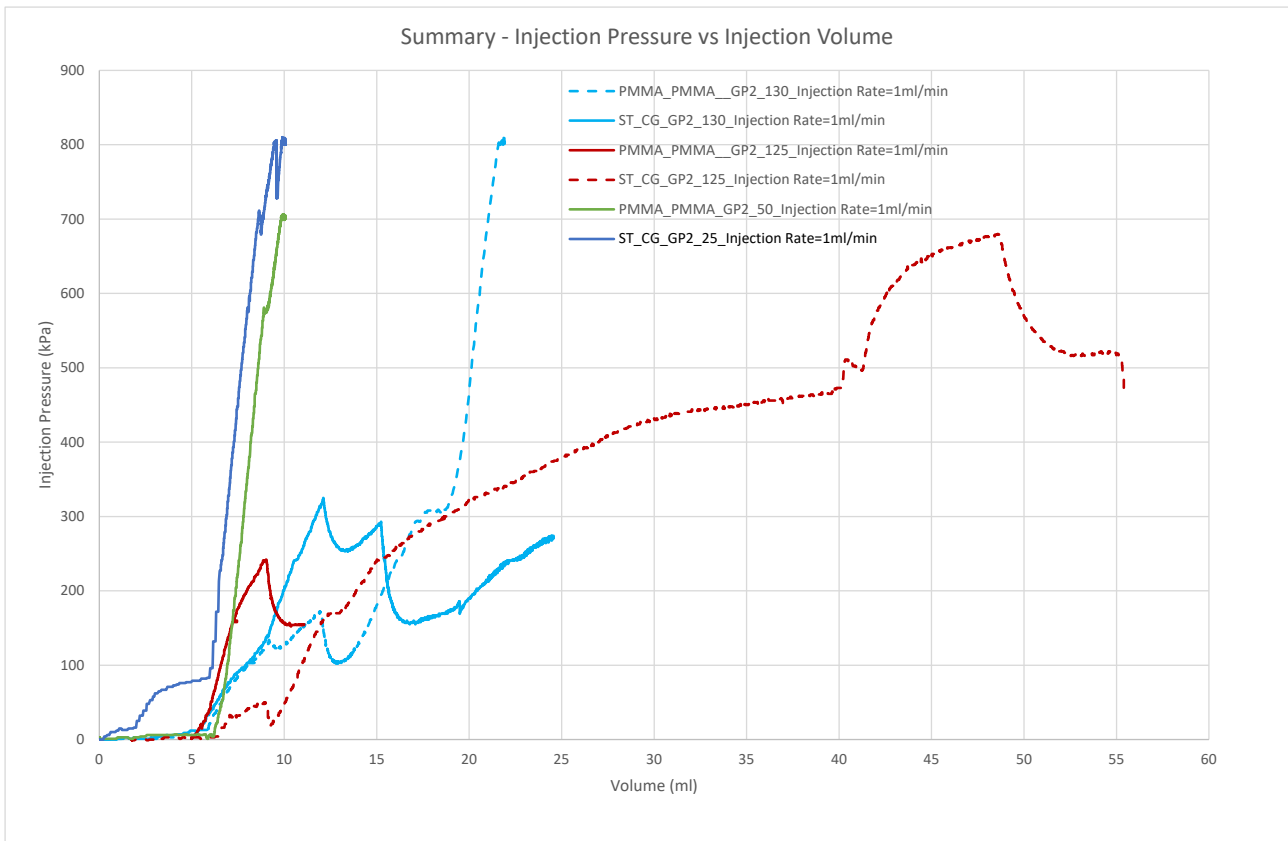


Figure 3-9 Summary of GP2 slurry injection. Injection pressure vs injection volume.

Table 3-3. Summary of observations on GP1 slurry injection

SAMPLE NAME*	FRACTURE APERTURE (MICRON)	HYDRAULIC APERTURE (MICRON)	INJECTION RATE (ML/MIN)	OBSERVATION
ST_CG_GP1_125	125	167	5	Flow through
ST_CG_GP1_150	150		10	Flow through
ST_CG_GP1_230	230		10	Flow through
ST_CG_GP1_350	350		10	Flow through

*- the sample name is coded as “fracture wall1_fracture wall2_sealant_fracture aperture”; ST – Steel, CG – Class G, SS - Siltstone

Table 3-4. Summary of observations on GP2 slurry injection

SAMPLE NAME*	FRACTURE APERTURE (MICRON)	HYDRAULIC APERTURE (MICRON)	INJECTION RATE (ML/MIN)	OBSERVATION
ST_CG_GP2_25	25	68	1	Blocked close to injection point
PMMA_PMMA_GP2_50	50	125	1	Flow through
PMMA_PMMA_GP2_125	125	132	1	Flow through
ST_CG_GP2_125	125	123	1	Flow through
ST_CG_GP2_130	130	190	1	Flow through

*- the sample name is coded as “fracture wall1_fracture wall2_sealant_fracture aperture”; ST – Steel, CG – Class G, SS - Siltstone

Polymer Resin 620-1 and 620-5 injection

Three compositions of polymer resins were evaluated for their injectivity into planar fractures, namely, 010620-1, 010620-5 and 020720-3 (or 620-1, 620-5 and 720-3 for short). The difference between the compositions is the components used as the diluter to reduce the viscosity of the base polymer resins.

The injection tests for the first two compositions, i.e., 620-1 and 620-5, were conducted at room temperature. The components with the required weights were mixed in a plastic container. Care was taken to minimize the amount of air trapped in the mixture while mixing. The fully mixed mixture was then placed in a vacuum chamber and a full vacuum was applied for at least 30 minutes at room temperature. The mixture was then transferred to a plastic syringe prior to the injection test.

Water injection was conducted at several constant rates prior to polymer resin injection to evaluate hydraulic aperture and fill up the fracture with water. The fracture sample was placed vertically and the polymer resin injection point was close to the bottom end of the fracture (Figure 3-4). This setup has the potential to maximize the displacement of water by the polymer resin inside the fracture.

A constant injection rate of 1ml/min or 2ml/min was adopted for most of the polymer resin injection tests. Prior to the polymer resin reaching the injection point, the injection was conducted at a higher rate to fill up the flexible nylon tubing. The volume of the polymer resin injected for each test ranged from 10ml to 30ml, far exceeding the fracture volumes. Following injection tests, all the fracture samples were placed vertically in the hot water bath to cure for at least 24 hours and continue to cure at room temperature for several days.

The summary plots of injection pressure versus injection volume curves for polymer resins 620-1 and 620-5 are presented in Figure 3-10 and Figure 3-11 respectively. The test conditions and observations for each test are presented in Table 3-5 and Table 3-6. The complete results including injection pressure, rate, force, and volume for individual injection tests are presented in Appendix C.

Polymer resin 720-3 injection

It was observed from the fracture surface after opening up the fracture samples following the shear bonding strength testing (Section 5) that a complete seal of the fracture by polymer resins 620-1 and 620-5 was not achieved, probably due to the incomplete displacement of water from the fracture by the polymer resin. Since polymer resin and water are immiscible and the former has a much higher viscosity than water, the polymer resin would flow along the path with minimum resistance within a fracture. This would leave the water in some areas with a smaller aperture to be by-passed and potentially forming leaking pathways to gas. Reducing viscosity of the polymer resin would allow it to reach areas with smaller aperture and therefore improve its sealing effectiveness.

Based on the observation from polymer resins 620-1 and 620-5 injection tests, some of the injection tests for polymer resin 720-3 were conducted at elevated temperature of 70°C. For such an injection test, the entire fracture sample was emersed in the hot water bath at 70°C and set up vertically (Figure 3-12). The syringe containing the polymer resin 720-3 was heated to 70°C in the hot water bath prior to injection and maintained at the elevated temperature during the injection.

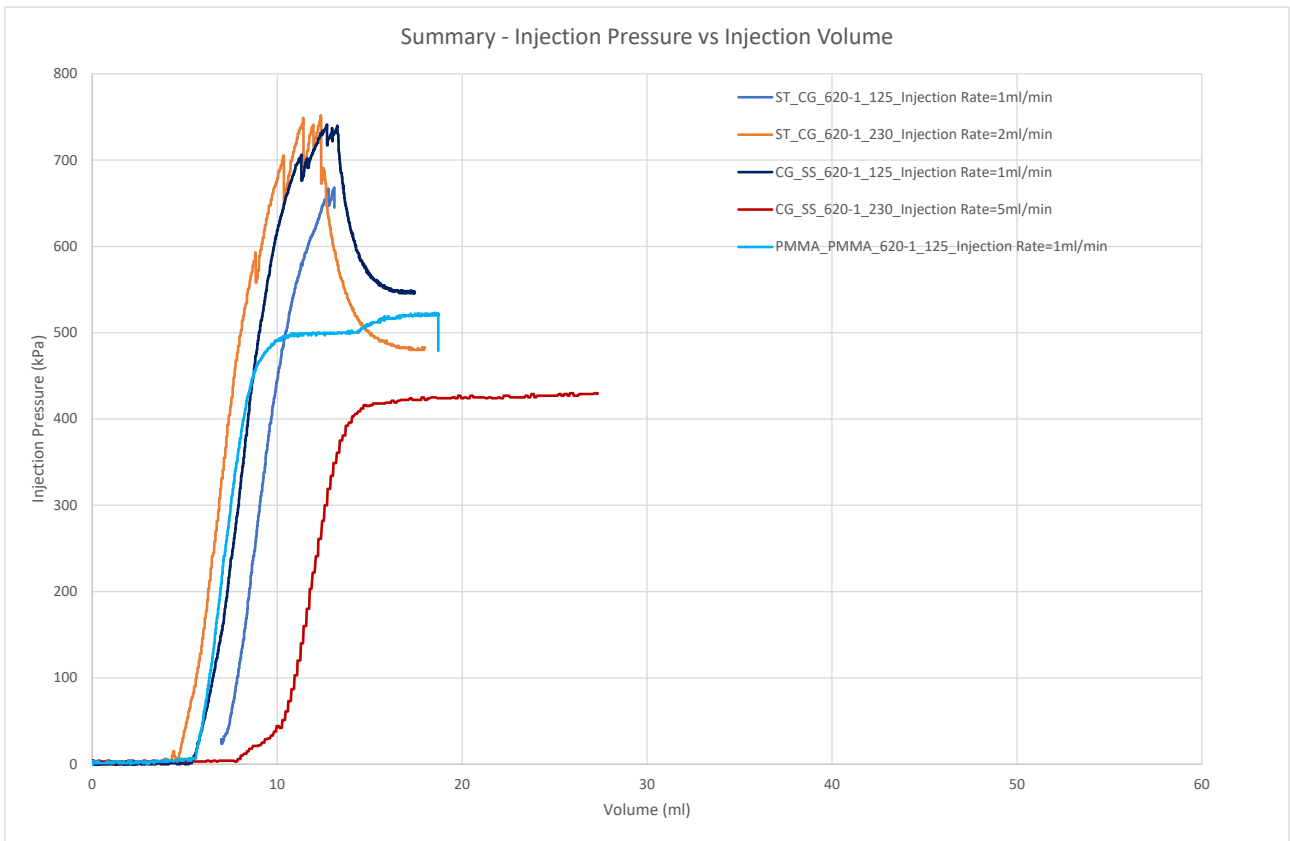


Figure 3-10. Summary of polymer resin 620-1 injection tests. Injection pressure vs injection volume

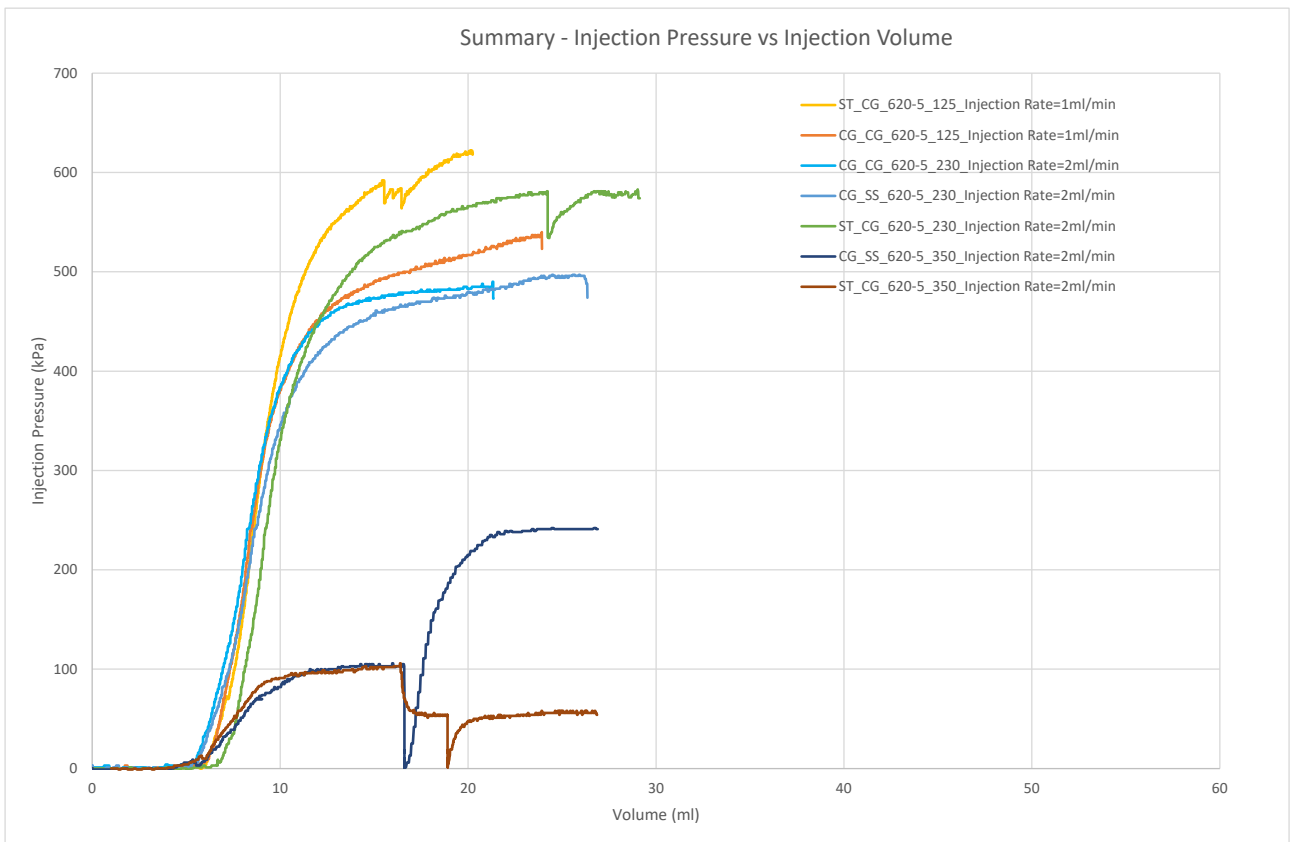


Figure 3-11 Summary of polymer resin 620-5 injection tests. Injection pressure vs injection volume.

Table 3-5. Summary of observations on polymer resin 620-1 injection

SAMPLE NAME	FRACTURE APERTURE (MICRON)	HYDRAULIC APERTURE (MICRON)	INJECTION RATE (ML/MIN)	OBSERVATION
CG_SS_620-1_125	125	132	1	Flow through
ST_CG_620-1_125	125	127	1	Flow through
ST_CG_620-1_230	230	198	2	Flow through
CG_SS_620-1_230	230	-	5	Flow through
PMMA_PMMA_620-1_125	125	144	1	Flow through

Table 3-6. Summary of observations on polymer resin 620-5 injection

SAMPLE NAME	FRACTURE APERTURE (MICRON)	HYDRAULIC APERTURE (MICRON)	INJECTION RATE (ML/MIN)	OBSERVATION
CG_CG_620-5_125	125	143	1	Flow through
CG_SS_620-5_125	125	142	1	Flow through
ST_CG_620-5_125	125	150	1	Flow through
CG_CG_620-5_230	230	242	2	Flow through
CG_SS_620-5_230	230	190	5	Flow through
ST_CG_620-5_230	230	223	2	Flow through
CG_SS_620-5_350	350	-	2	Flow through
ST_CG_620-5_230	350	-	2	Flow through

Furthermore, a commercially available solid-free water-based primer and bonding agent (ARDEX P51, Appendix D) was used as a pre-flush fluid for the polymer resin 720-3. The primer, diluted with water with a ratio of 1 to 3, was injected into the fracture prior to the polymer injection. The objective was to evaluate if the primer and bonding agent would improve the sealability and bonding strength of the polymer resin.

The procedure for the polymer resin 720-3 injection at elevated temperature was slightly different from that for the polymer resins 620-1 and 620-5. Following visual observation of the polymer resin flowing out of the fracture from the open end of the fracture sample, variety of injection rates was applied. This included stopping for a short period of polymer resin injection and then re-starting the injection. This would allow the heavier polymer resin to move downwards and settle at the lower part of the fracture and the lighter water to move upwards if any water was trapped in the polymer resin. Further injection of polymer resin would displace more water from the fracture, therefore improving the sealing effectiveness and the fracture bonding strength.

The summary plot of injection pressure versus injection volume curves for polymer resin 720-3 is presented in Figure 3-13. The test conditions and observations for each test are presented Table 3-7. Complete results including injection pressure, rate, force, and volume for individual injection tests are presented in Appendix C.

The major observations from all the polymer resin injection tests are

- The specially formulated polymer resin 720-3 was able to penetrate planar fractures with an aperture as narrow as 25 μm under an elevated temperature of 70 $^{\circ}\text{C}$;
- All the three polymer resins were able to penetrate planar fractures with an aperture greater than 125 μm at room temperature; and
- For some of the injection tests for polymer resins 620-1 and 620-5, a steady state of polymer resin flow was achieved, i.e., for a constant injection rate, a constant injection pressure was obtained.

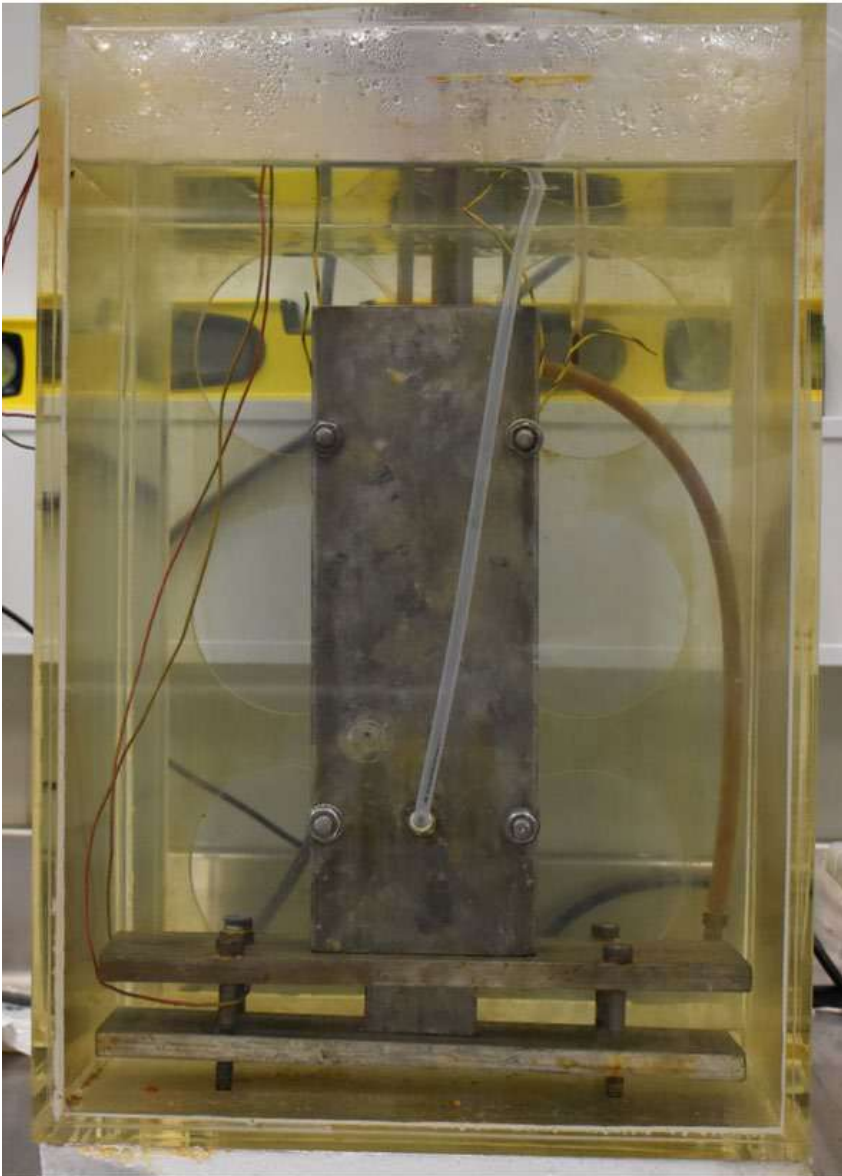


Figure 3-12 Photo of a fracture sample set up in hot water bath

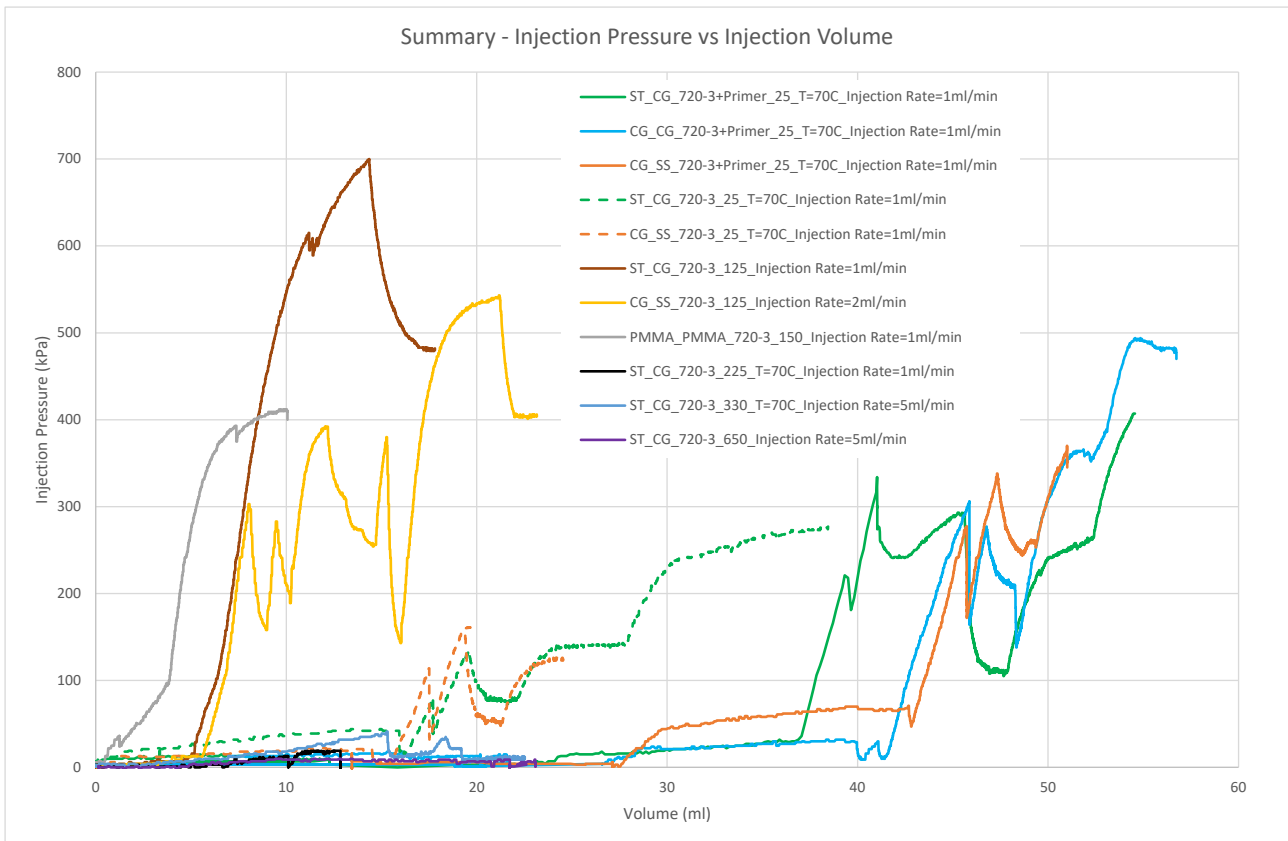


Figure 3-13 Summary of polymer resin 720-3 injection tests. Injection pressure and injection volume.

Table 3-7. Summary of observations on polymer resin 720-3 injection

SAMPLE NAME	PRIMER	TEMPERATURE (DEG C)	FRACTURE APERTURE (MICRON)	HYDRAULIC APERTURE (MICRON)	INJECTION RATE (ML/MIN)	OBSERVATION
ST_CG_720-3_25_T=70C		70	25	50	1	Flow through
ST_CG_720-3+Primer_25_T=70C	Primer	70	25	76	1	Flow through
CG_CG_720_3+Primer_25_T=70C	Primer	70	25	82	1	Flow through
CG_SS_720-3_25_T=70C		70	25	83	1	Flow through
CG_SS_720-3+Primer_25_T=70C	Primer	70	25	66	1	Flow through
ST_CG_720-3_225_T=70C		70	225	230	1	Flow through
CG_SS_720-3_125			125	128	1	Flow through
ST_CG_720-3_125			125	133	2	Flow through
ST_CG_720-3_650			650		5	Flow through
ST_CG_720-3_330_T=70C		70	330		5	Flow through
PMMA/PMMA_720-3_350			350		2	Flow through
PMMA/PMMA_720-3_150			150	150	1	Flow through

4 FRACTURE SEALING PERFORMANCE EVALUATION

4.1 Testing apparatus

The effectiveness of the sealant materials in sealing synthetic planar fracture to gas leakage was assessed after the sealant was cured. A fit-for-purpose testing apparatus was set up for fracture sealing performance evaluation. As shown in Figure 4-1, the apparatus consists of a gas cylinder with a volume of 1000 cm³, two ball valves, two pressure transducers, a gas pressure regulator and a pressure gauge. The fracture sample was connected to the test apparatus using a flexible nylon tube, which was kept as short as possible to reduce the volume between the gas cylinder and the fracture injection point. Prior to connecting to the test apparatus, the injection hole in the fracture sample was cleaned by drilling out the cured sealant material deposited in the injection hole.

The work principle of the testing apparatus is similar to that for the unsteady state permeameter developed by Jones (1972). The procedures for performing a sealability test were as follows

- The ball valve V2 was closed and the ball valve V1 was open, the gas cylinder was charged with workshop compressed air to an initial pressure (500kPa to 700kPa) via a quick fitting. The gas pressure could be regular if required;
- The ball valve V1 was closed and the source of the compressed air was disconnected from the apparatus. The gas pressure in the cylinder was monitored with time using PT1 for a period of time to ensure gas tightness of the testing apparatus; and
- When a constant gas pressure was achieved, the ball valve V2 was fully open. The pressure changes with time for both PT1 and PT2 together with the room temperature were recorded.

If the fracture was not completely sealed with the cured sealant material, the compressed air would flow (leak) through the fracture and the gas pressure in the cylinder would decline with time, rapidly at first and getting more and more slowly. The fracture sample was immersed under water in a plastic container to identify leaking location if complete seal was not achieved for the fracture sample.

4.2 Gas flow in planar fractures

Assuming a Darcy flow in a porous rock core sample, Jones (1972) derived a relationship between the rate of pressure declination and the permeability of the rock core sample using an unsteady state permeameter as follows

$$\frac{-V_t[1+\delta G(c)]}{p_0(t)} \left[\frac{dp_0(t)}{dt} \right] = \frac{k_l A}{29,390 \mu L} [p_0(t) + 2(p_a + b)] \quad (2)$$

where V_t is the volume of the gas cylinder in cm³, δ is a constant equal to 2/3 of the ratio of the pore volume of the core sample to the volume of the gas cylinder, $G(c)$ is related to a correction

factor accounting for non-constant mass flow rate, $p_0(t)$ is the gas pressure at upstream end surface of the core sample in psig, k_i is Klinkenberg or “liquid” permeability of the core sample in md, A and L are the cross section area in cm^2 and length of the core sample in cm, μ is the viscosity of the gas in cP, p_a is atmospheric pressure in psia, and b is Klinkenger slip factor in psi. Jones (1972) showed that since $G[c]$ has a value lies between 0.5 and 0.6 for the pressure of interest, the term $\delta G[c]$ in Equation 2 is very small, therefore could be negligible.

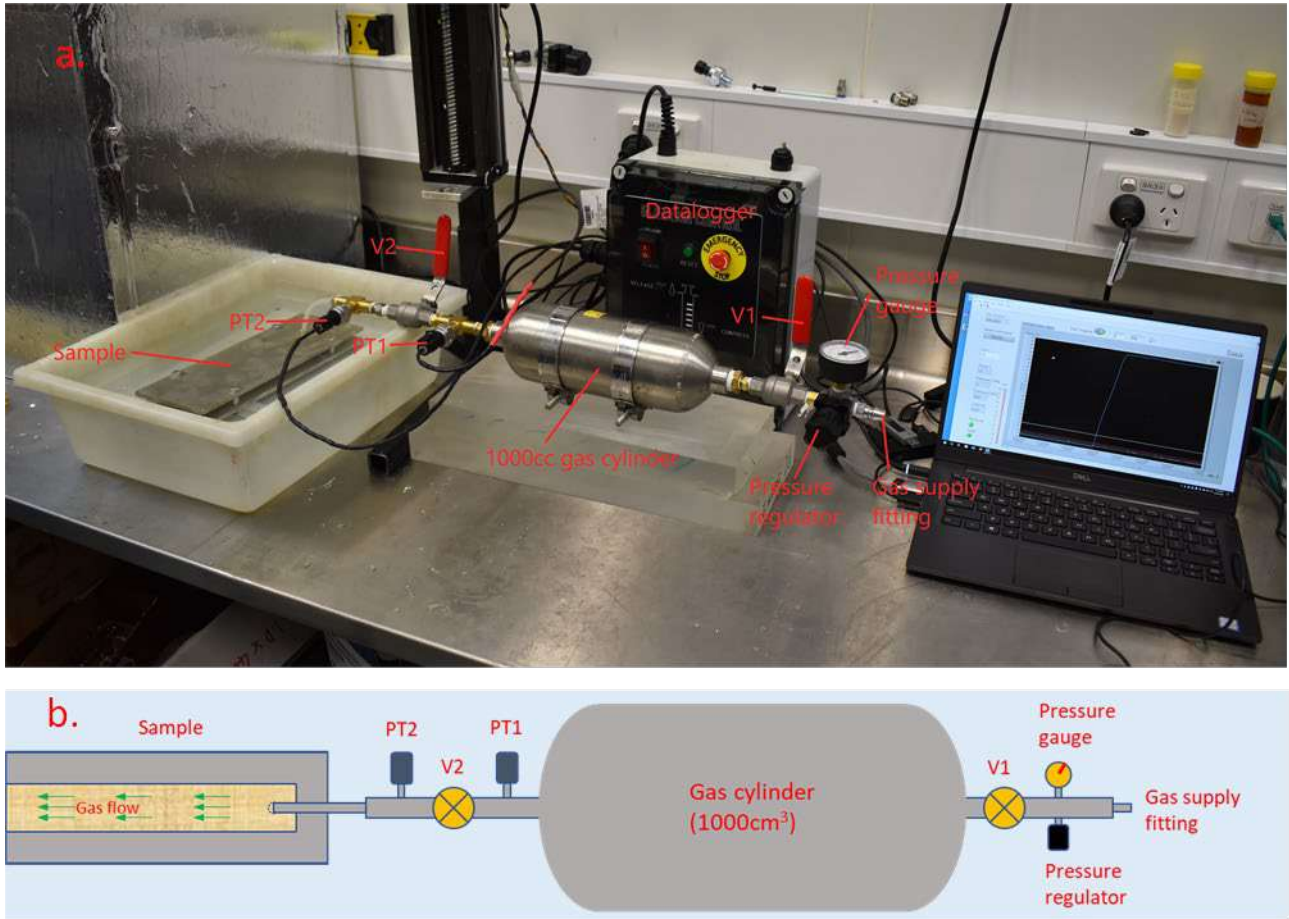


Figure 4-1 Testing apparatus for assessing fracture sealing performance, a). Photo of the testing set up, and b). Schematic of the apparatus

Inspection of Equation 2 shows that the instant slope of the pressure vs time curve at a given time t since the opening of the valve $V2$, $\frac{dp_0[t]}{dt}$, is related to the permeability of the rock core sample.

4.3 Results and analyses

Since it was observed from the sealability tests, the sealing behaviour for the planar fracture varied widely for different sealants, ranging from almost no seal to complete seal, there is no need to calculate exact values of permeability or conductivity for each planar fractures using Equation 2. Instead, the sealing behaviour is broadly categorized as complete seal, partial seal and no seal based on the initial slope of the pressure vs time curves, i.e.,

- Complete seal. Initial slope of the pressure vs time curve is equal to zero
- No seal. Initial slope of the pressure vs time curve is almost vertical

- Partial seal. Initial slope of the pressure vs time curves is between the complete seal and no seal.

The pressure vs time curves for all the sealability tests are presented in Figure 4-2 to Figure 4-7 and the observations on sealability are summarised in Table 4-1 to Table 4-6 for all the fracture sealing materials respectively. As shown, the effectiveness of sealing a planar fracture appears to be the lowest for polymer resin 620-1 and 620-5, followed by GP1, Class G and GP2. Note that in Figure 4-4 the result for the fracture sample ST_CG_GP2_130 is invalid, because the injection hole was blocked (tested sample photo in Figure 5-9 and Appendix C). The polymer resin 720-3 appears to be the most effective sealant among all the sealants tested in sealing the planar fractures. About half of the sealability tests have shown a complete seal while the rest shown a partial seal. The sealing mechanisms will be discussed further in Section 5.

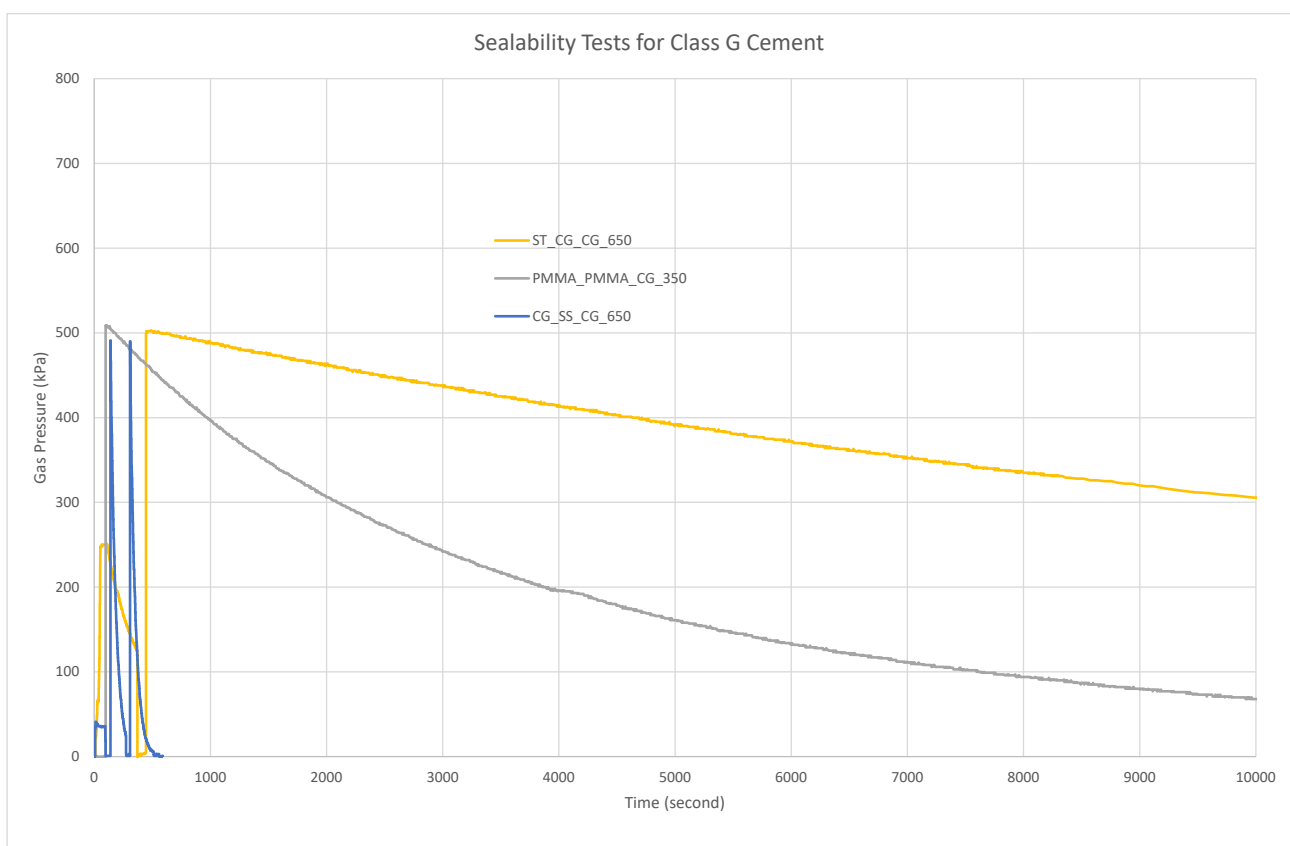


Figure 4-2 Gas pressure vs time for planar fractures sealed with Class G cement slurries

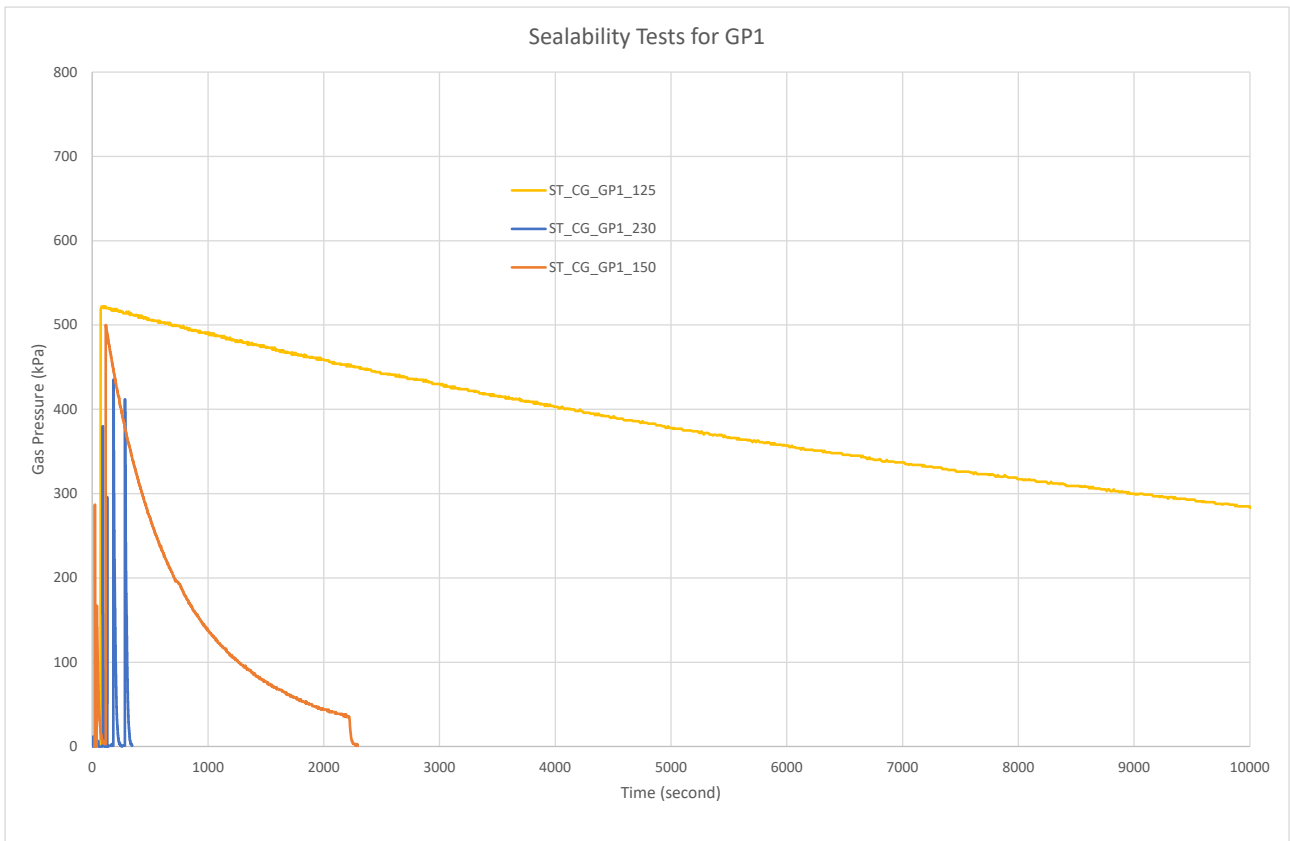


Figure 4-3. Gas pressure vs time for planar fractures sealed with geopolymer 1 slurries



Figure 4-4. Gas pressure vs time for planar fractures sealed with geopolymer 2 slurries

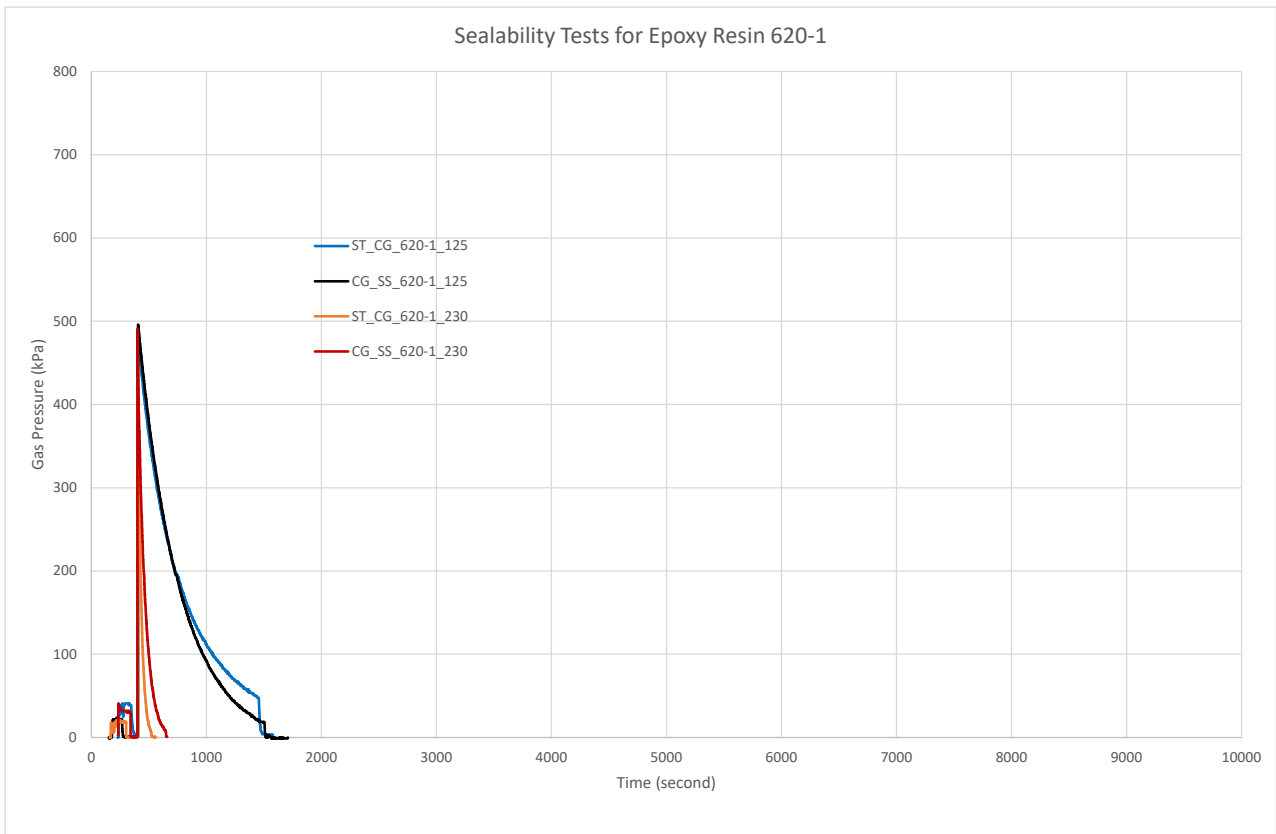


Figure 4-5. Gas pressure vs time for planar fractures sealed with polymer resin 620-1.

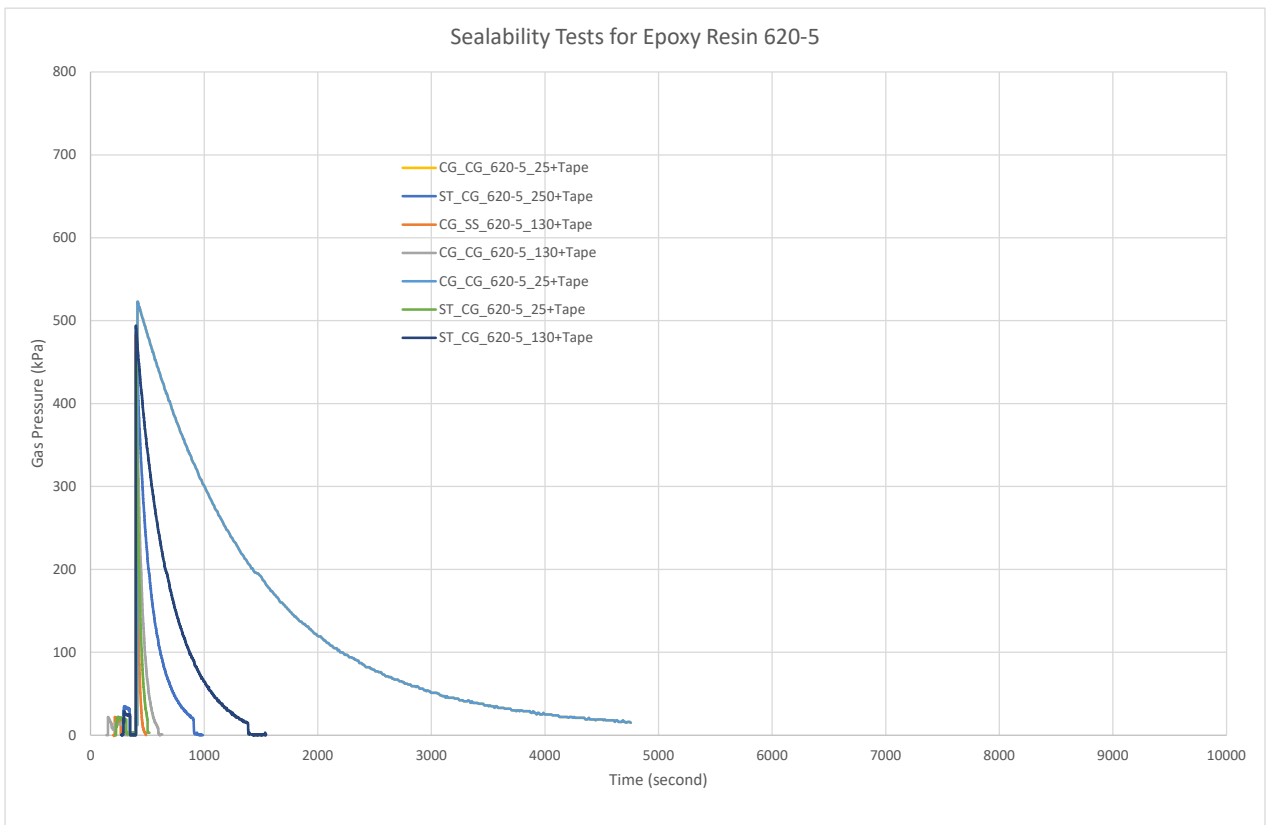


Figure 4-6. Gas pressure vs time for planar fractures sealed with polymer resin 620-5.

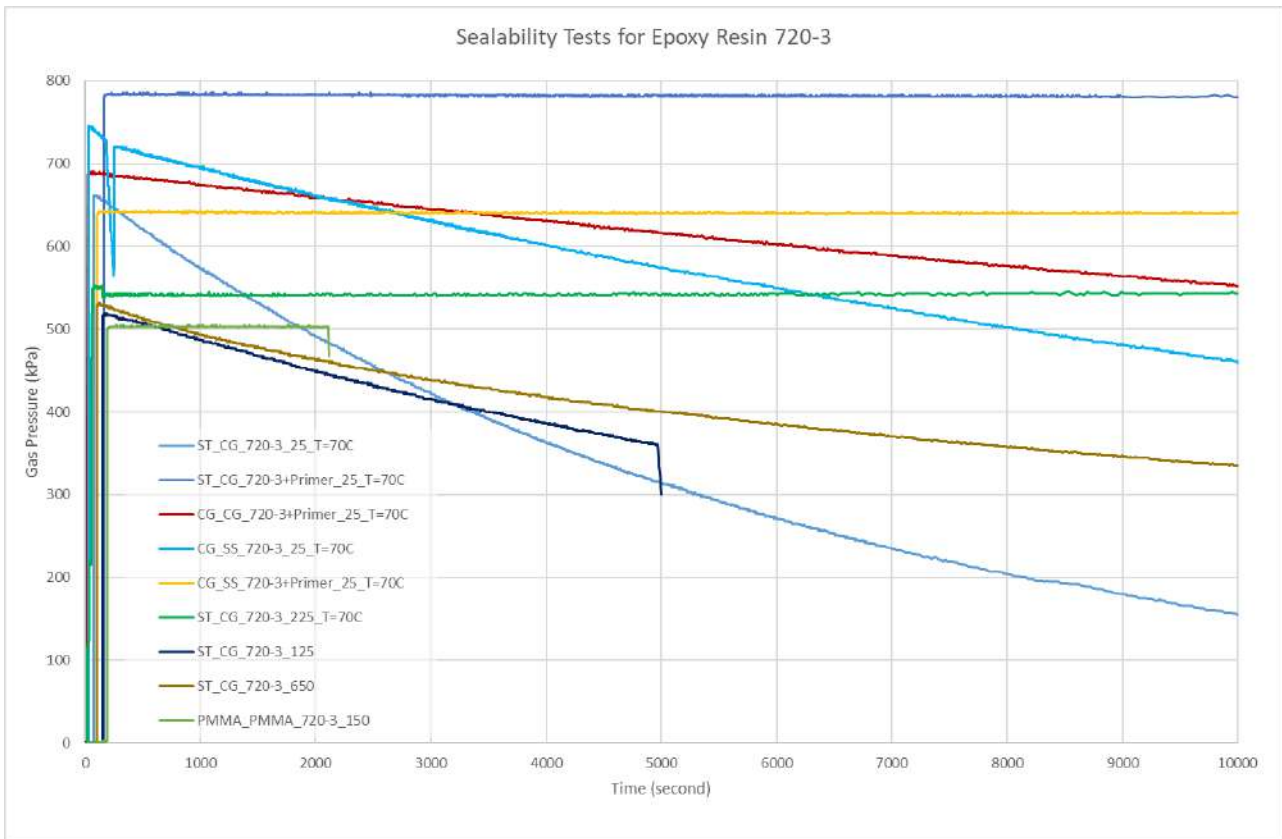


Figure 4-7. Gas pressure vs time for planar fractures sealed with polymer resin 720-3.

Table 4-1 Summary of observations on sealability for Class G cement

SAMPLE NAME	SHIM THICKNESS (MICRON)	HYDRAULIC APERTURE (MICRON)	SEALABILITY
ST_CG_CG_650	650		Partial seal
CG_SS_CG_650	650		Partial seal
PMMA_SS_CG_350	350		Not Tested
PMMA_PMMA_CG_350	350		Not Tested
PMMA_PMMA_CG_250	250	281	Not Tested

Table 4-2 Summary of observations on sealability for GP1

SAMPLE NAME	SHIM THICKNESS (MICRON)	HYDRAULIC APERTURE (MICRON)	SEALABILITY
ST_CG_GP1_125	125	167	Partial seal
ST_CG_GP1_150	150		Partial seal
ST_CG_GP1_230	230		No seal
ST_CG_GP1_350	350		Not tested

Table 4-3 Summary of observations on sealability for GP2

SAMPLE NAME	SHIM THICKNESS (MICRON)	HYDRAULIC APERTURE (MICRON)	SEALABILITY
ST_CG_GP2_25	25	68	Seal/partial seal
PMMA_PMMA_GP2_50	50	125	Not tested
PMMA_PMMA_GP2_125	125	132	Not tested
ST_CG_GP2_125	125	123	Almost no seal
ST_CG_GP2_130	130	190	Inconclusive, injection hole blocked

Table 4-4 Summary of observations on sealability for polymer resin 620-1

SAMPLE NAME	SHIM THICKNESS (MICRON)	HYDRAULIC APERTURE (MICRON)	SEALABILITY
CG_SS_620-1_125	125	132	Almost no seal
ST_CG_620-1_125	125	127	Almost no seal
ST_CG_620-1_230	230	198	Almost no seal
CG_SS_620-1_230	230	-	Almost no seal
PMMA_PMMA_620-1_125	125	144	Not tested

Table 4-5 Summary of observations on sealability for polymer resin 620-5

SAMPLE NAME	SHIM THICKNESS (MICRON)	HYDRAULIC APERTURE (MICRON)	SEALABILITY
CG_CG_620-5_125	125	143	Partial seal
CG_SS_620-5_125	125	142	No seal
ST_CG_620-5_125	125	150	No seal
CG_CG_620-5_230	230	242	No seal
CG_SS_620-5_230	230	190	No seal
ST_CG_620-5_230	230	223	Almost no seal
CG_SS_620-5_350	350	-	Almost no seal
ST_CG_620-5_230	350	-	Almost no seal

Table 4-6 Summary of observations on sealability for polymer resin 720-3

SAMPLE NAME	SHIM THICKNESS (MICRON)	HYDRAULIC APERTURE (MICRON)	SEALABILITY
ST_CG_720-3_25_T=70C	25	50	Partial seal
ST_CG_720-3+Primer_25_T=70C	25	76	Seal
CG_CG_720_3+Primer_25_T=70C	25	82	Partial seal
CG_SS_720-3_25_T=70C	25	83	Partial seal
CG_SS_720-3+Primer_25_T=70C	25	66	Seal

ST_CG_720-3_225_T=70C	225	230	Seal
CG_SS_720-3_125	125	128	Not tested
ST_CG_720-3_125	125	133	Partial seal
ST_CG_720-3_650	650		Partial seal
ST_CG_720-3_330_T=70C	330		Not tested
PMMA/PMMA_720-3_350	350		Not tested
PMMA/PMMA_720-3_150	150	150	Seal

5 BONDING STRENGTH PERFORMANCE EVALUATION

5.1 Direct shear strength testing apparatus and testing procedure

The bonding strength of the sealant materials with fracture walls, i.e., carbon steel casing, cement sheath and formation rock, is an important parameter in assessing the suitability of the sealant materials in sealing small fractures. A fit-for-purpose direct shear strength testing jig was designed and manufactured. The shear strength testing jig together with an Instron loading frame forms the shear bonding strength testing apparatus. The major advantage of the direct shear bonding strength testing jig is that it can test the full size fracture sample without having to re-sample to fit into a standard direct shear testing apparatus, hence, to maintain a zero to negligible disturbance to the fragile sealed fracture samples.

Figure 5-1 shows a schematic and photo of the direct shear strength testing apparatus. A sealed fracture sample was sandwiched between two stiff steel plates with adjustable supports. Two PTFE sheets were inserted between the fracture sample and the steel plate on the un-supported side of the sample to reduce the friction between the sample and the steel plate. The testing jig was held together by compressing 8 springs to a length of 61mm from their original lengths of 75mm at the free state. Each spring has a stiffness of 4.85N/mm, and the total force generated by 8 springs was approximately 540N, equivalent to a nominal normal stress of 40kPa applied to the fracture. As shown in Figure 5-1, the springs were loosely fitted on 8 threaded bolts inside the steel tubings which has a length of 60mm. Note that a 1mm gap was left between the tightening nuts and the end of steel tubings. The nominal normal stress was kept constant for all the direct shear strength tests. If required, the normal stress could be varied by compressing the springs to different lengths.

The assembled direct shear strength testing jig was then installed in the Instron loading frame. Care was taken to ensure the testing jig was accurately aligned with the Instron loading system. Direct shear strength testing was conducted by applying a constant displacement rate of approximately 0.3mm/min. At least 3mm shear displacement was applied to each test sample or until a nominal residual strength was observed.

Experiments were designed and performed to evaluate the frictional force between the PTFE sheets. It was found that the friction force between the PTFE sheets was approximately 100N. Note that to ensure a consistent frictional force was induced for each direct shear bonding strength test, no lubricant was applied to the PTFE sheets.

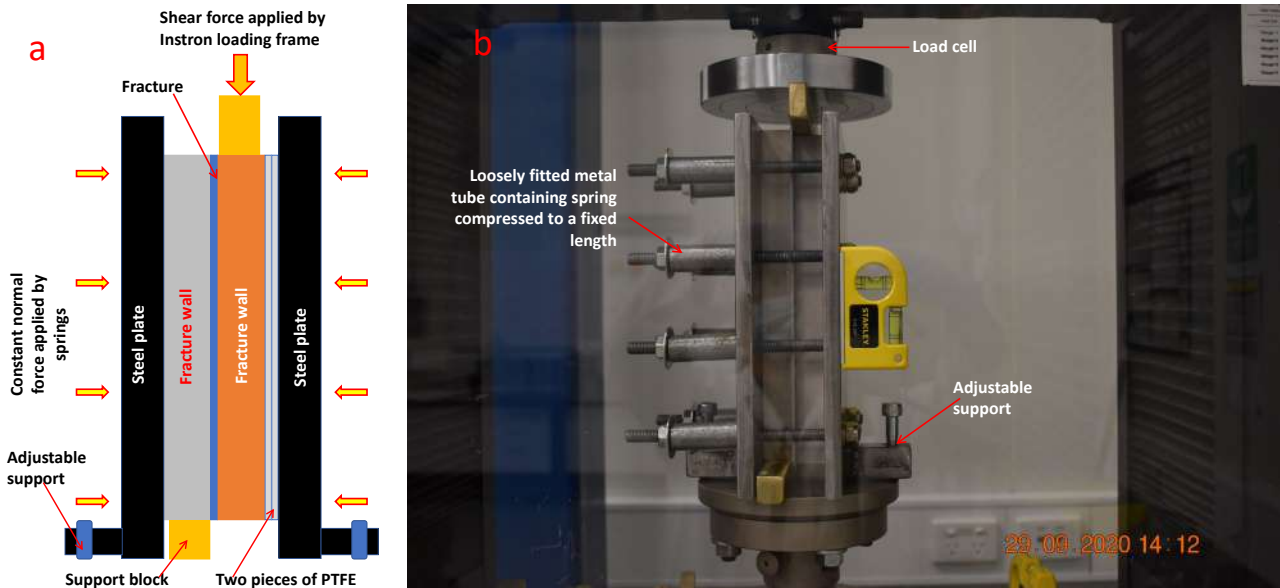


Figure 5-1 Shear bonding strength testing apparatus, a). Schematic of the shear strength testing jig, b). Photo of the testing jig installed in an Instron loading frame.

5.2 Results and analyses

The results of direct shear bonding strength tests are presented as the curves of shear force vs shear displacement. The curves are grouped in terms of sealant material type, and plotted in Figure 5-2 to Figure 5-7.

As shown in Figure 5-2 to Figure 5-7, the shear force shows a maximum (or peak) value before reaching a nominal constant value with shear displacement. The peak value is defined as the peak shear strength and the nominal constant value post-peak defined as residual strength. The peak shear strength is calculated from the peak shear force as

$$\sigma_s = \frac{F_p}{A} \quad (3)$$

where σ_s is the peak shear strength in MPa, F_p is peak shear force in N with deduction of the frictional force between the PTFE sheets, and A is the fracture area in mm^2 surrounded by the shim and is a constant for all the fractures (Figure 3-4a).

The peak shear bonding strengths derived based on Equation 3 for each test are summarised in Table 5-1 to Table 5-6. For the fractures sealed with Class G cement and geopolymers, the shear bonding strength is very low, ranging from 45kPa to 150kPa. In fact, two fracture samples sealed with GP1 were separated due to gravity during sample handling and set up for testing. The fractures sealed with Polymer Resins 620-1 and 620-5 have a slightly higher shear bonding strength, ranging below 100kPa to over 400kPa.

A significantly higher shear bonding strength is obtained for fractures sealed with Polymer Resin 720-3 injected at the simulated downhole temperature condition (70°C). Injection of the primer solution prior to the polymer resin injection increased the shear bonding strength further by a considerable amount. However, the fractures injected with the same polymer resin at room temperature have shear bonding strength similar to those of the other two polymer resins 620-1

and 620-5. Note that all the fracture samples once sealed (injected) with the sealants were cured in the hot water bath at 70°C for 24 to 48 hours and continued to cure under water at room temperature until tested for shear bonding strength, typically within a week.

The high shear bonding strength achieved for fracture samples sealed at the elevated temperature may be explained based on viscosity of the polymer resin and injection pressure. As shown in Section 2, the viscosity of the polymer resin 720-3 is significantly lower at 70°C than at room temperature (approximately 23 deg C), the polymer resin was able to penetrate into small apertures within the fracture and the small voids/spaces formed between the shim and fracture wall under an injection pressure similar to that for fracture samples sealed at room temperature. Despite the best effort in grinding the fracture wall slabs as smooth and flat as possible, small voids and unevenness on the fracture wall surface is unavoidable. These voids and apertures formed due to the surface unevenness may not be accessible when the viscosity of the polymer resin was high at room temperature although subject to an elevated injection pressure. Furthermore, for the fracture samples sealed at room temperature, the polymer viscosity within the fracture would decrease when placed into the hot water bath, however, no injection pressure would be applied, hence, some of the small voids and apertures would remain un-accessible to the polymer resin during curing.

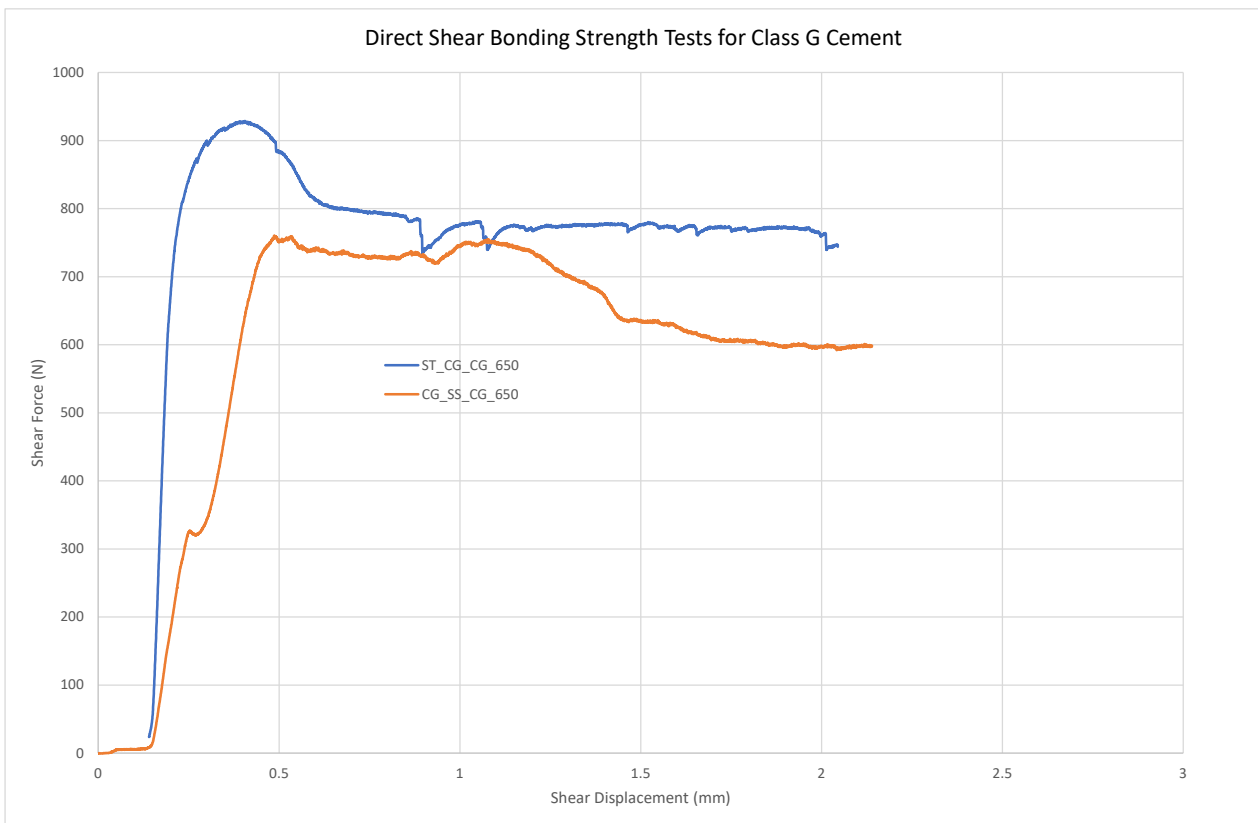


Figure 5-2 Shear force vs shear displacement curves for direct shear bonding strength tests for fractures sealed with Class G cement

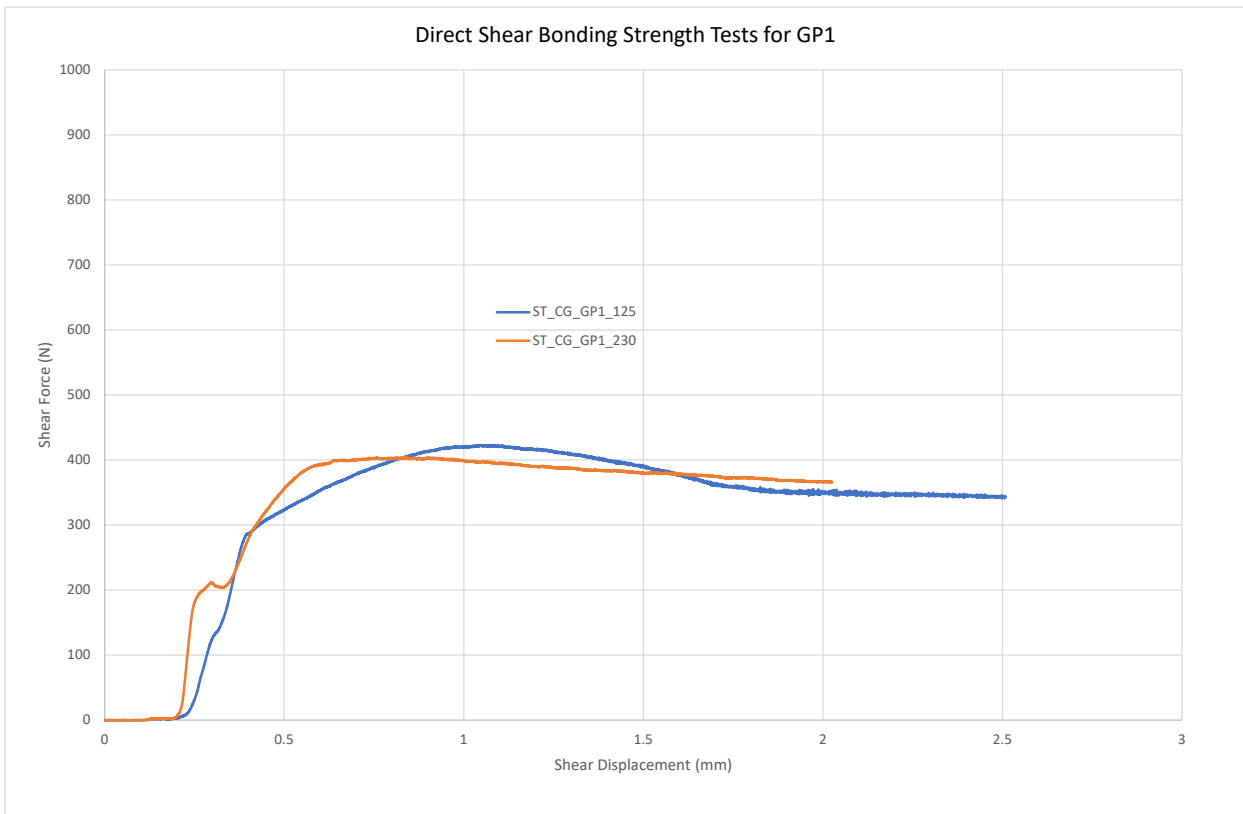


Figure 5-3 Shear force vs shear displacement curves for direct shear bonding strength tests on fractures sealed with GP1

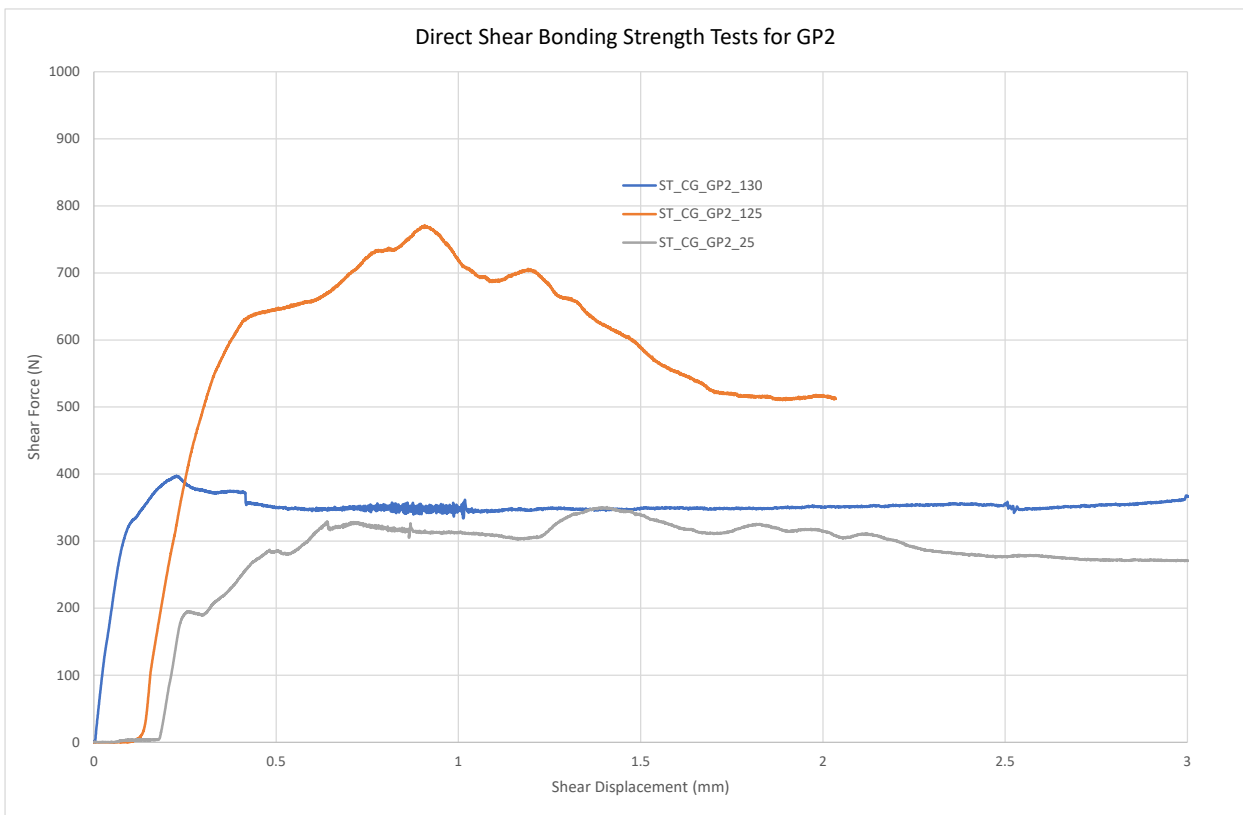


Figure 5-4 Shear force vs shear displacement curves for direct shear bonding strength tests for fractures sealed with GP2.

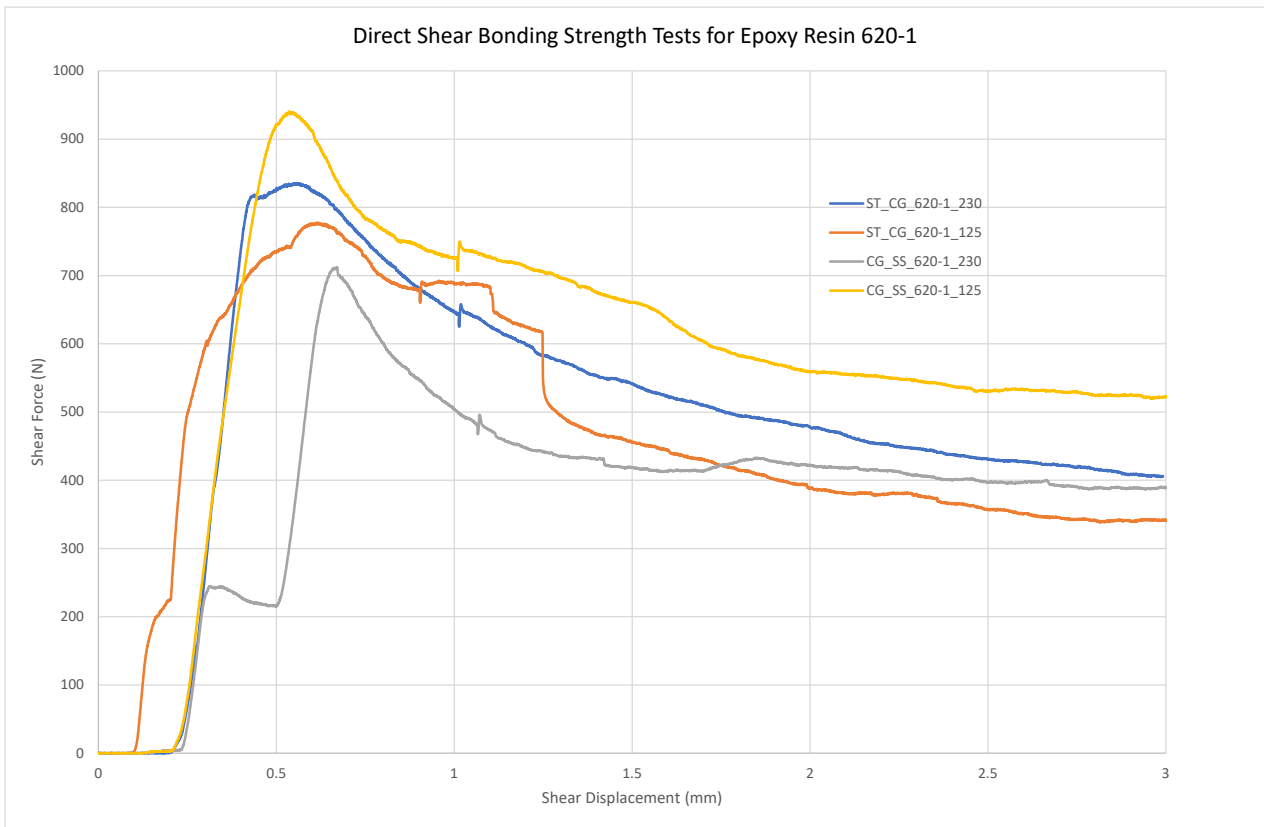


Figure 5-5 Shear force vs shear displacement curves for direct shear bonding strength tests for fractures sealed with Polymer Resin 620-1

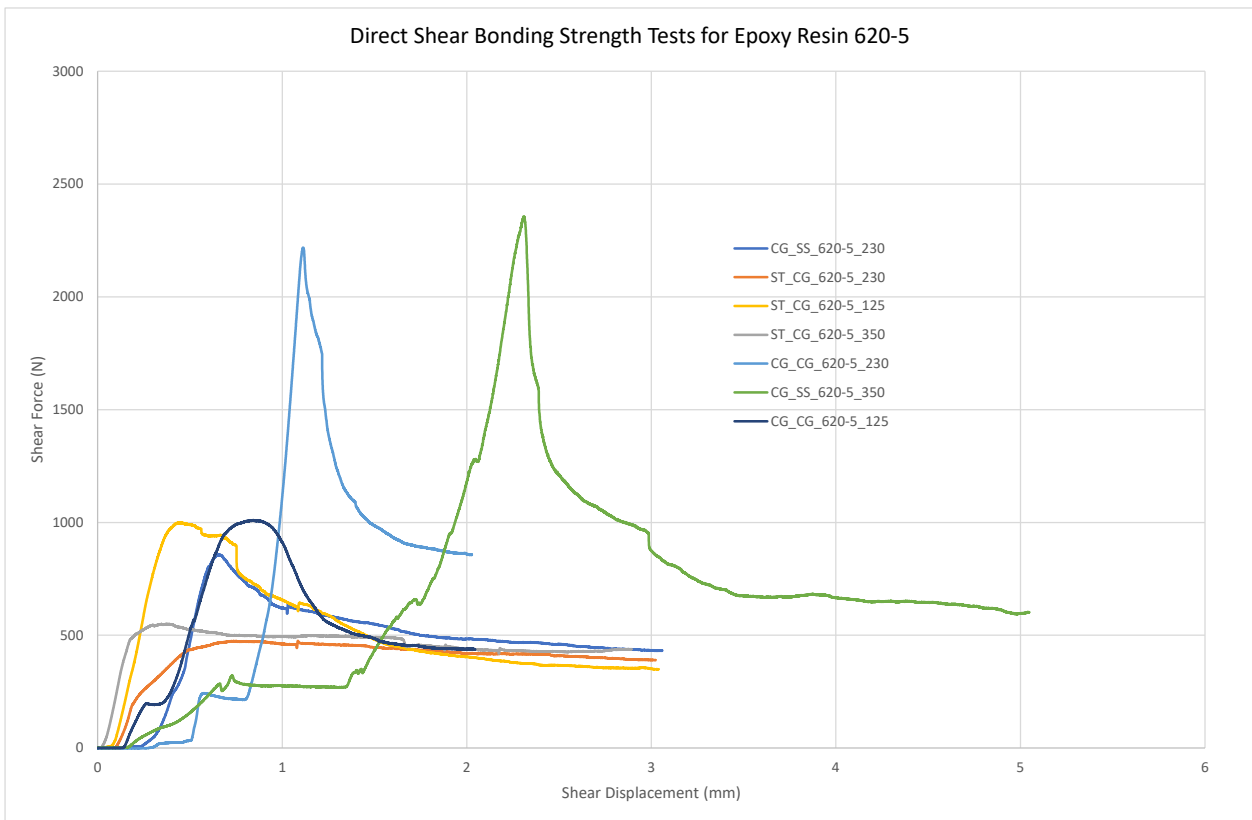


Figure 5-6 Shear force vs shear displacement curves for direct shear bonding strength tests for fractures sealed with Polymer Resin 620-5.

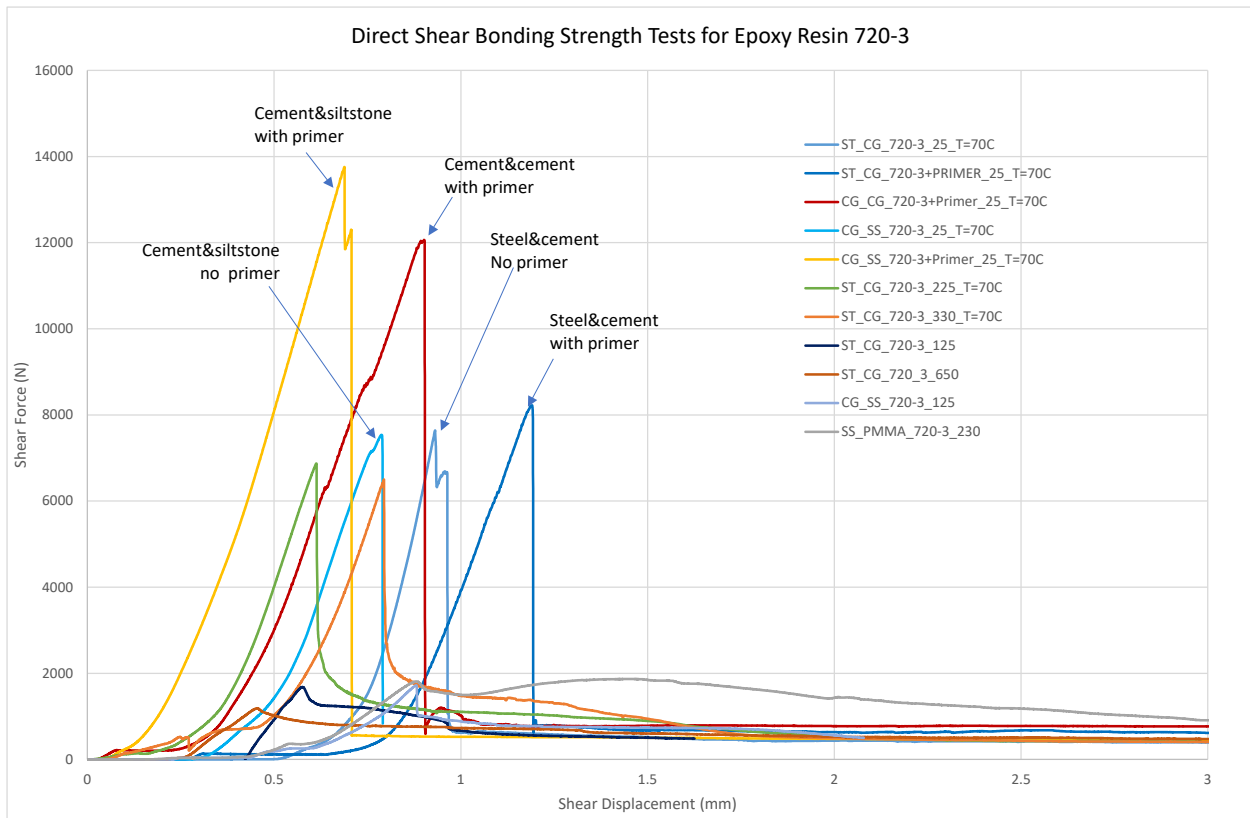


Figure 5-7 Shear force vs shear displacement curves for direct shear bonding strength tests for fractures sealed with Polymer Resin 720-3.

Table 5-1 Summary of direct shear bonding strength for Class G cement

SAMPLE NAME	SHIM THICKNESS (MICRON)	HYDRAULIC APERTURE (MICRON)	SHEAR BONDING STRENGTH (KPA)
ST_CG_CG_650	650		150
CG_SS_CG_650	650		120
PMMA_SS_CG_350	350		Not Tested
PMMA_PMMA_CG_350	350		Not Tested
PMMA_PMMA_CG_250	250	281	Not Tested

Table 5-2 Summary of direct shear bonding strength for GP1

SAMPLE NAME	SHIM THICKNESS (MICRON)	HYDRAULIC APERTURE (MICRON)	SHEAR BONDING STRENGTH (KPA)
ST_CG_GP1_125	125	167	59
ST_CG_GP1_150	150		Failure due to handling
ST_CG_GP1_230	230		55
ST_CG_GP1_350	350		Failure due to handling

Table 5-3 Summary of direct shear bonding strength for GP2

SAMPLE NAME	SHIM THICKNESS (MICRON)	HYDRAULIC APERTURE (MICRON)	SHEAR BONDING STRENGTH (KPA)
ST_CG_GP1_25	25	68	45
PMMA_PMMA_GP2_50	50	125	Not Tested
PMMA_PMMA_GP2_125	125	132	Not Tested
ST_CG_GP2_125	125	123	122
ST_CG_GP2_130	130	190	54

Table 5-4 Summary of direct shear bonding strength for polymer resin 620-1

SAMPLE NAME	SHIM THICKNESS (MICRON)	HYDRAULIC APERTURE (MICRON)	SHEAR BONDING STRENGTH (KPA)
CG_SS_620-1_125	125	132	152
ST_CG_620-1_125	125	127	123
ST_CG_620-1_230	230	198	134
CG_SS_620-1_230	230	-	111
PMMA_PMMA_620-1_125	125	144	Not tested

Table 5-5 Summary of direct shear bonding strength for polymer resin 620-5

SAMPLE NAME	SHIM THICKNESS (MICRON)	HYDRAULIC APERTURE (MICRON)	SHEAR BONDING STRENGTH (KPA)
CG_CG_620-5_125	125	143	165
CG_SS_620-5_125	125	142	
ST_CG_620-5_125	125	150	163
CG_CG_620-5_230	230	242	385
CG_SS_620-5_230	230	190	140
ST_CG_620-5_230	230	223	72
CG_SS_620-5_350	350	-	409
ST_CG_620-5_230	350	-	82

Table 5-6 Summary of direct shear bonding strength for polymer resin 720-3

SAMPLE NAME	SHIM THICKNESS (MICRON)	HYDRAULIC APERTURE (MICRON)	SHEAR BONDING STRENGTH (KPA)
ST_CG_720-3_25_T=70C	25	50	1370
ST_CG_720-3+Primer_25_T=70C	25	76	1476
CG_CG_720_3+Primer_25_T=70C	25	82	2175
CG_SS_720-3_25_T=70C	25	83	1352
CG_SS_720-3+Primer_25_T=70C	25	66	2483

ST_CG_720-3_225_T=70C	225	230	1231
CG_SS_720-3_125	125	128	284
ST_CG_720-3_125	125	133	287
ST_CG_720-3_650	650		198
ST_CG_720-3_330_T=70C	330		1164
PMMA/PMMA_720-3_350	350		Not tested
PMMA/PMMA_720-3_150	150	150	Cracks generated in PMMA

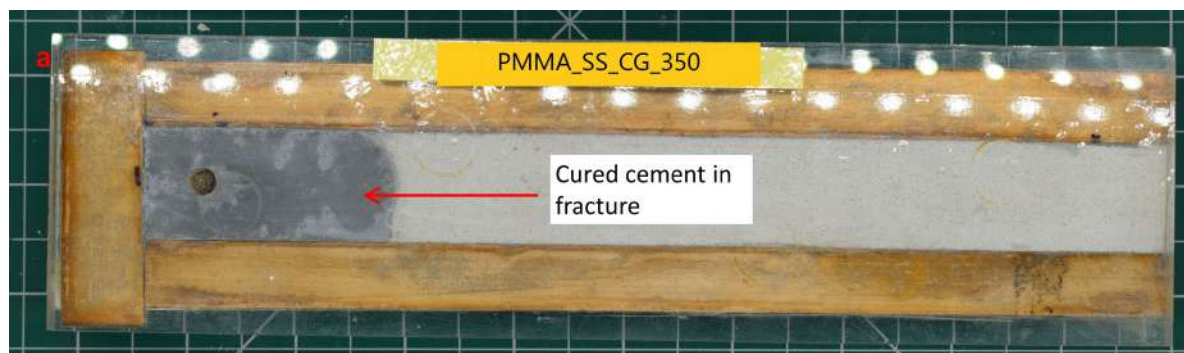
5.3 Fracture sealing – observations on fracture surfaces

Following the destructive direct shear bonding strength tests, the fracture samples were opened up and photos were taken. Photos for all the fracture samples are presented in Appendix C. Observation on deposition of the cured sealant materials on the fracture surface is useful in gaining a better understanding in terms of injectivity, sealability and bonding strength for different fracture sealing materials

5.3.1 Class G cement

Photos of two typical fracture samples sealed with Class G cement are presented in Figure 5-8. The apertures of the two fracture samples are 350 μ m (PMMA_SS_CG_350) and 650 μ m (ST_CG_CG_650) respectively. It was observed during the slurry injection tests, the cement slurry was able to penetrate into the smaller fracture (350 μ m) fracture for a short distance and then blocked. For the sample with a larger aperture (650 μ m), the cement slurry was able to penetrate the entire fracture length.

It can be seen from Figure 5-8 that the seal formed from the cured cement appears to be continuous and intact. However, sealability test on the sample ST_CG_CG_650 showed that gas leakage was still possible. The gas pressure in the gas cylinder reduced from 500kPa to 300kPa in about 2.5 hours (Figure 4-2). Furthermore, despite the reasonably good seal on the fracture surface (partial seal), the fracture had a small shear bonding strength (150kPa) (Figure 5-2).



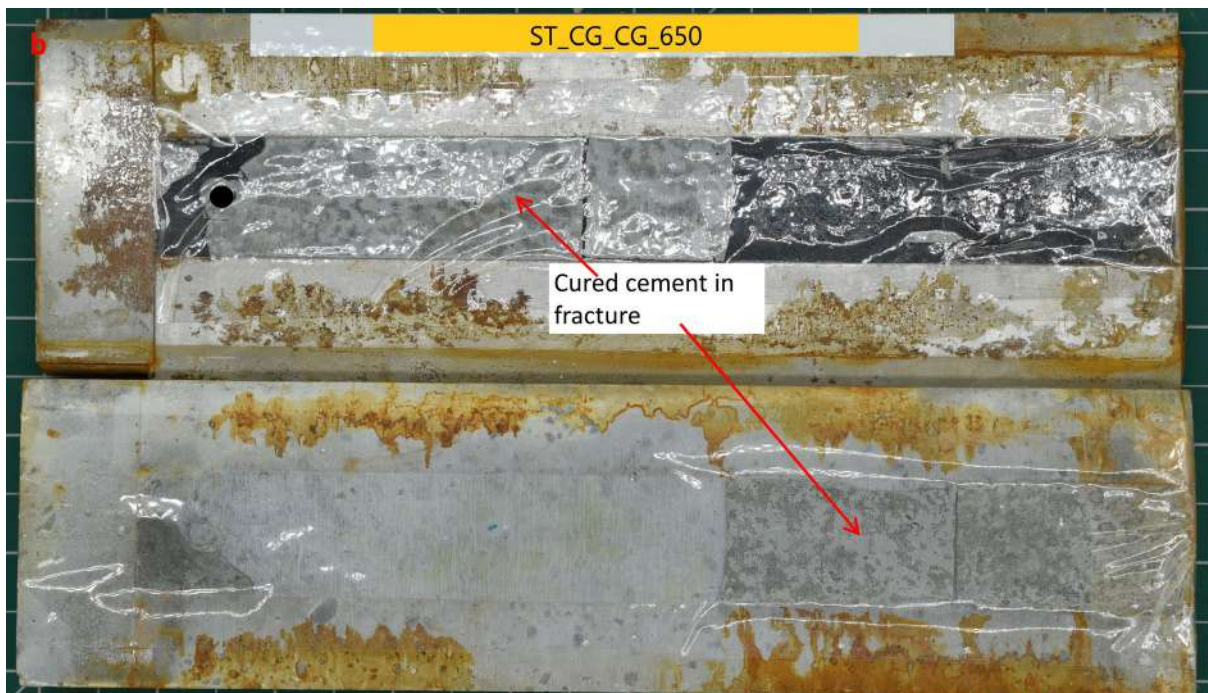


Figure 5-8. Photos for fracture samples PMMA_SS_CG_350 and ST_CG_CG_650 sealed with Class G cement slurry, a). Cement slurry flow blocked close to injection point for the 350 μ m aperture fracture, b). Cement slurry flowed through entire length of the 650 μ m aperture fracture.

5.3.2 Geopolymers

Photos of two typical fracture samples sealed with GP2 slurry are presented in Figure 5-9. The apertures of the samples are 25 μ m and 130 μ m respectively. The GP2 slurry injection tests showed that the slurry flow was blocked shortly following the injection for the 25 μ m aperture fracture. The blockage is confirmed from Figure 5-9a. The GP2 slurry was able to be injected into the entire length of the fracture sample with a 130 μ m aperture (Figure 5-9b).

Figure 5-9 showed that the seal formed from the cured GP2 appeared to be continuous with some visible cracks. However, it is uncertain when the cracks were formed, i.e., during the curing of the GP2 slurry or generated during the direct shear bonding strength testing. The sealability test showed that the fracture sample ST_CG_GP2_25 initially had good seal, gas leakage occurred sometimes later. The sealability for the sample ST_CG_GP2_130 is inclusive since the injection hole was block. Both fracture samples had a very low shear bonding strength with the shear strength of the partially sealed fracture being less than half of that of the fully sealed fracture sample.

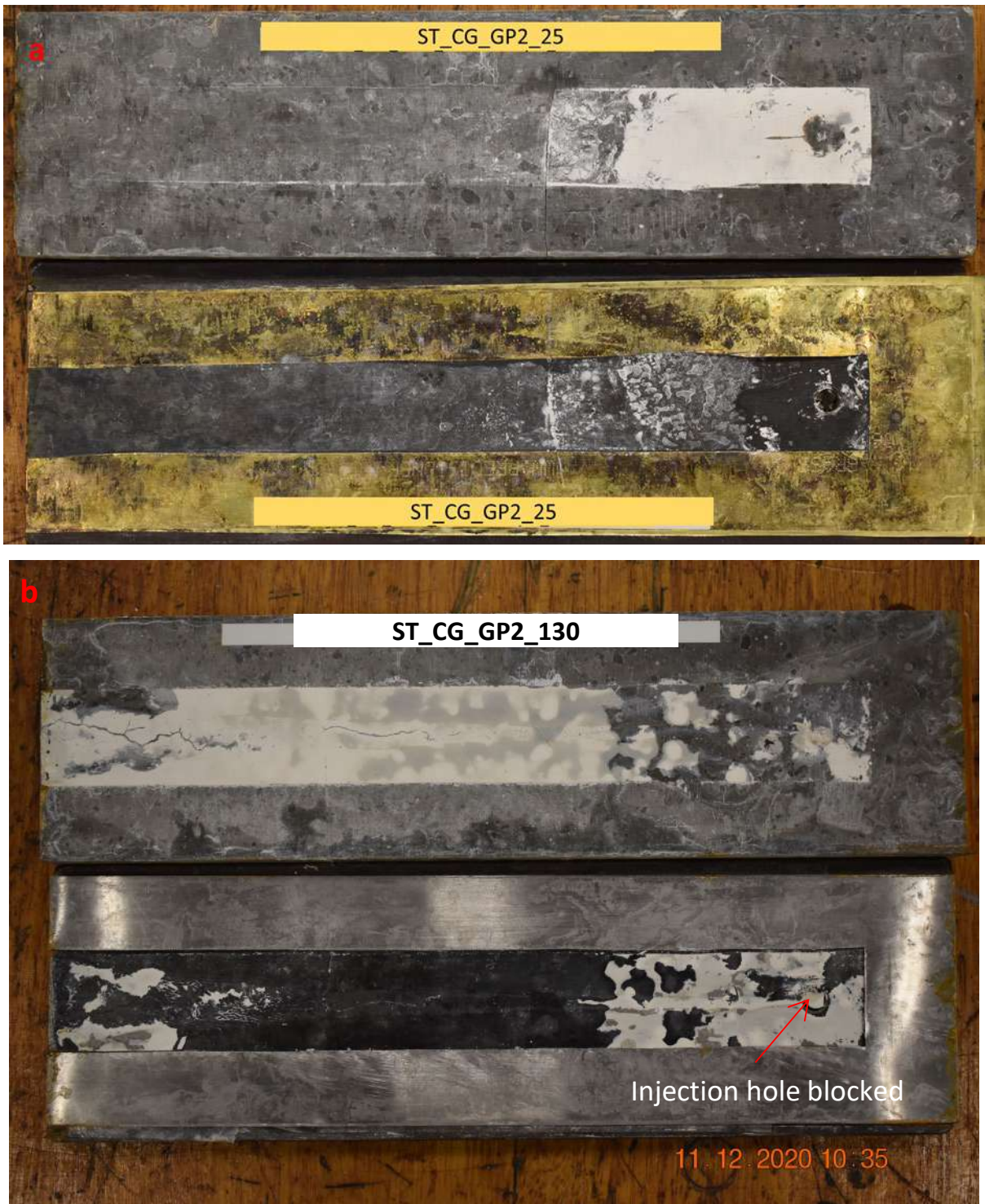


Figure 5-9 Photos for fracture samples ST_CG_GP2_25 and ST_CG_GP2_130 sealed with GP2 slurry, a). GP2 slurry flow blocked close to injection point for the 25 μ m aperture fracture, b). GP2 slurry flowed through entire length for the 130 μ m aperture fracture.

5.3.3 Polymer resins

Photos of two typical fracture samples sealed with polymer resin are presented in Figure 5-10. The apertures of the two fracture samples are 230 μ m and 25 μ m respectively. The fracture sample ST_CG_620-1_230 was injected with polymer resin 620-1 at room temperature, whilst the sample

ST_CG_720-3_25 was injected with polymer resin 720-3 preceded by the primer solution at 70°C in hot water bath. Both polymer resins were injected and flew through the entire fracture lengths. However, sealability tests demonstrated that the fracture sample injected with polymer resin 620-1 had generated little seal to gas whilst the one injected with polymer resin 720-3 at elevated temperature had a good seal to gas. The result of direct shear bonding tests showed that the shear bonding strength is correlated with sealability of the fracture sample. The fracture sample generated a good seal had a significantly higher shear bonding strength.

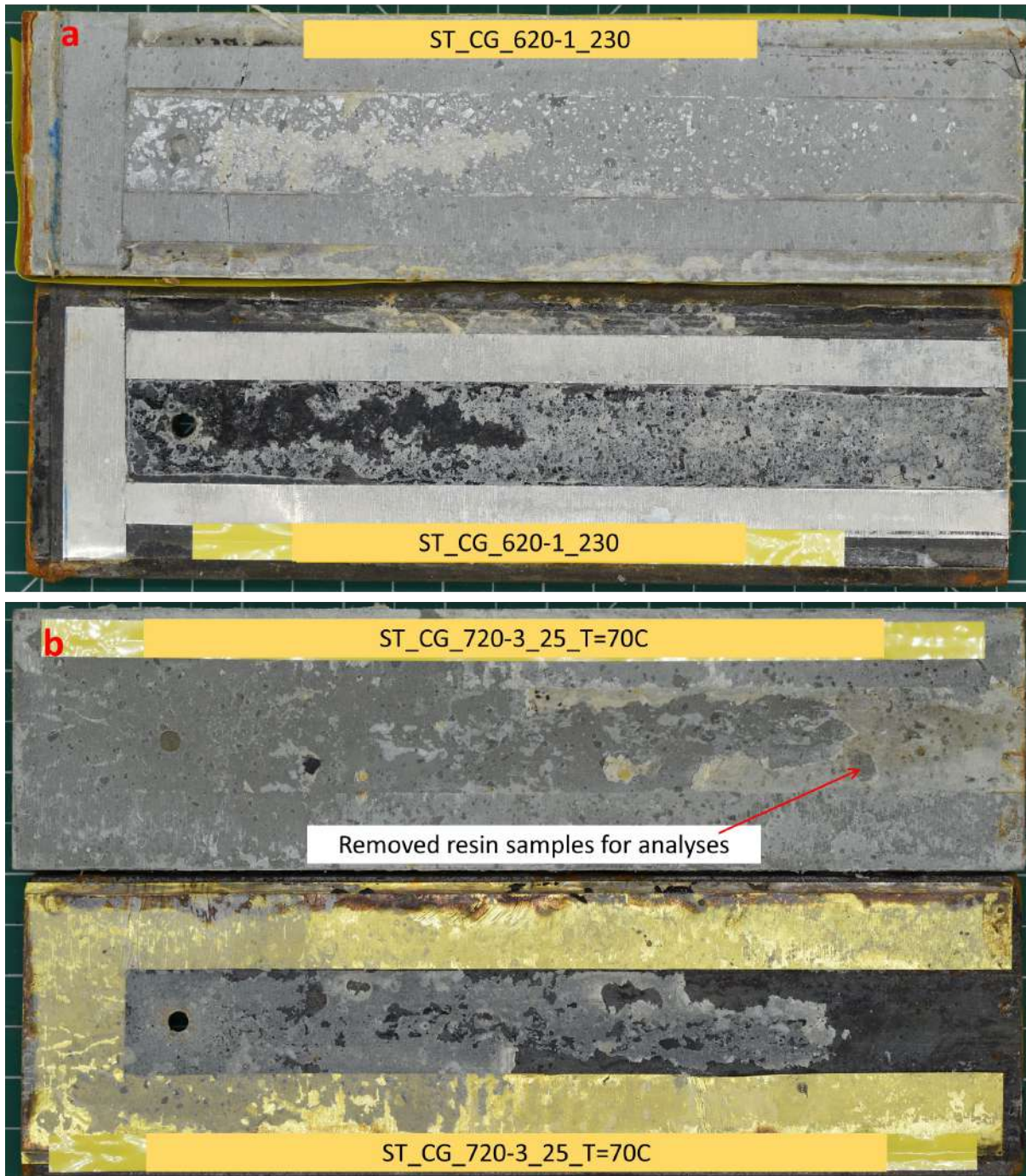


Figure 5-10 Photos for fracture samples ST_CG_620-1_230 and ST_CG_720-3_5_T=70C sealed with polymer resins, a). 620-1 with a fracture aperture of 230um injected at room temperature, b). 720-3 with a fracture aperture of 25um injected at 70°C.

Figure 5-10a showed that there were many small cavities in the cured polymer resin for the fracture sample ST_CG_620-1_230. This is most likely due to water trapped in the polymer resin during injection at room temperature. A polymer resin and water mixing test was carried out in a glass container by adding 10%wt of water to the polymer resin and then fully mixed at room temperature. The mixture was moved to an oven at 70°C to cure for 24 hours. It was observed the mixture was able to cure with the water trapped inside the polymer resin. The trapped water within polymer resin could be responsible for the observed poor sealability and shear bonding strength. This assessment may be supported by the photo in Figure 5-10b where the trapped water was much less and the fracture sample showed a good sealability and higher shear bonding strength.

5.4 SEM and FIR studies on primer enhanced bonding strength mechanisms

As demonstrated in the shear bonding strength tests in Section 5.2, the fracture samples treated (flushed) with the primer prior to polymer resin injection had a considerably higher shear bonding strength than that without primer treatment. To gain a better understanding on the mechanisms how the primer application helped improve the mechanical strength, small pieces of the cured polymer resin film were taken from the following fracture samples:

- ST_CG_720-3_25_T=70C
- ST_CG_720-3+Primer_T=70C
- CG_CG_720-3+Primer_25_T=70C
- CG_SS_720-3_25_T=70C
- CG_SS_720-3+Primer_25_T=70C

One polymer resin sample was taken from each fracture sample and both sides of the polymer resin film were analysed using SEM (Scanning Electron Microscope), a total of 10 examination sites.

5.4.1 SEM analyses

The samples were mounted on aluminium stubs with double-sided conductive carbon tape. These samples were then iridium coated using a Cressington 208HRD sputter coater. The thickness of the iridium coating was approximately 4 nm (60 mA for 50 seconds). Conductive coating is necessary to prevent charge accumulation in an electron microscope to obtain clear images, especially for insulating material. The samples were imaged using a Hitachi TM3030Plus Tabletop SEM (Scanning Electron Microscope). The images were obtained the secondary electron (SE) detector to highlight topographical features. Energy dispersive spectroscopy (EDS) was used to identify elements present within the samples. The EDS system used was AZTEC, manufactured by Oxford Instruments Pty Ltd. An accelerating voltage of 15 kV was used for imaging and EDS analysis.

The SEM studies identified following two potential mechanisms that may be responsible for the observed shear bonding strength increase:

- The primer contributed to the reduction in water trapped on the interface between the carbon steel and the polymer resin.

Figure 5-11 shows the SEM images for the polymer resin film bonding to the carbon steel surface with and without application of the primer solution. Reduction in water inclusion is evident for the polymer resin film where the primer solution was applied. Since water inclusion has no resistance to shear stress, reduction of water inclusion in polymer resin would directly contribute to improved shear bonding strength of the fracture sample. However, since the primer solution is water based, it is unclear how the primer solution helped reduce the water inclusion in polymer resin, which warrants further investigation in future.

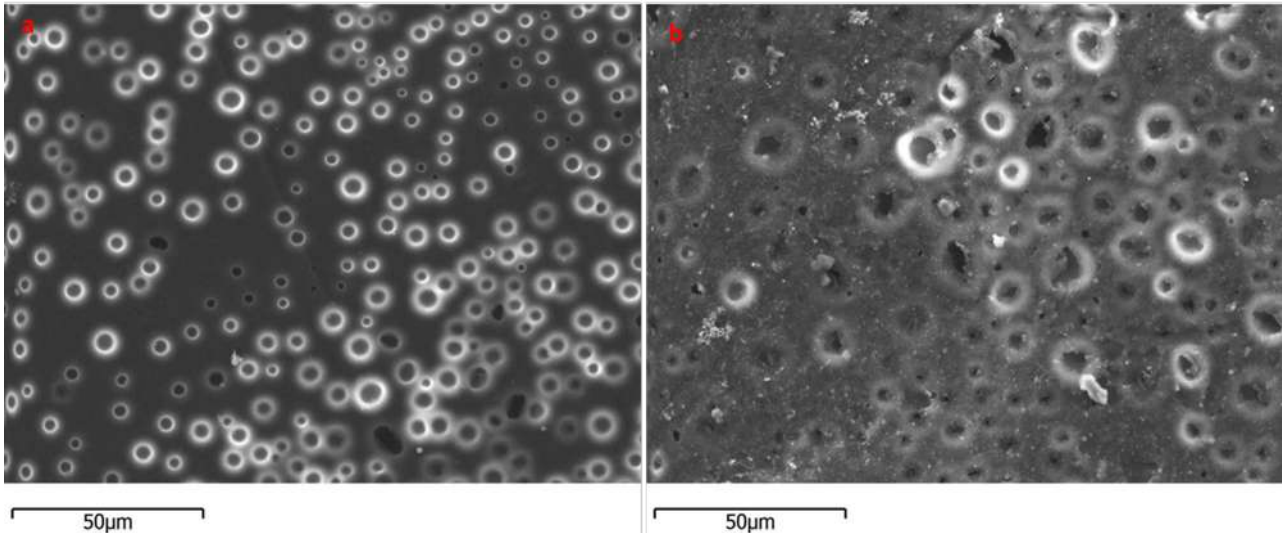


Figure 5-11 SEM images of polymer resin film bonding with carbon steel for the fracture samples, a) ST_CG_720-3_25_T=70C without application of the primer solution and b) ST_CG_720-3+Primer_25_T=70C with application of the primer solution.

- The primer acting as bonding promoter

Figure 5-12 shows SEM images of the polymer resin films for the fracture samples CG_SS_720-3_25_T=70C and CG_SS_720-3+Primer_25_T=70C, i.e., one fracture sample without treatment of the primer solution (Figure 5-12a, c) and the other treated with the primer solution (Figure 5-12b, d). Figure 5-12a,b shows the images of the polymer resin film bonding to the siltstone slabs and Figure 5-12c,d shows the images bonding to the Class G cement slabs. It is clear that the polymer resin film surfaces treated with the primer solution are much rougher and more porous, whether they were bonding to the siltstone or Class G cement slabs, than those without primer treatment. This implies a strong “tear and pull” when subject to a shear displacement along the interfaces, an indication of an enhanced shear bond strength.

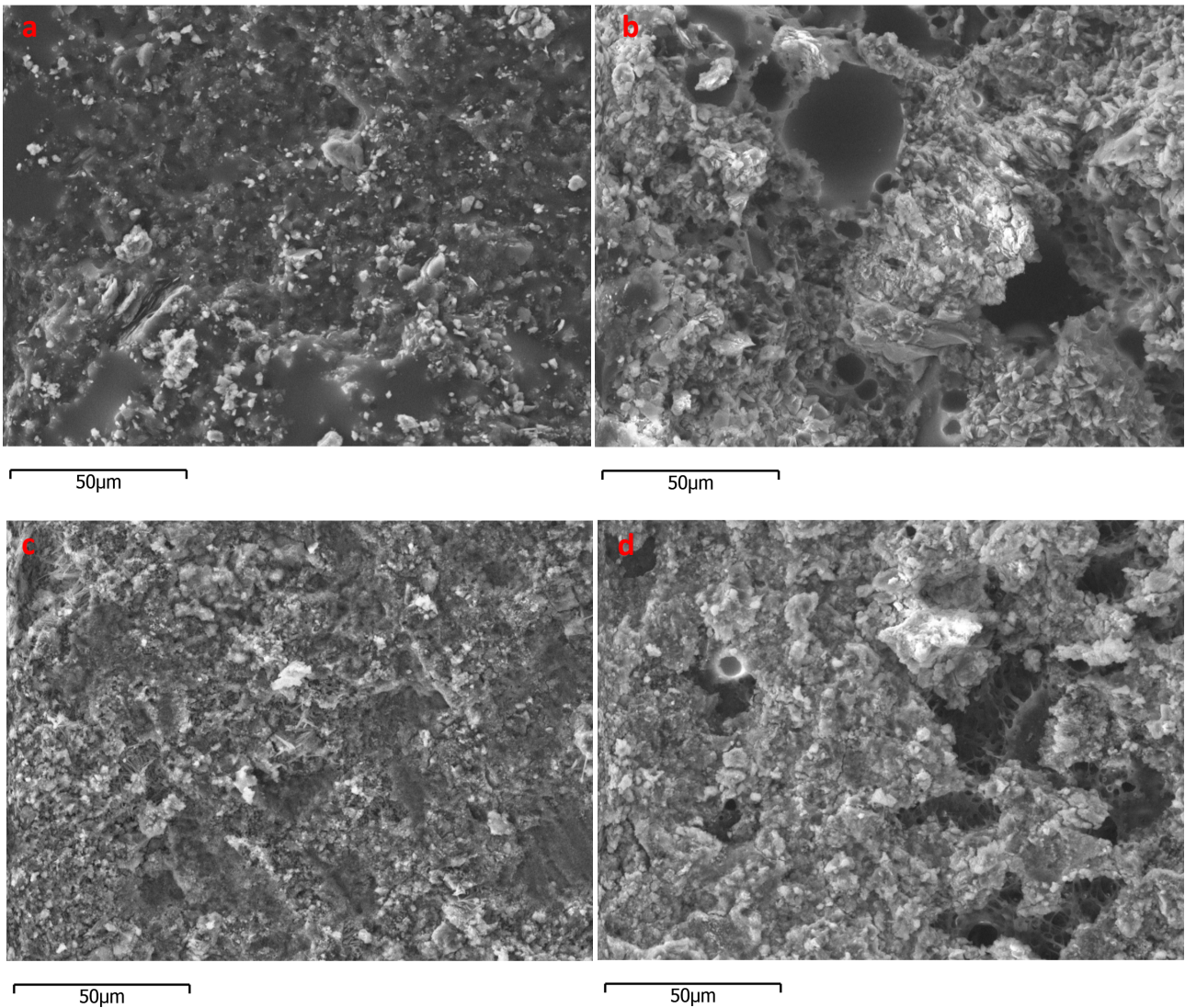


Figure 5-12 SEM images of polymer resin surface. Images a (no primer treatment) and b (primer treatment) in contact with siltstone, Image c (no primer treatment) and d (primer treatment) in contact with cement

5.4.2 FTIR analyses

To verify that the observed enhancement in shear bonding strength was indeed induced due to the primer solution, a FTIR (Fourier Transform Infrared Spectrometer) study on the polymer resin film samples, the same ones used for the SEM analyses, was carried out. The FTIR tool (NICOLET 6700, ATR method, DTGS KBr detector, 4000-525cm⁻¹ range) was used to verify the presence of the primer on the surface of the polymer resin film samples.

The primer ADEX P51 – Acrylic Copolymer contains 10 to 60%wt of Polyvinyl acetate/maleinate copolymer (Appendix D). Their chemical structures are shown in Figure 5-13

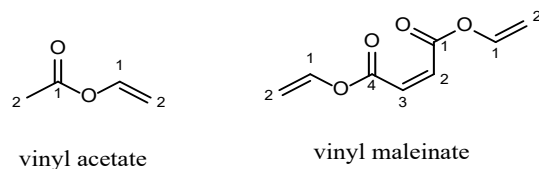


Figure 5-13 Chemical structures of Acrylic Copolymer.

Acetate and Maleinate are two main components of P51 acrylic primer. FTIR absorption peak of carbonyl ester (O=C-O) stretching vibration occurs around $1730\text{-}1750\text{cm}^{-1}$. This peak is well distinguished because there are no other polymer resin peaks locate in this region.

A total of six FTIR analyses were performed on the polymer resin film samples retrieved from carbon steel, cement and siltstone surfaces which were treated with or without primer solution. The FTIR Spectra of the analyses are presented in Figure 5-14.

The presence of the primer can be clearly identified from the polymer resin surface bonding to the carbon steel surface that was treated with the primer solution, as shown in Figure 5-14a. No such FTIR absorption peak exists for the fracture sample with no treatment by the primer solution.

The FTIR absorption peak is not as clear on the polymer resin surfaces bonding to the cement (Figure 5-14b) and siltstone surfaces (Figure 5-14c), but a peak can still be identified. The reason for the lower FTIR absorption peak is probably due to the bonding strength of the polymer resin with the cement and siltstone surfaces and a thin layer of the cement or the siltstone materials could cover the polymer resin surface which may be difficult for the beam to penetrate since the beam can only penetrate 1-2 micron deep from the polymer resin surface.

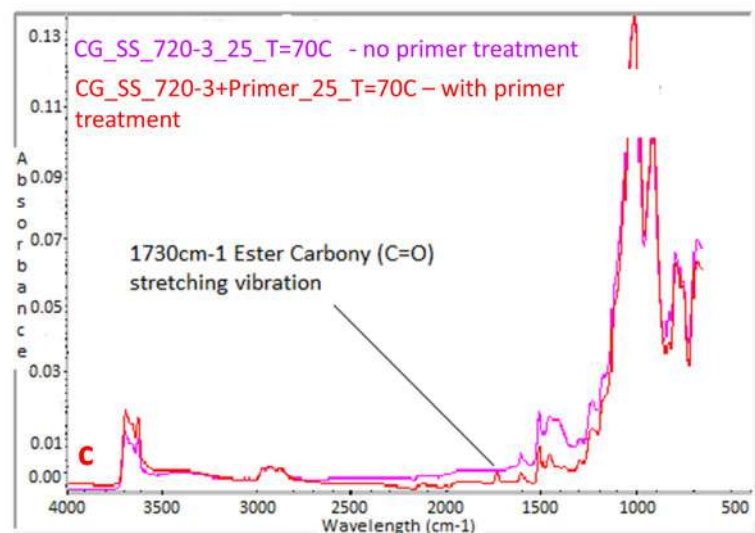
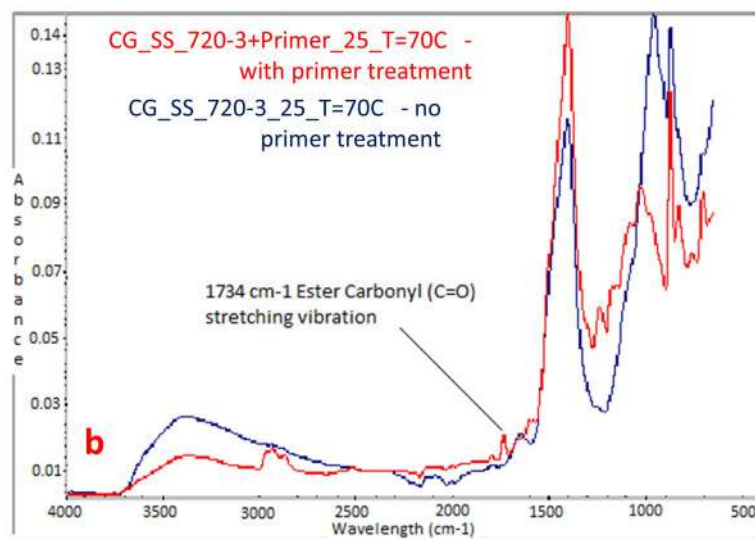
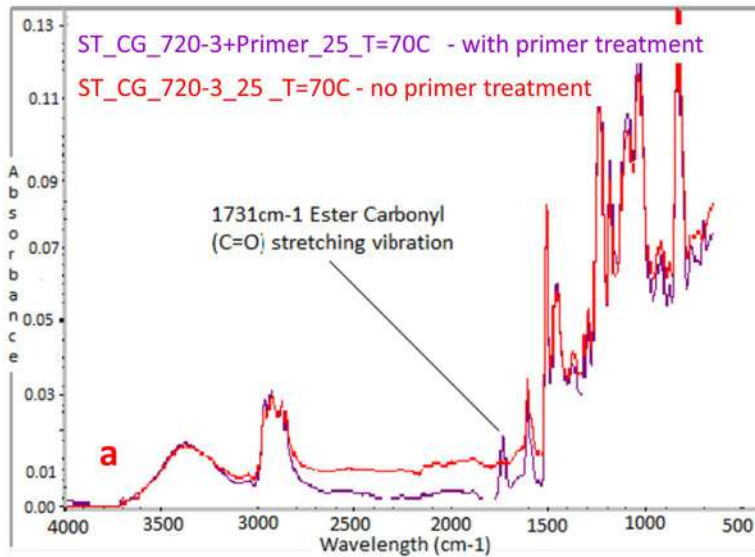


Figure 5-14. FTIR Spectra of polymer resin film samples, a) bonding to carbon steel surface, b) bonding to cement surface, and c) bonding to siltstone surface.

6 SUMMARY, CONCLUSIONS AND SUGGESTIONS FOR FURTHER STUDIES

A comprehensive experimental study has been conducted to evaluate the performance of five potential fracture sealing materials. The new (or alternative to conventional cement) fracture sealing materials, including two geopolymers and three thermal-activated polymer resins, were selected after screening a large number of potential candidate materials. The selected sealing materials were characterized for their rheological, physical, and mechanical properties.

The new fracture sealing materials were firstly evaluated for their injectivity into sand packs. They were then assessed for their performance in sealing synthetic planar fractures, in terms of injectivity, sealability and shear bonding strength. To accomplish this assessment, a set of novel and fit-for-purpose experimental testing apparatus were developed. This included a sealant injection system, a gas sealability test apparatus and a direct shear bonding strength jig.

Around 40 planar fracture samples were tested to evaluate the performance of the fracture sealing materials. The synthetic planar fracture was formed by inserting a pre-cut metal shim with a given thickness between two smooth test slabs, which were then clamped together by bolts. The fracture length and width were kept constant for all the fracture samples whilst the apertures varied from 25 μm to 650 μm with great majority less than 400 μm . The test slab materials ranged from carbon steel, cured Class G cement and siltstone. The sealing materials were injected into the planar fracture from the sealed end of the fracture and flew out from the other end open to atmosphere. The fracture samples filled with the sealing material were then cured at 70°C in a hot water bath for 24 to 48 hours. The major findings from the experimental study are as follows:

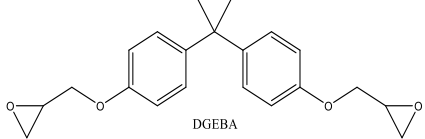
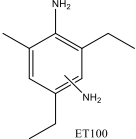
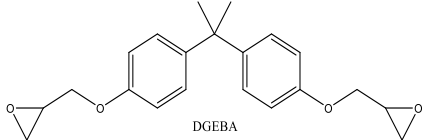
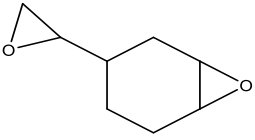
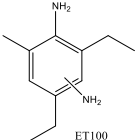
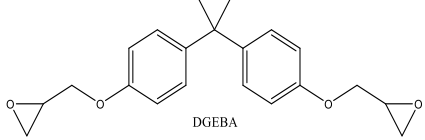
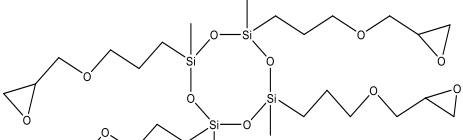
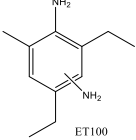
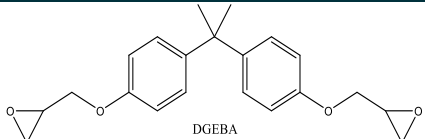
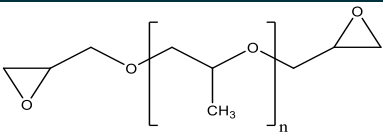
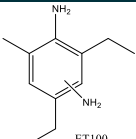
- It was observed from the sand pack experiments that both the geopolymer and thermal-activated polymer resin were able to be injected into the sand pack to consolidate and form a solid sand pack upon curing, while it was not possible to inject the conventional Class G cement slurry into the sand pack. The particle sizes of the sand packs were between 250 μm and 425 μm ;
- The results of the injectivity test on the planar fractures showed that the thermal-activated polymer resins were able to penetrate a planar fracture with an aperture as narrow as 25 μm , whilst the minimum fracture aperture that could be injected through was approximately 50 μm for the geopolymer and 350 μm for the conventional Class G cement slurry;
- It was observed that the seal to gas generated in the planar fractures from Class G cement and geopolymer slurries ranged from almost no seal to partial seal. Partial to complete seal was achieved with one of the thermal-activated polymer resins (code name 720-3) when the injection was conducted at 70°C, although the seal was poor if the injection was conducted at room temperature. The sealability of the thermal-activated polymer resin had improved further by applying a water-based primer solution prior to the polymer resin injection;

- The shear bonding strength of the fracture sample was in general very low for the Class G cement and geopolymer slurries, averaged around 100kPa with a normal stress of 40kPa. In comparison, the shear bonding strength generated from one of the thermal-activated polymer resins (code name 720-3) was almost ten times higher when the injection was conducted at 70°C. Application of the primer solution enhanced the shear bonding strength further significantly.
- The SEM and FTIR studies on the polymer resin samples taking from the cured fracture samples revealed that the mechanism of the primer solution in enhancing sealability and shear bonding strength was due to reduction in water inclusion on the bonding interface.

The experimental study so far demonstrated that the thermal-activated polymer resin (code name 720-3) is a promising sealant material in sealing small fractures where conventional oil well cement would likely fail. Further laboratory experimental studies are recommended to evaluate its performance in sealing small/micro fractures, and the longevity and effectiveness of the seal under simulated downhole pressure, temperature, and other adverse downhole conditions, prior to field trials.

Appendix A Chemical Structure and DSC Spectra for Polymer Resins

Table A.1. Chemical Structures for fracture sealing materials

BND#	Polymer Resin	Diluent	Curing Agent
010620-0	 <p>DGEBA Diglycidyletherbisphenol A</p>		 <p>ET100 Mixture of 3,5-diethyltoluene-2,4-diamine(80%) and 3,5-diethyltoluene-2,6-diamine(20%)</p>
010620-1	 <p>DGEBA Diglycidyletherbisphenol A</p>	 <p>ECHO 1,2-Epoxy cyclohexyl-4-Oxirane</p>	 <p>ET100 Mixture of 3,5-diethyltoluene-2,4-diamine(80%) and 3,5-diethyltoluene-2,6-diamine(20%)</p>
010620-5	 <p>DGEBA Diglycidyletherbisphenol A</p>	 <p>D4-Epoxy</p>	 <p>ET100 Mixture of 3,5-diethyltoluene-2,4-diamine(80%) and 3,5-diethyltoluene-2,6-diamine(20%)</p>
020720-3	 <p>DGEBA Diglycidyletherbisphenol A</p>	 <p>PPGDGE Poly(propylene glycol) diglycidyl ether</p>	 <p>ET100 Mixture of 3,5-diethyltoluene-2,4-diamine(80%) and 3,5-diethyltoluene-2,6-diamine(20%)</p>

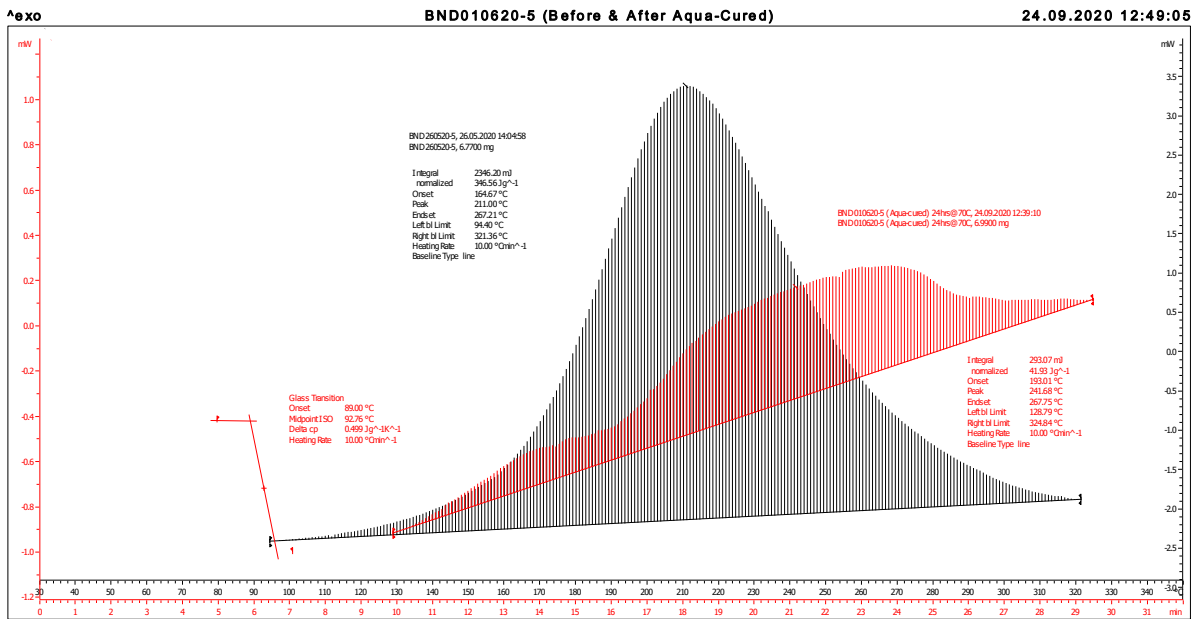


Figure A. 1. DSC Spectra for BND010620-5 (DGEBA+20%wtD4-Epoxy/ET100) (Before & After Cured); T_g=92.8°C and %Curing = 87.9.

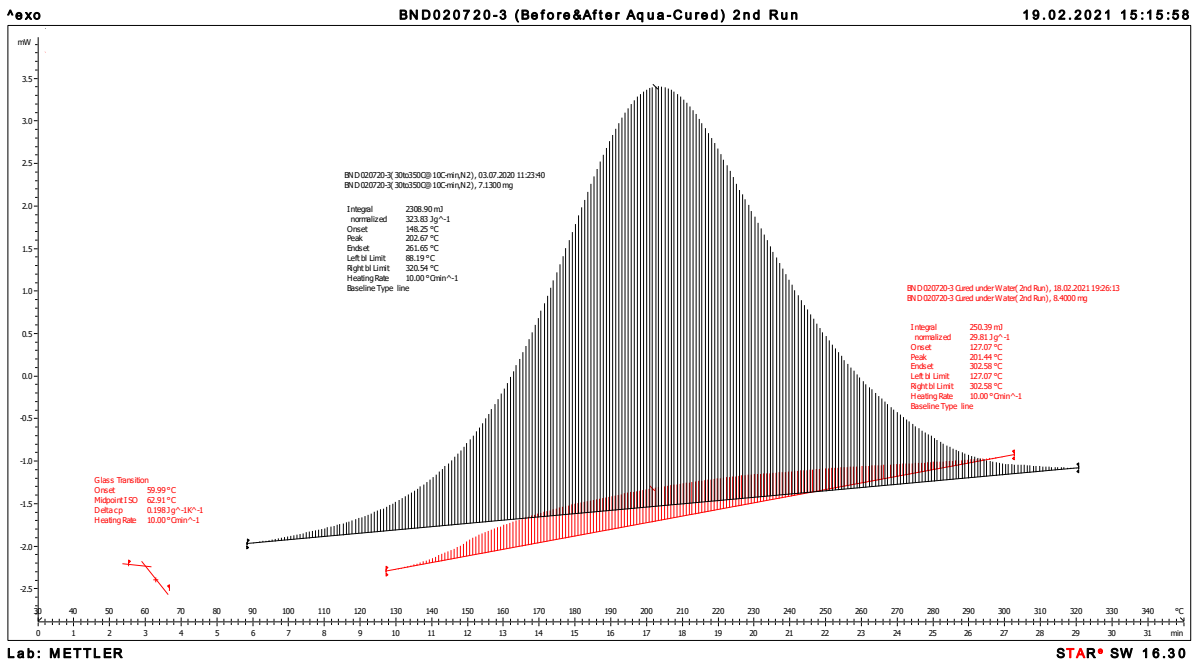


Figure A. 2. DSC Spectra for BND020720-3 (DGEBA+20%wt PPGDGE/ET100) (Before & After Cured); T_g=62.9°C & 80.0°C; %Curing = 90.8

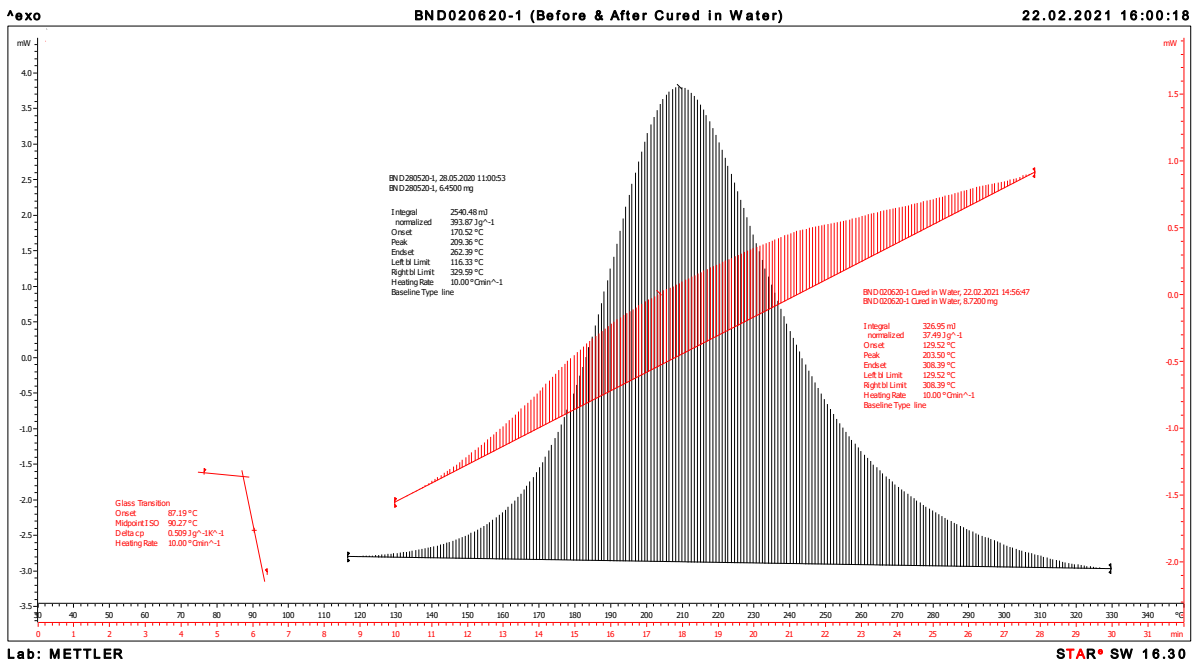


Figure A. 3. DSC Spectra for BND010620-1 (DGEBA+10%wt ECHO/ET100) (Before & After Cured in Water); Tg=90.3C, %Curing = 90.5

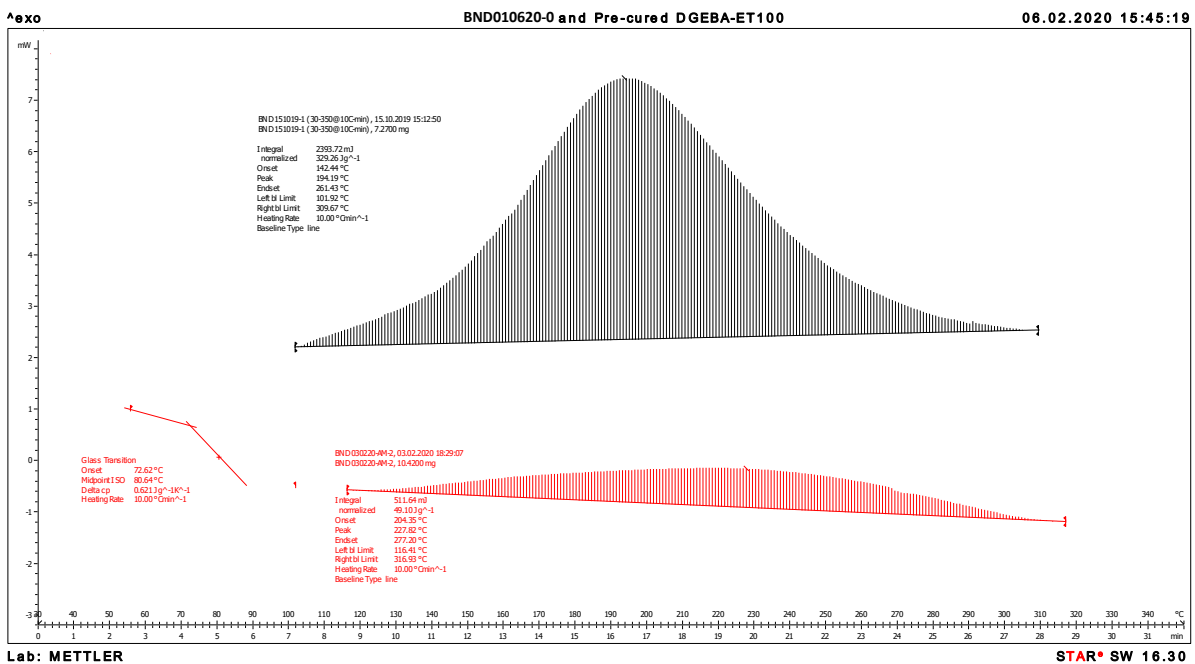


Figure A. 4. DSC Spectra for BND010620-0 (DGEBA/ET100) (Before & After Cured in Water); Tg=80.6C %Curing = 85.1

Appendix B Mechanical Properties of Cured Fracture Sealing Materials

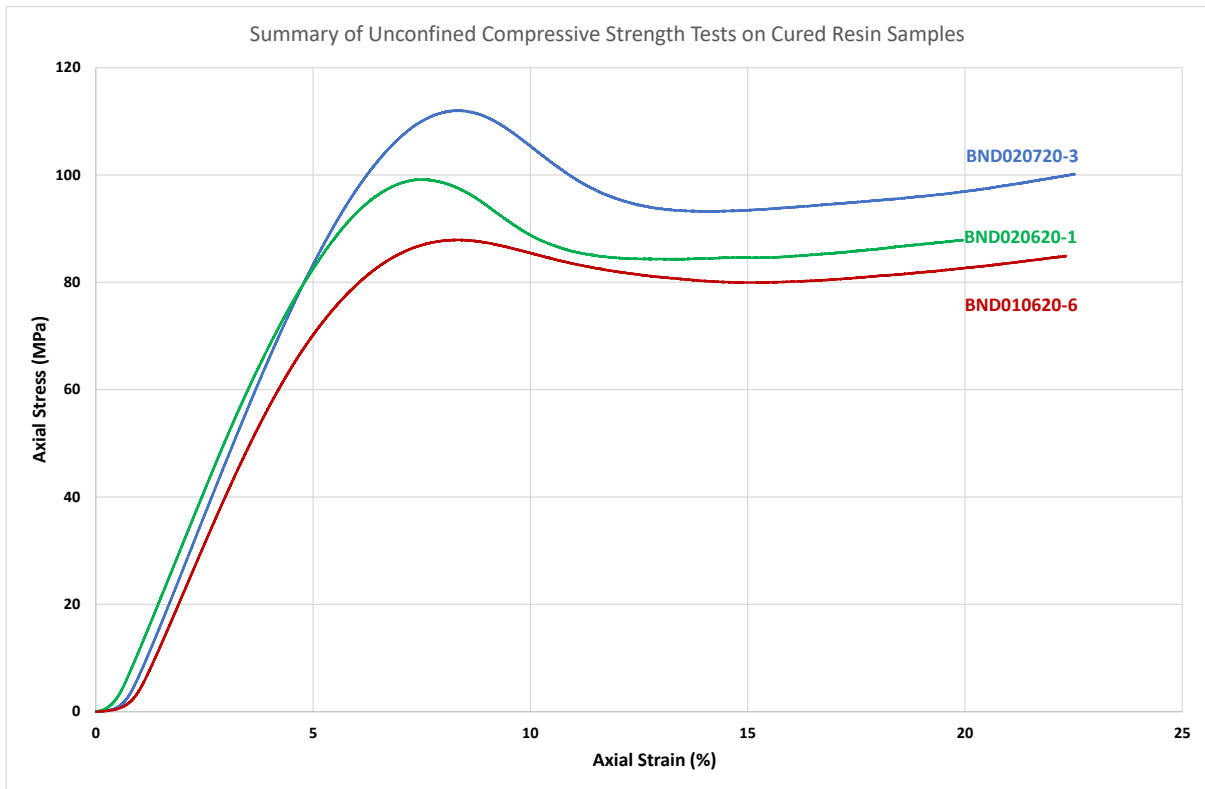


Figure B. 1. Axial stress vs strain curves for fully cured polymer resin samples.

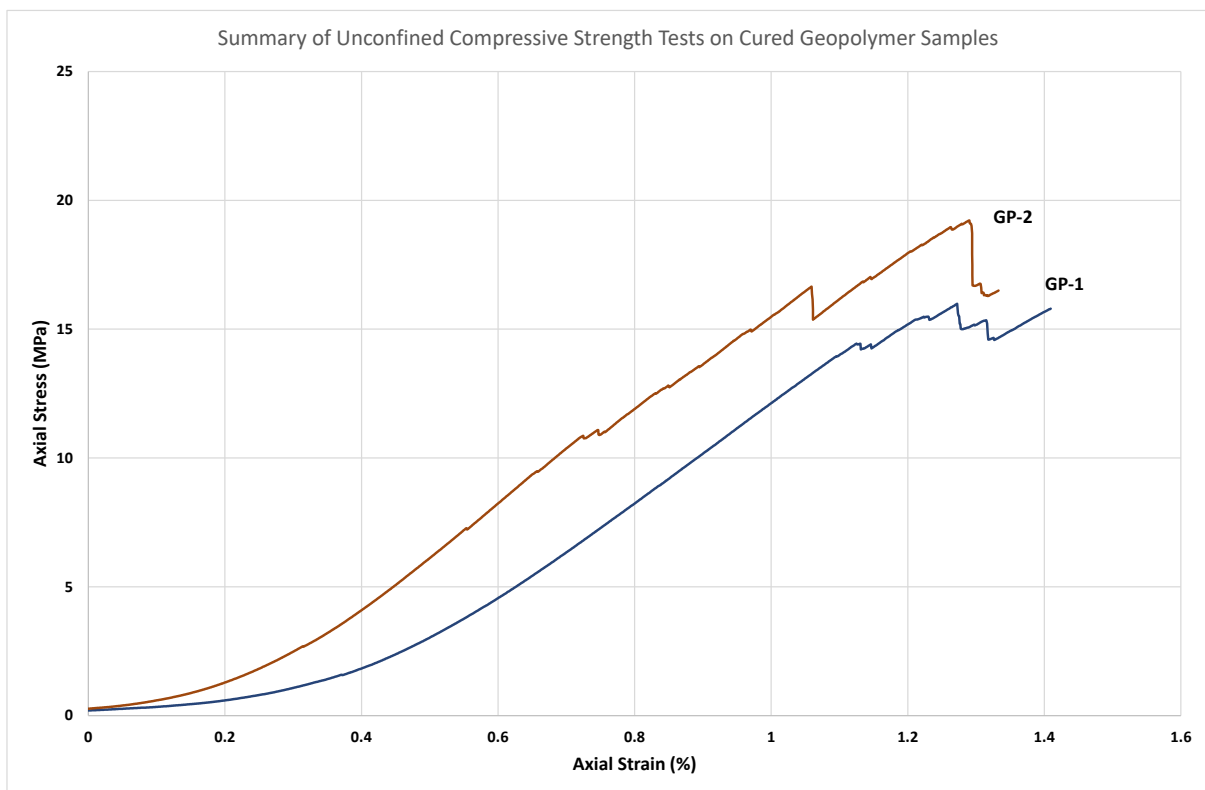


Figure B. 2. Axial stress vs strain curves for fully cured geopolymer samples.

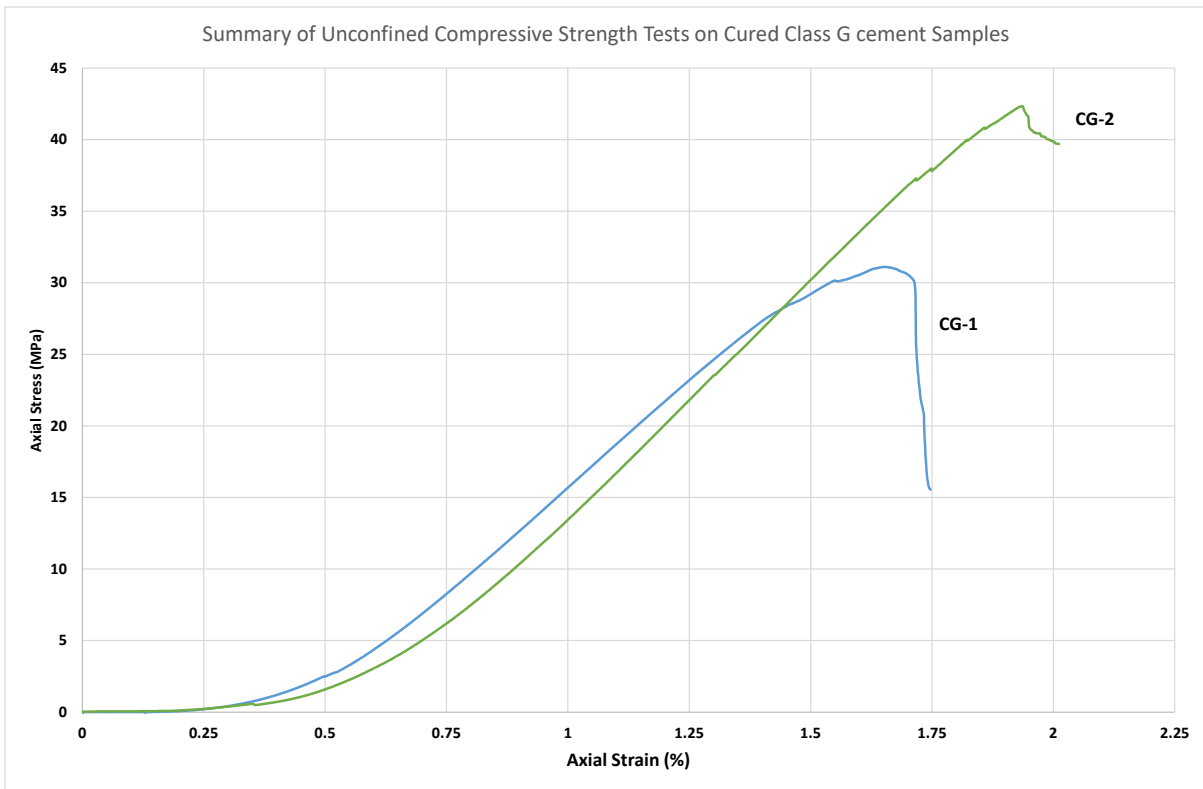


Figure B. 3. Axial stress vs strain curves for fully cured Class G cement samples.



Figure B. 4. Photos of the tested samples for polymer resins, geopolymer and Class G cement, showing ductile deformation for polymer resin and brittle failure for geopolymer and Class G cement.

Appendix C. Results of Injectivity Tests and Photos of Tested Fracture Samples

CG Injectivity Tests

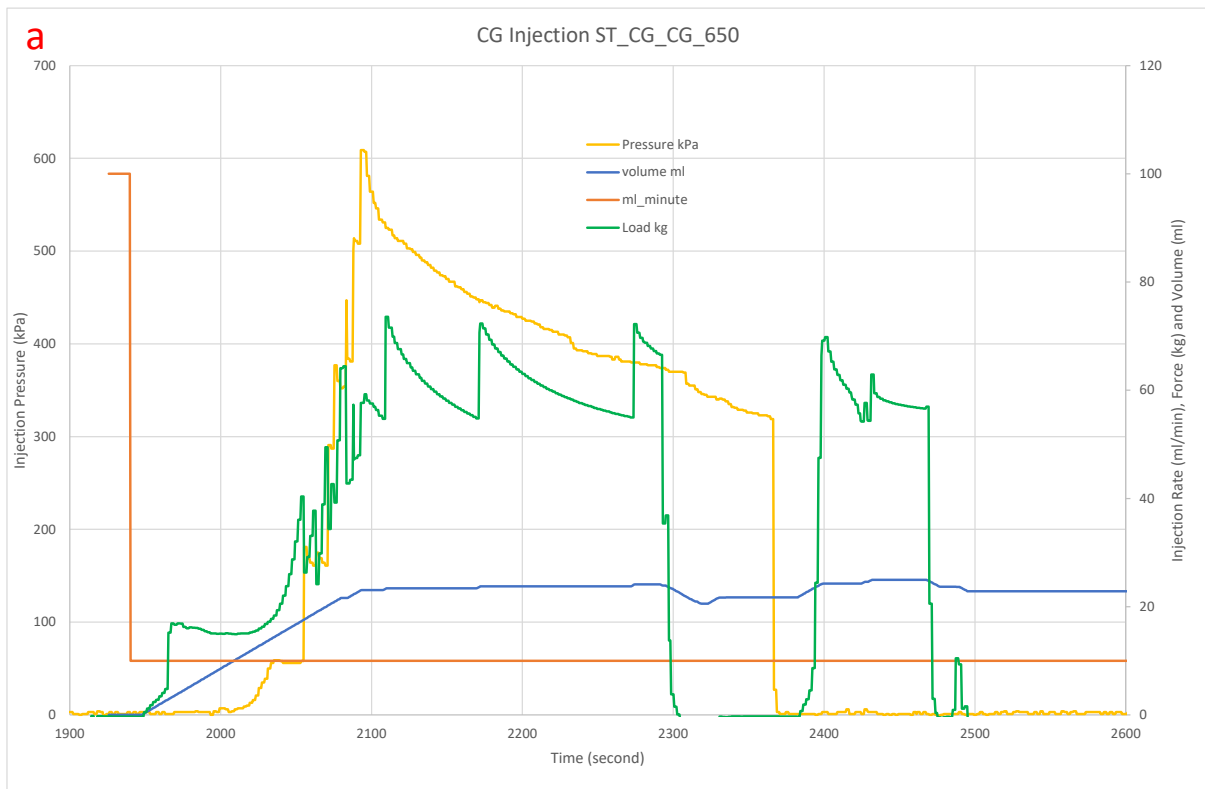


Figure C. 1. Injection test for fracture sample ST_CG_CG_650, a) Injection pressure, rate, force and volume vs time, and b) Photo of tested sample after shear bonding strength test.

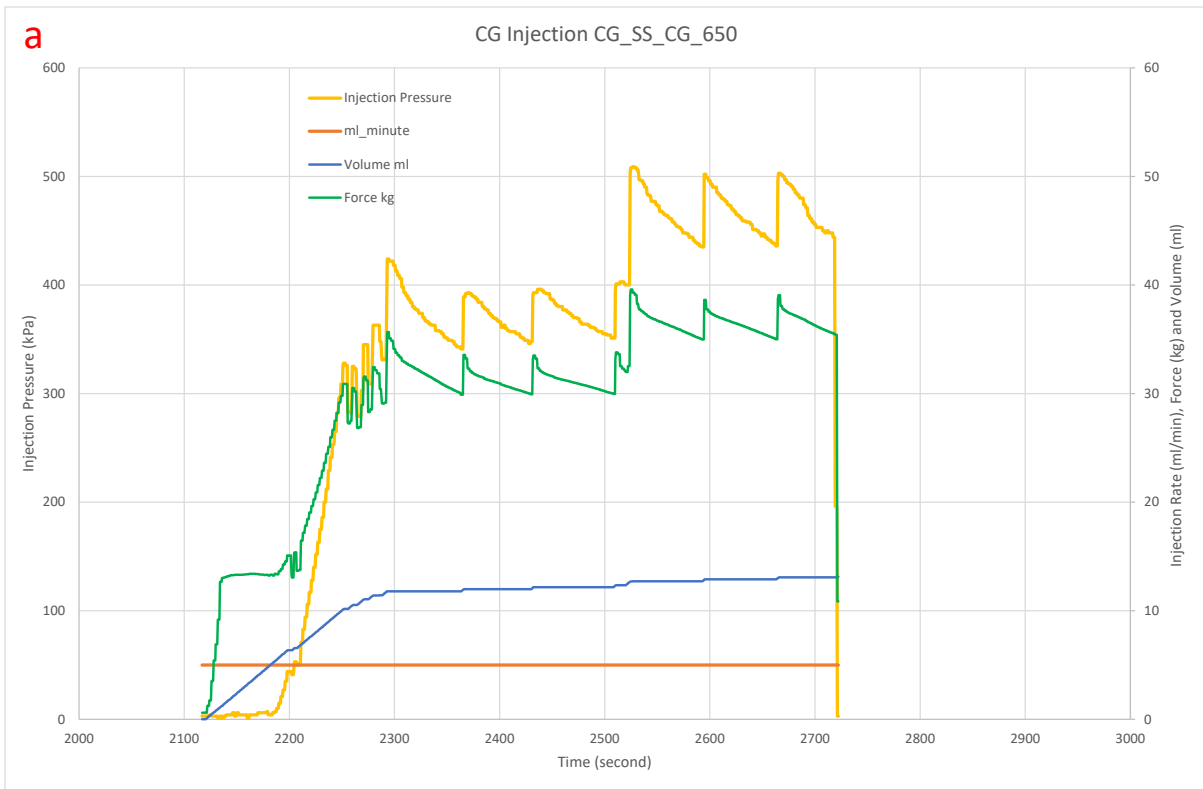


Figure C. 2. Injection test for fracture sample CG_SS_CG_650, a) Injection pressure, rate, force and volume vs time, and b) Photo of tested sample following shear bonding strength test.

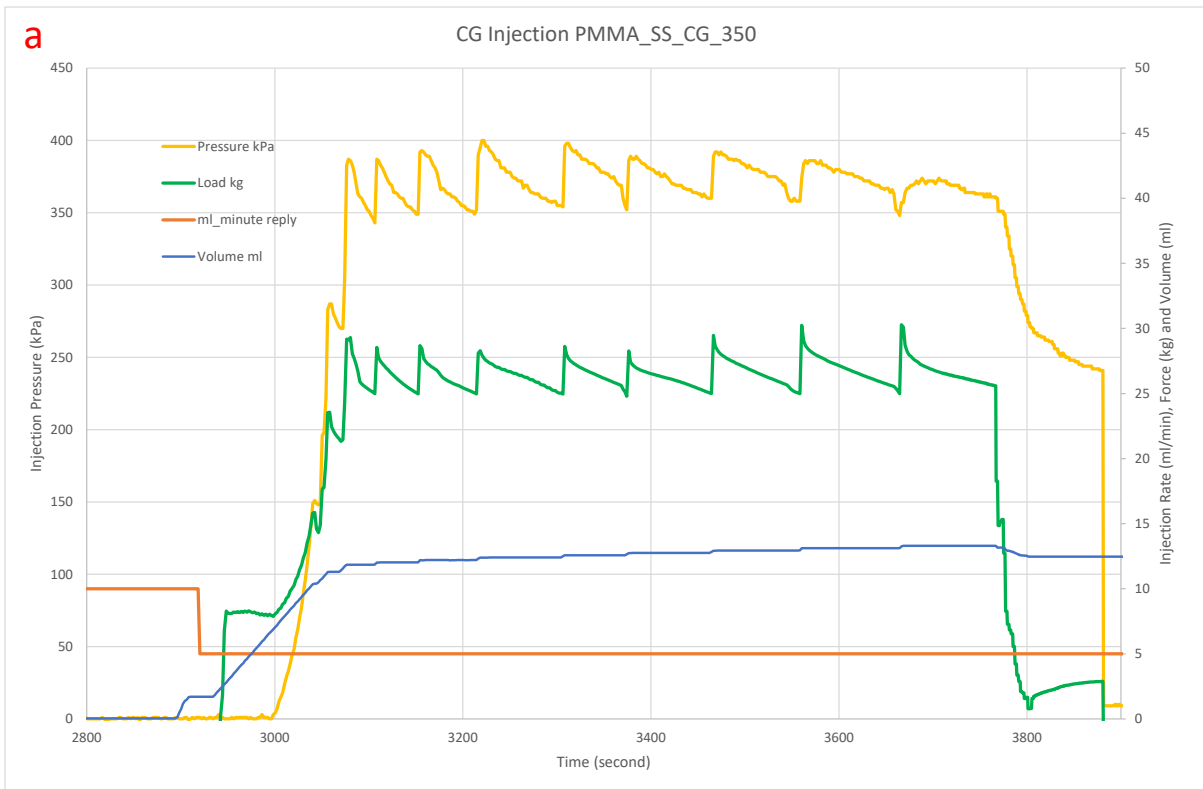


Figure C. 3. Injection test for fracture sample PMMA_SS_CG_350, a) Injection pressure, rate, force and volume vs time, and b) Photo of tested sample.

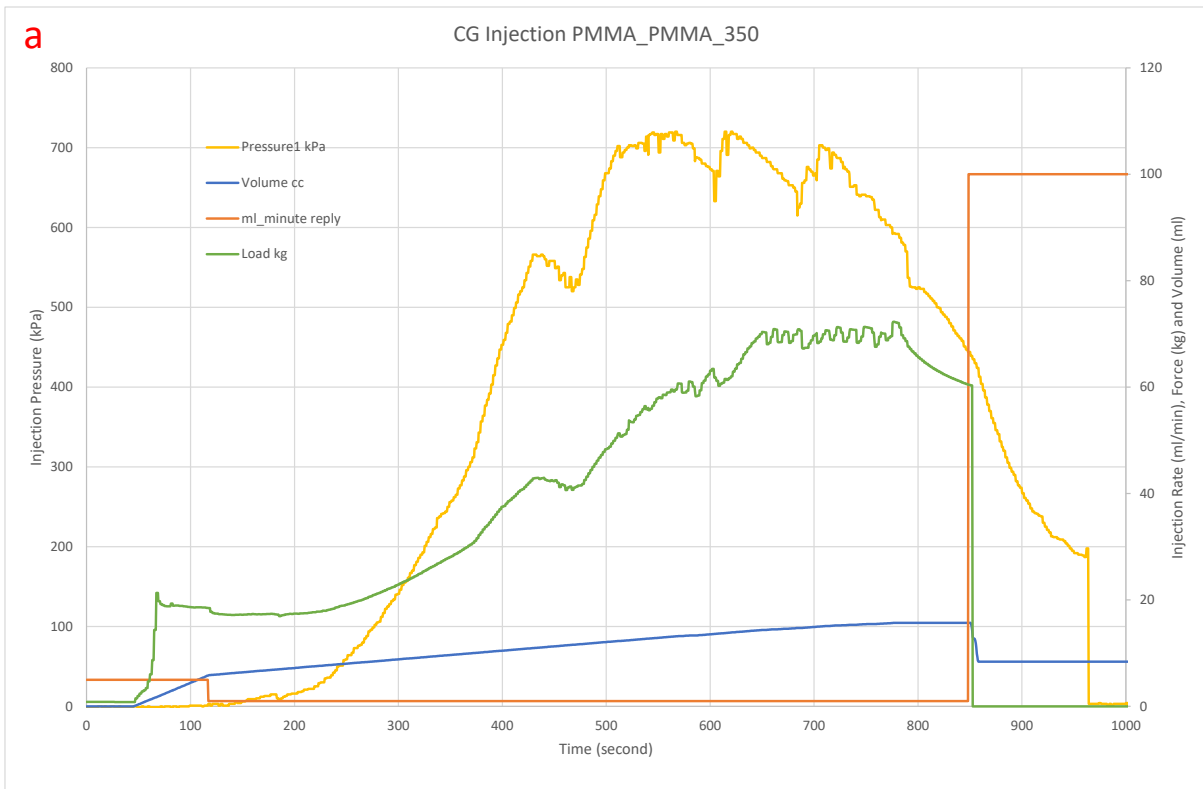


Figure C. 4. Injection test for fracture sample PMMA_PMMA_CG_350, a) Injection pressure, rate, force and volume vs time, and b) Photo of tested sample.

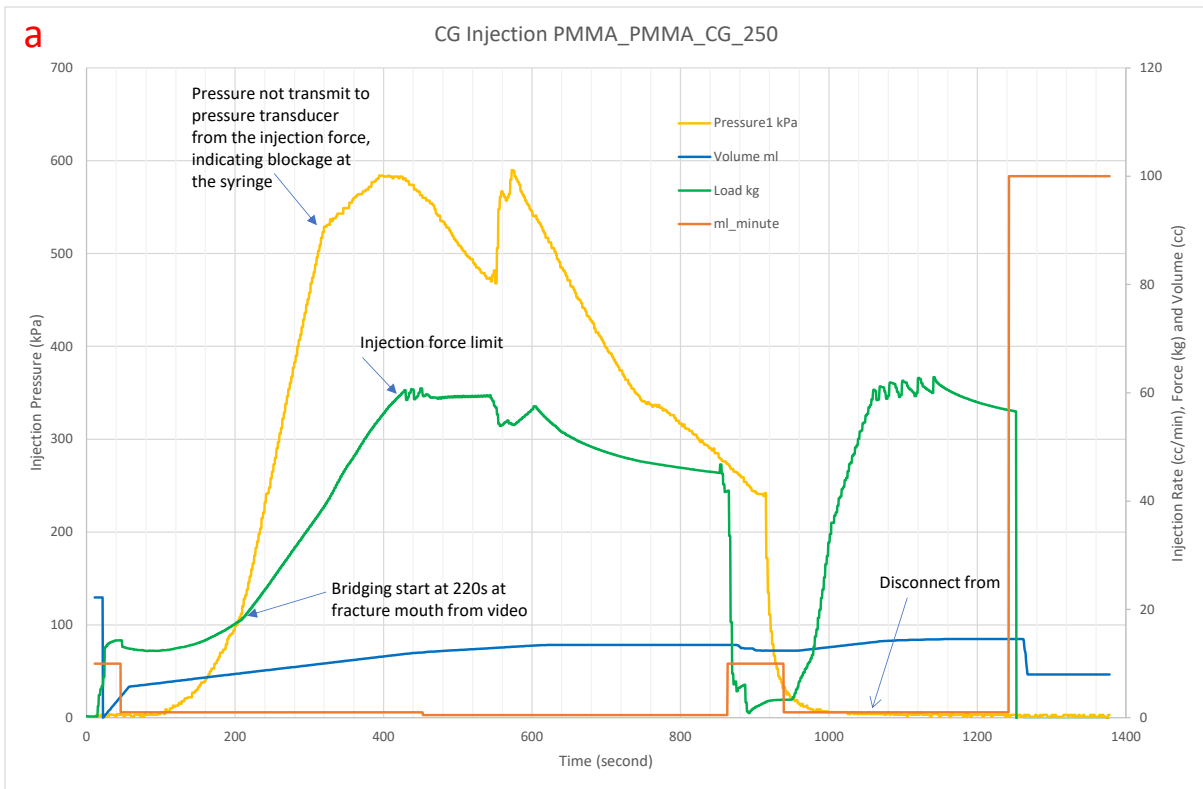


Figure C. 5. Injection test for fracture sample PMMA_PMMA_CG_250, a) Injection pressure, rate, force and volume vs time, and b) Photo of tested sample.

GP1 Injectivity Tests

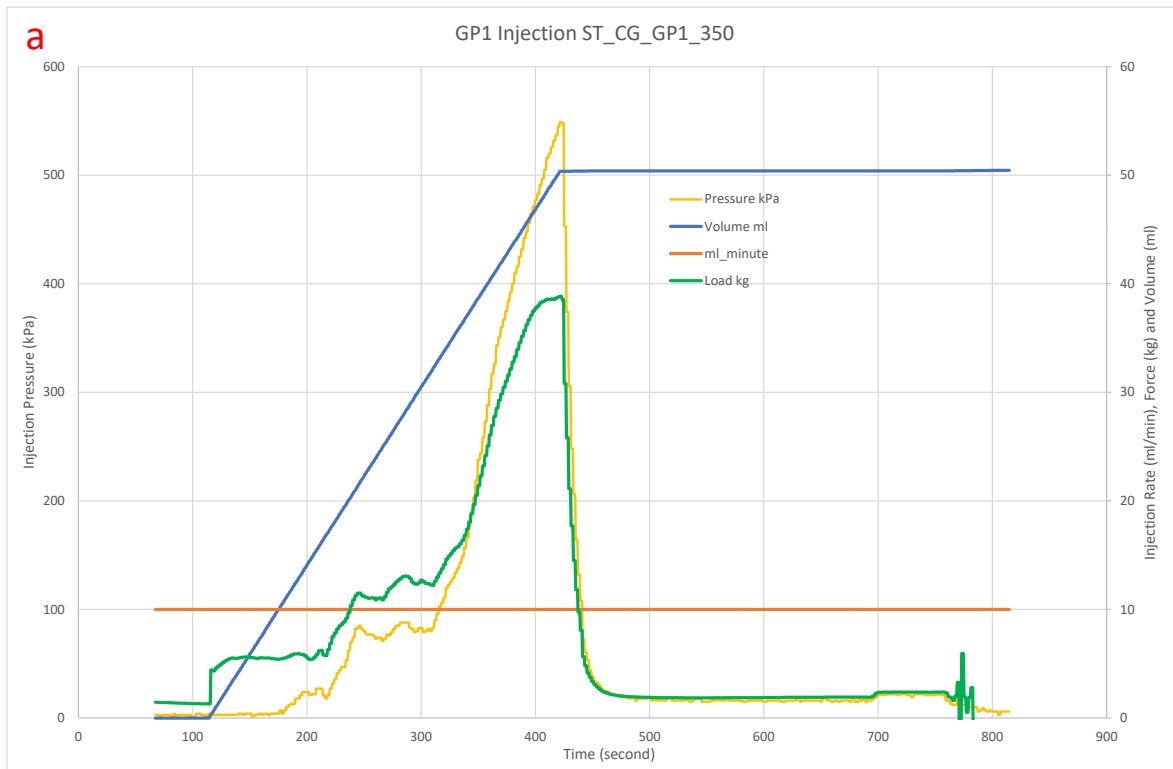


Figure C. 6. Injection test for fracture sample ST_CG_GP1_350, a) Injection pressure, rate, force and volume vs time, and b) Photo of tested sample after shear bonding strength test.

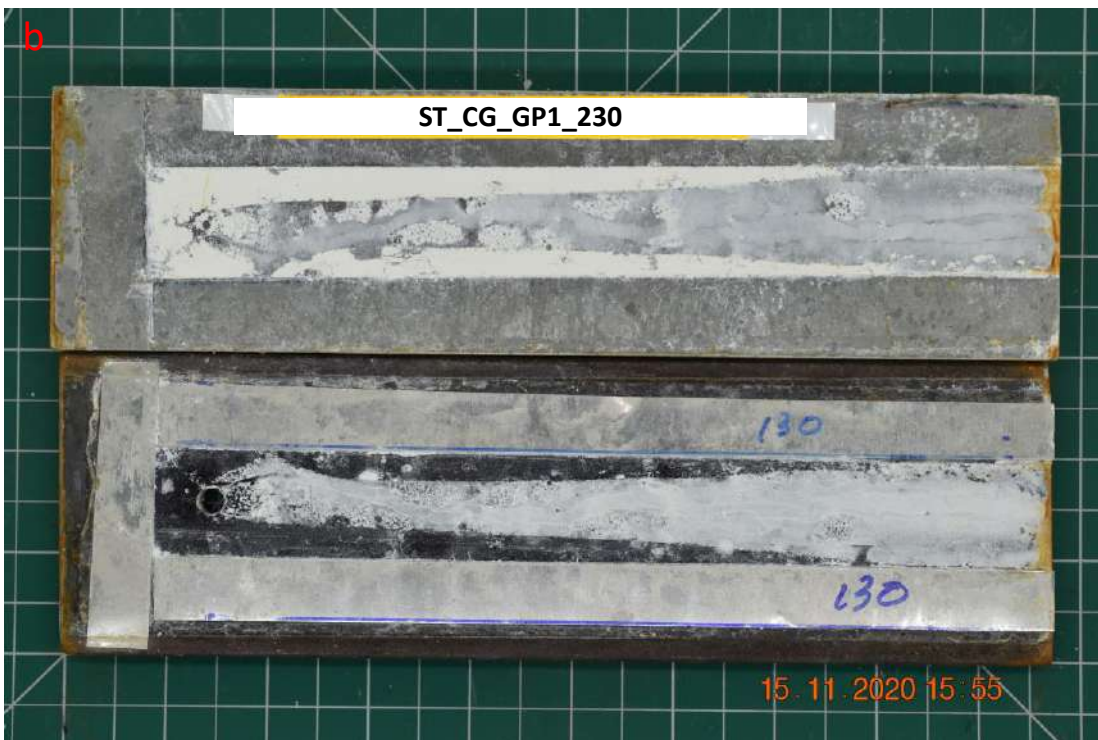
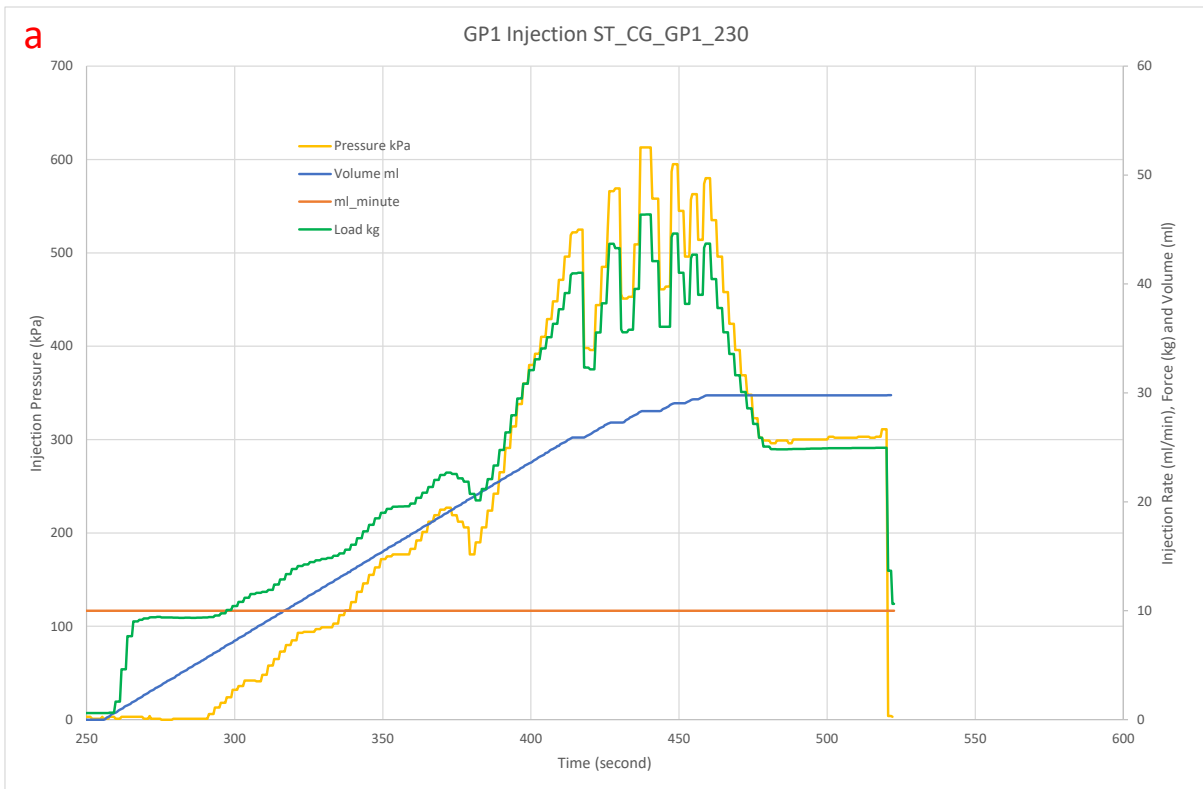


Figure C. 7. Injection test for fracture sample ST_CG_GP1_230, a) Injection pressure, rate, force and volume vs time, and b) Photo of tested sample following shear bonding strength test.

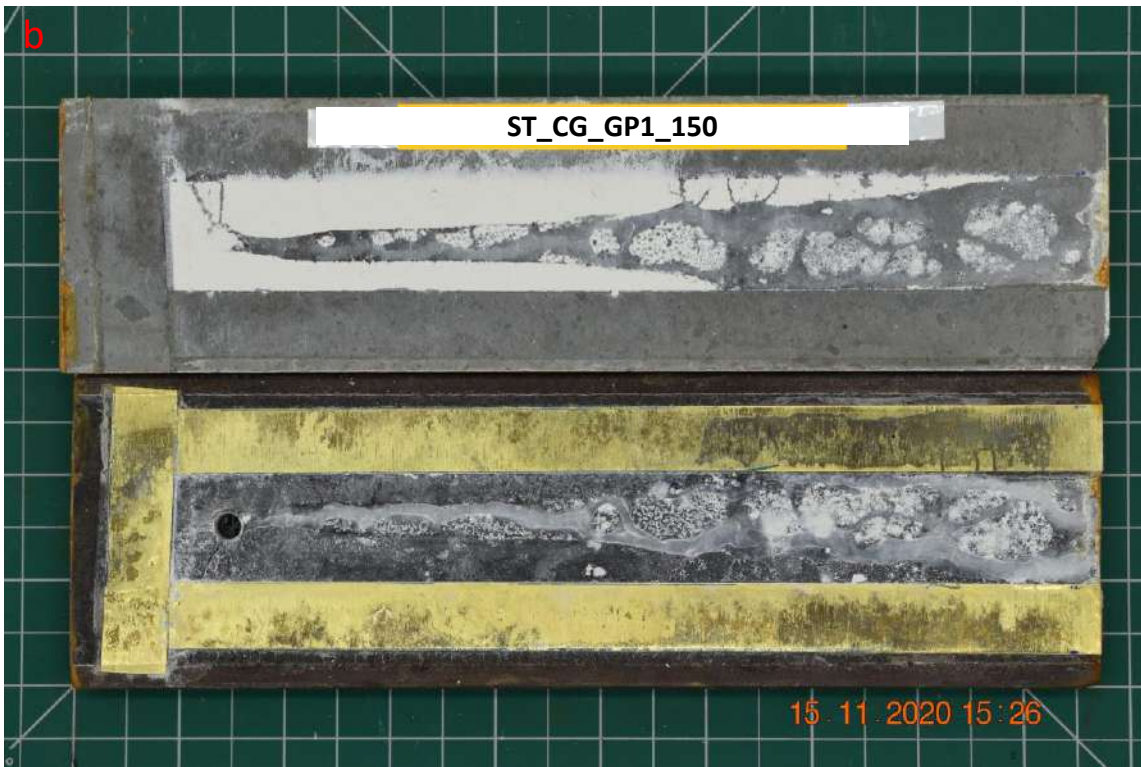
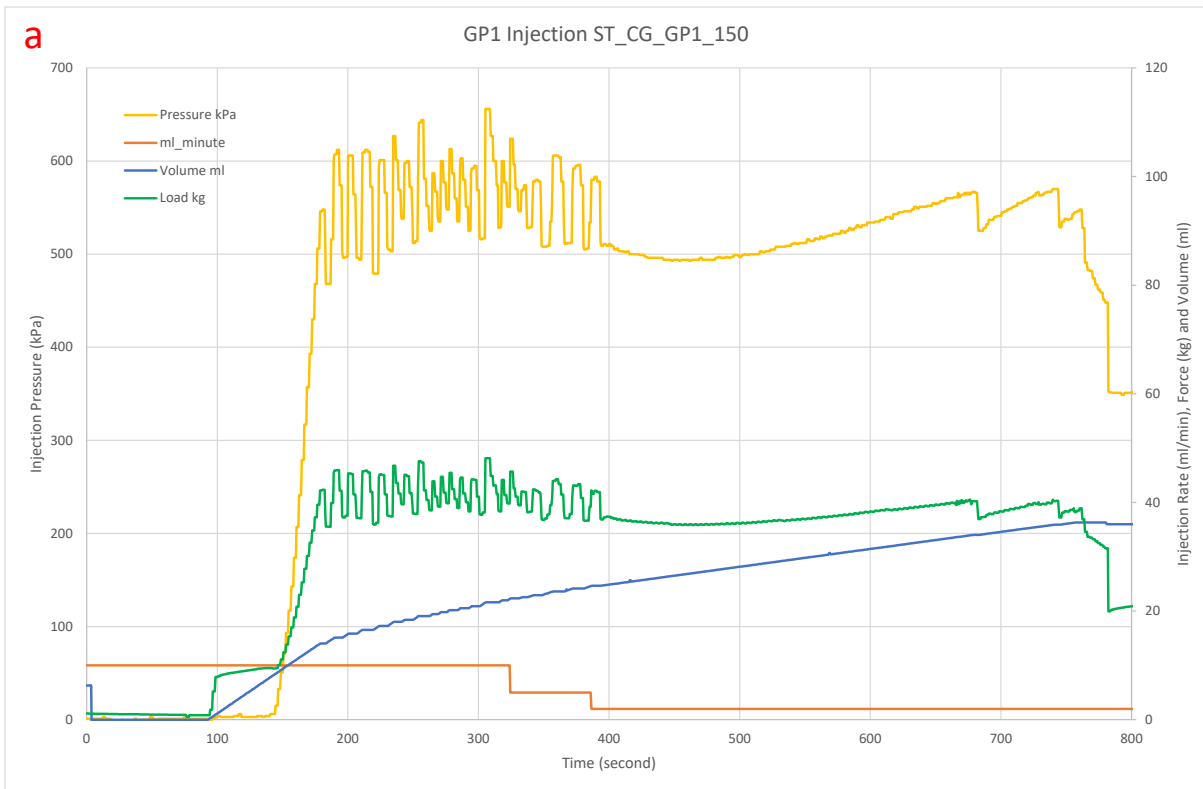


Figure C. 8. Injection test for fracture sample ST_CG_GP1_150, a) Injection pressure, rate, force and volume vs time, and b) Photo of tested sample.

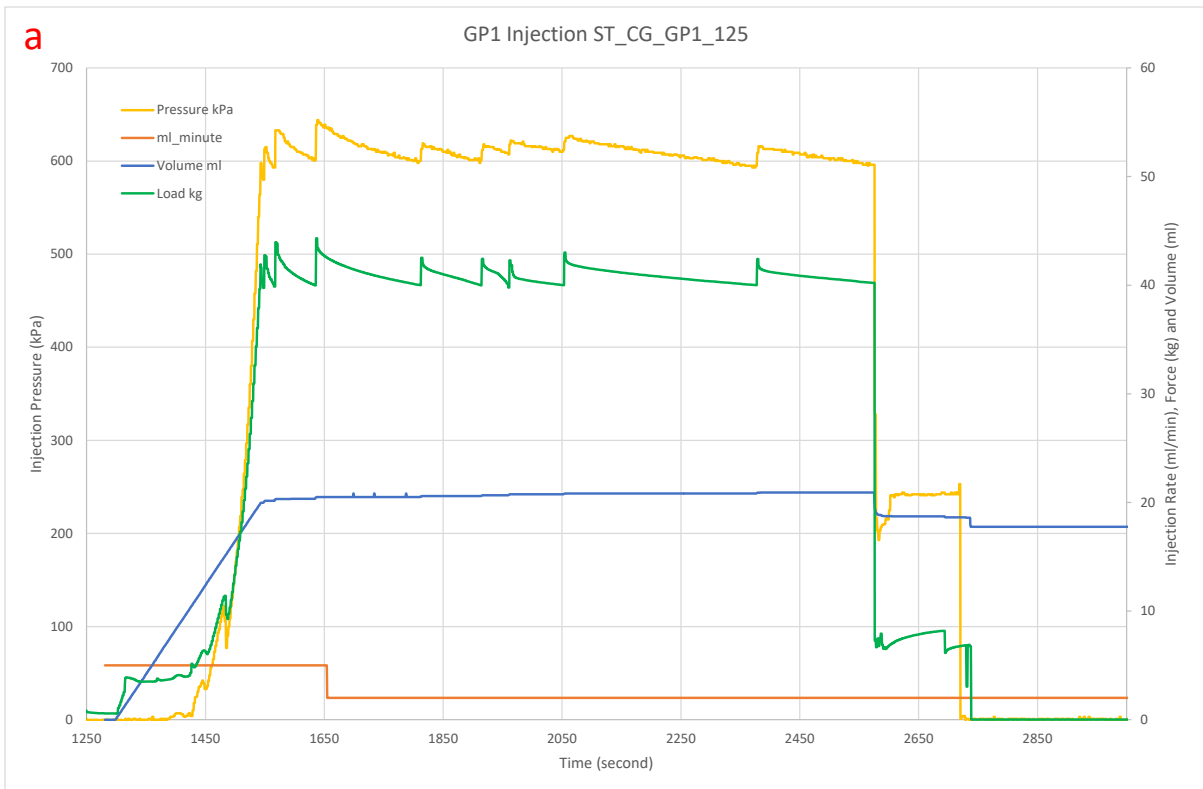


Figure C. 9. Injection test for fracture sample ST_CG_GP1_125, a) Injection pressure, rate, force and volume vs time, and b) Photo of tested sample.

GP2 Injectivity Tests

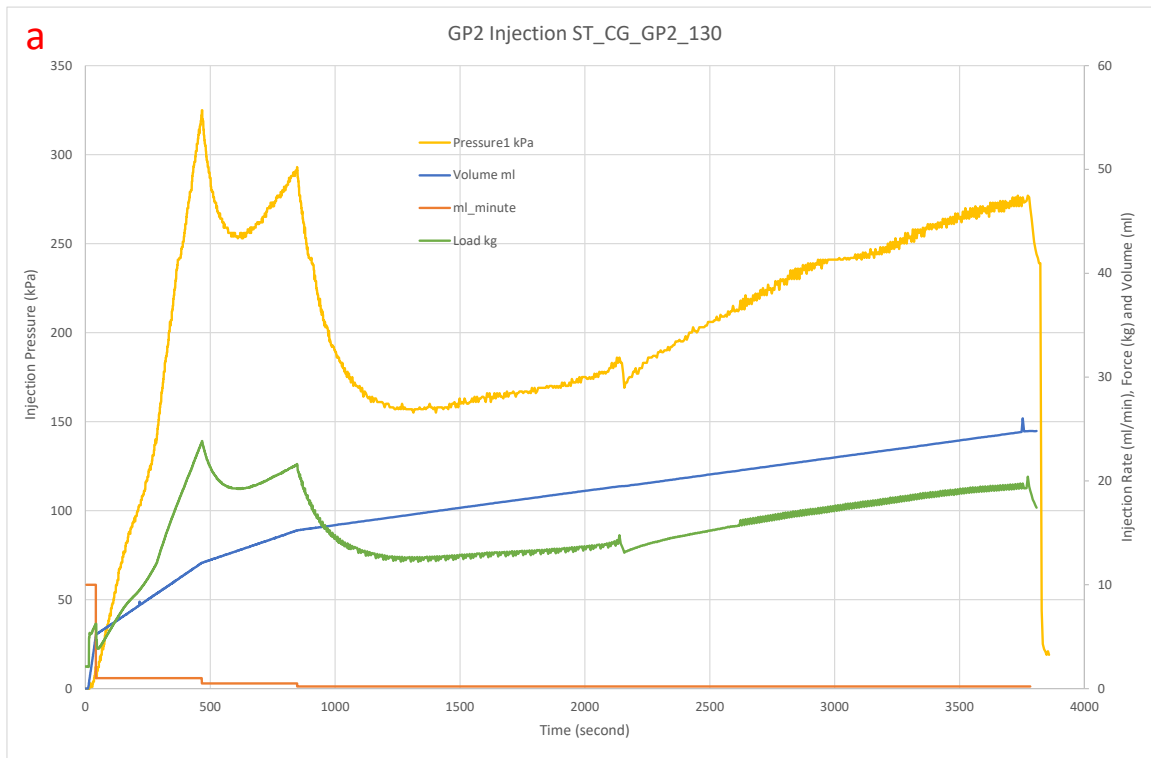


Figure C. 10. Injection test for fracture sample ST_CG_GP2_130, a) Injection pressure, rate, force and volume vs time, and b) Photo of tested sample after shear bonding strength test.

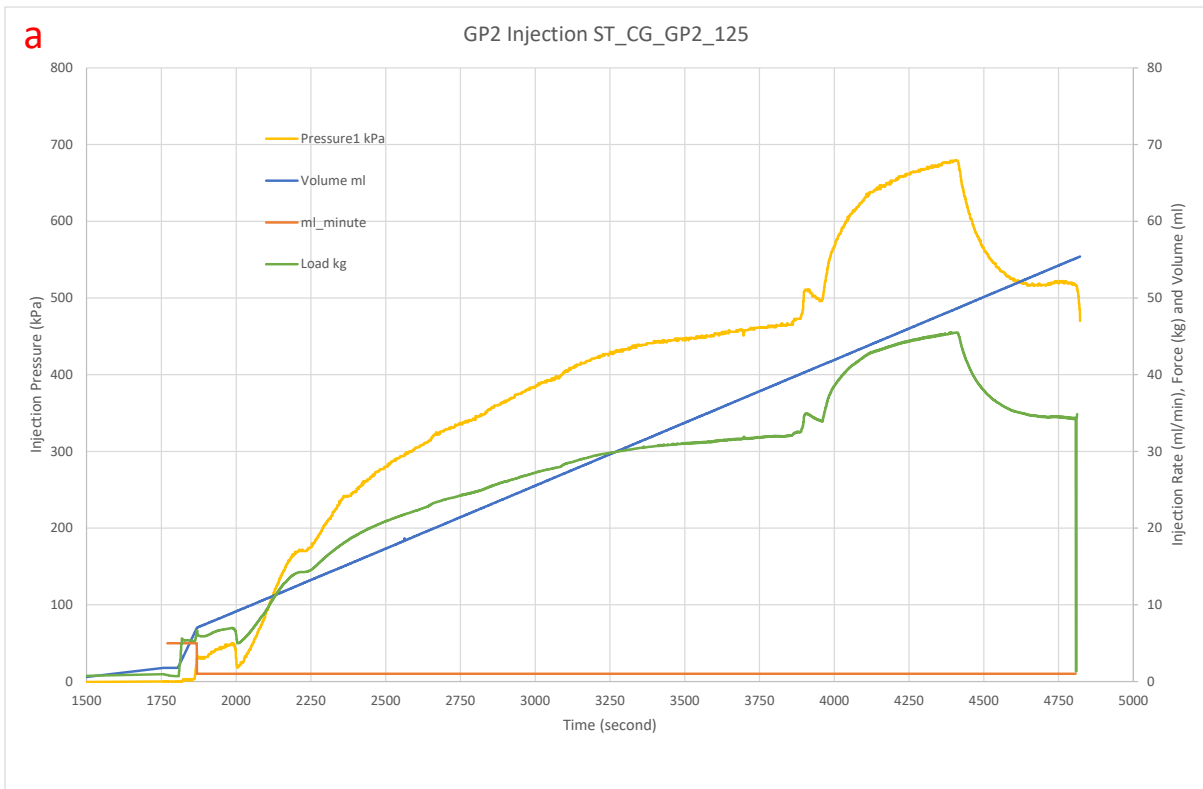


Figure C. 11. Injection test for fracture sample ST_CG_GP2_125, a) Injection pressure, rate, force and volume vs time, and b) Photo of tested sample following shear bonding strength test.

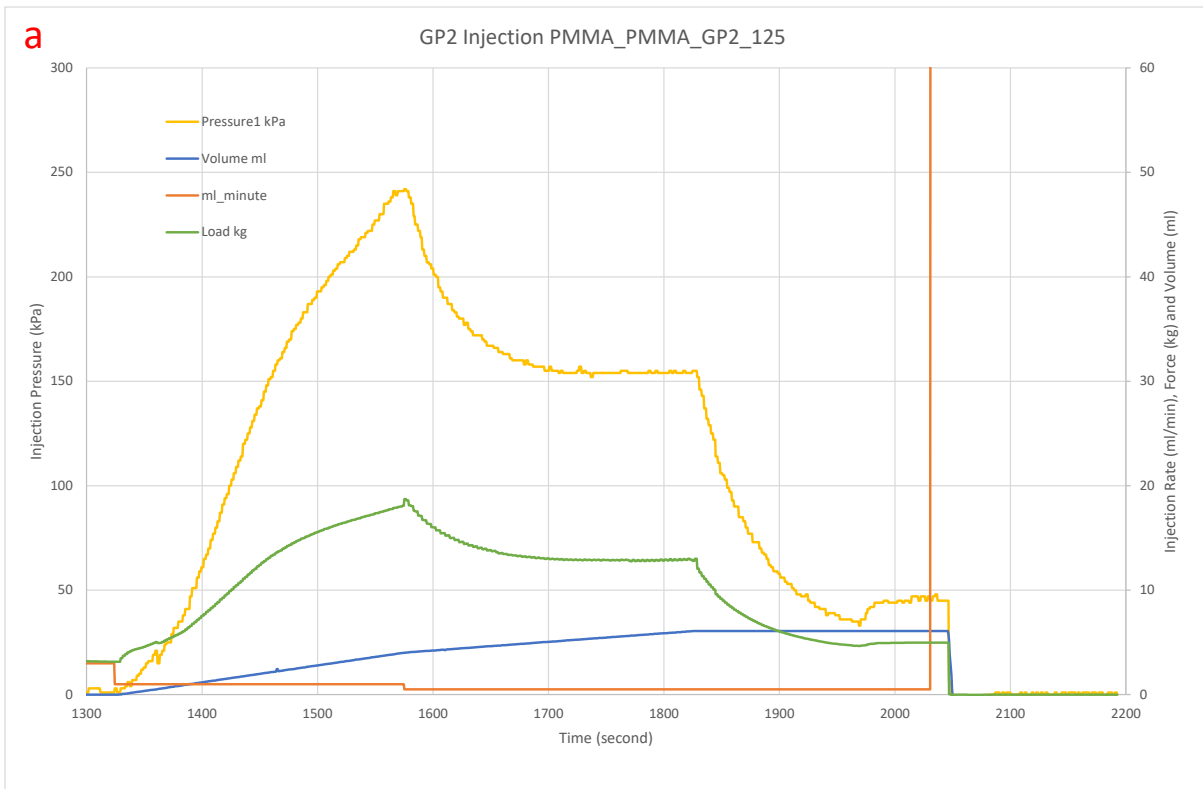


Figure C. 12. Injection test for fracture sample PMMA_PMMA_GP2_125, a) Injection pressure, rate, force and volume vs time, and b) Photo of tested sample.

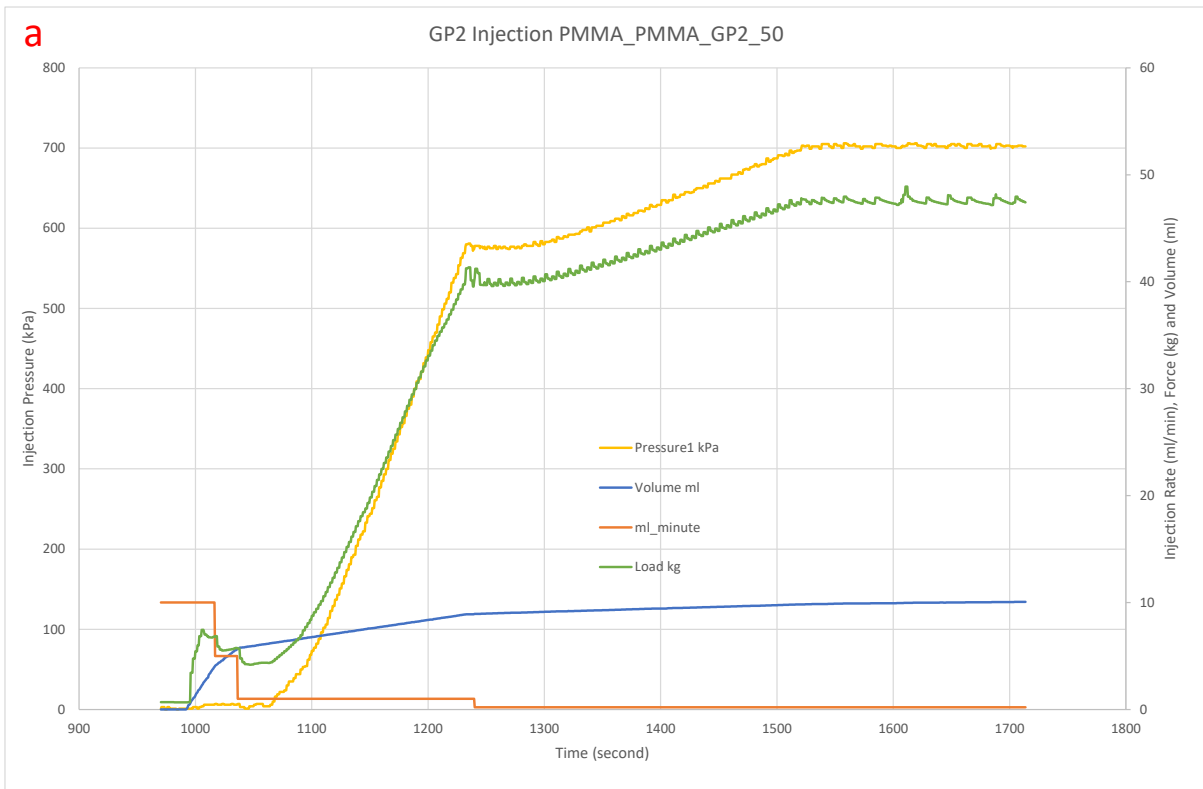


Figure C. 13. Injection test for fracture sample PMMA_PMMA_GP2_50, a) Injection pressure, rate, force and volume vs time, and b) Photo of tested sample.

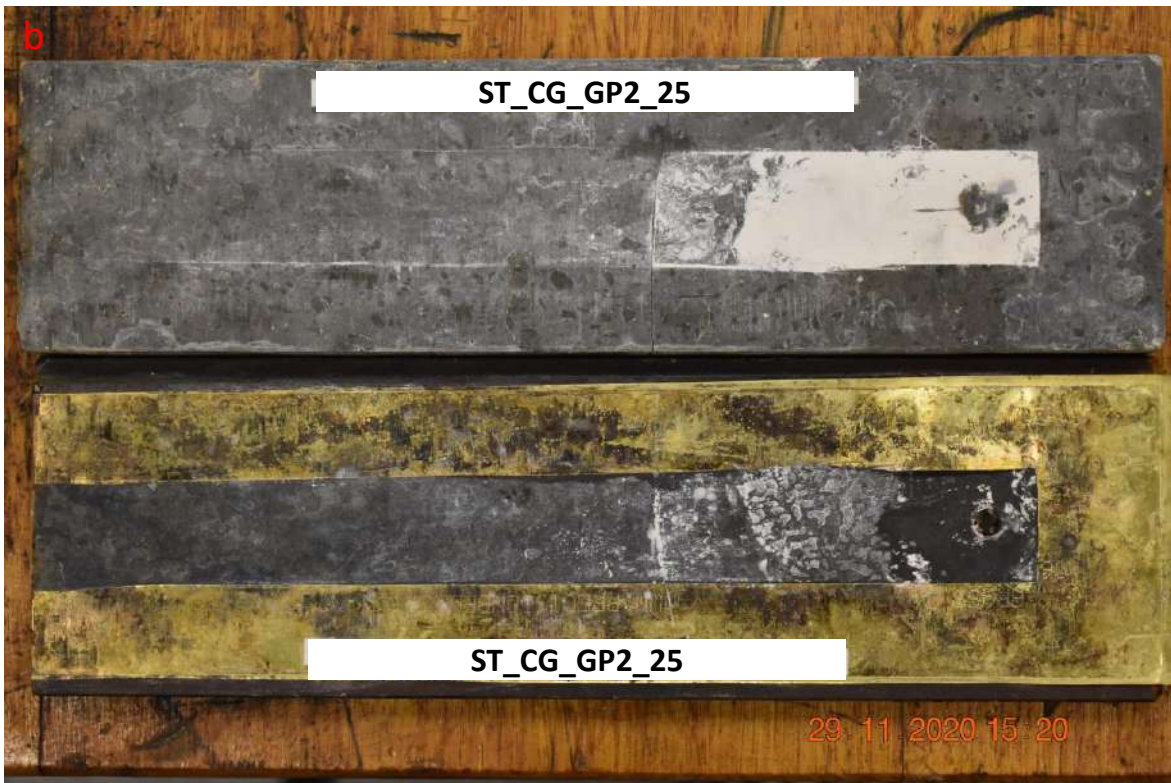
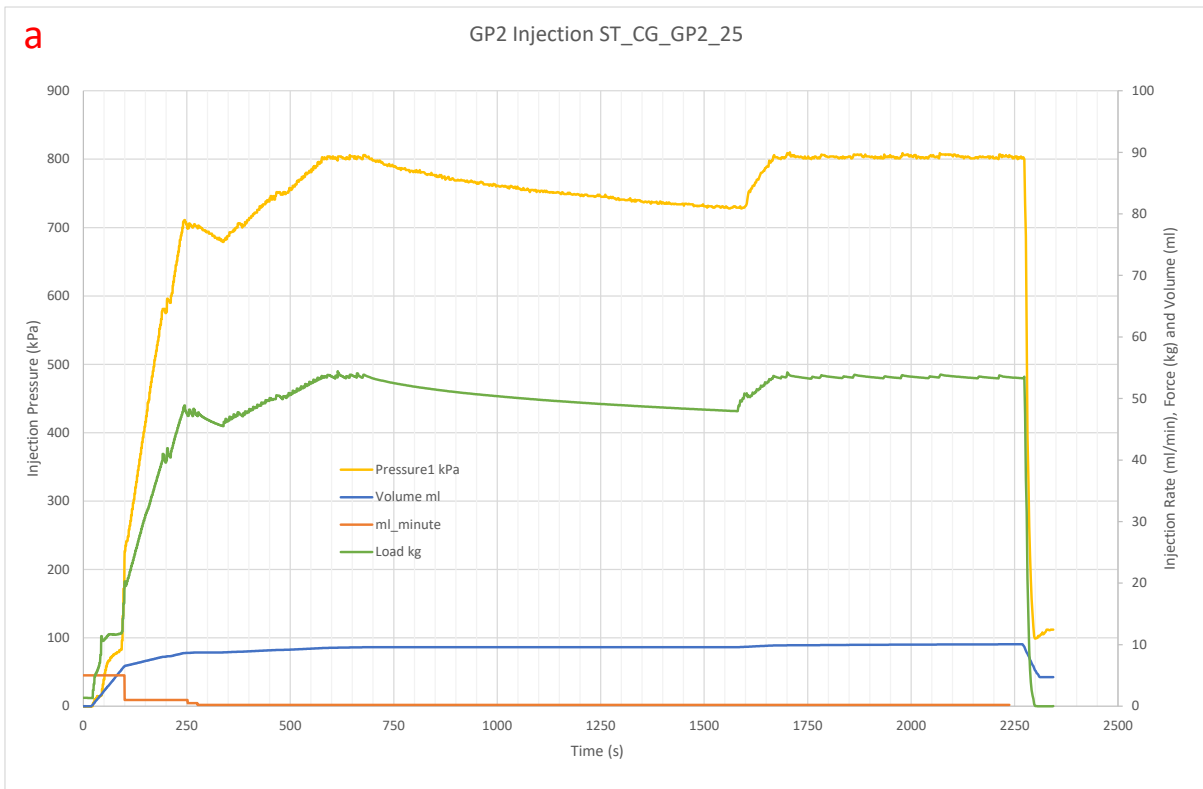


Figure C. 14. Injection test for fracture sample ST_CG_GP2_25, a) Injection pressure, rate, force and volume vs time, and b) Photo of tested sample.

Polymer Resin 010620-1 Injectivity Tests

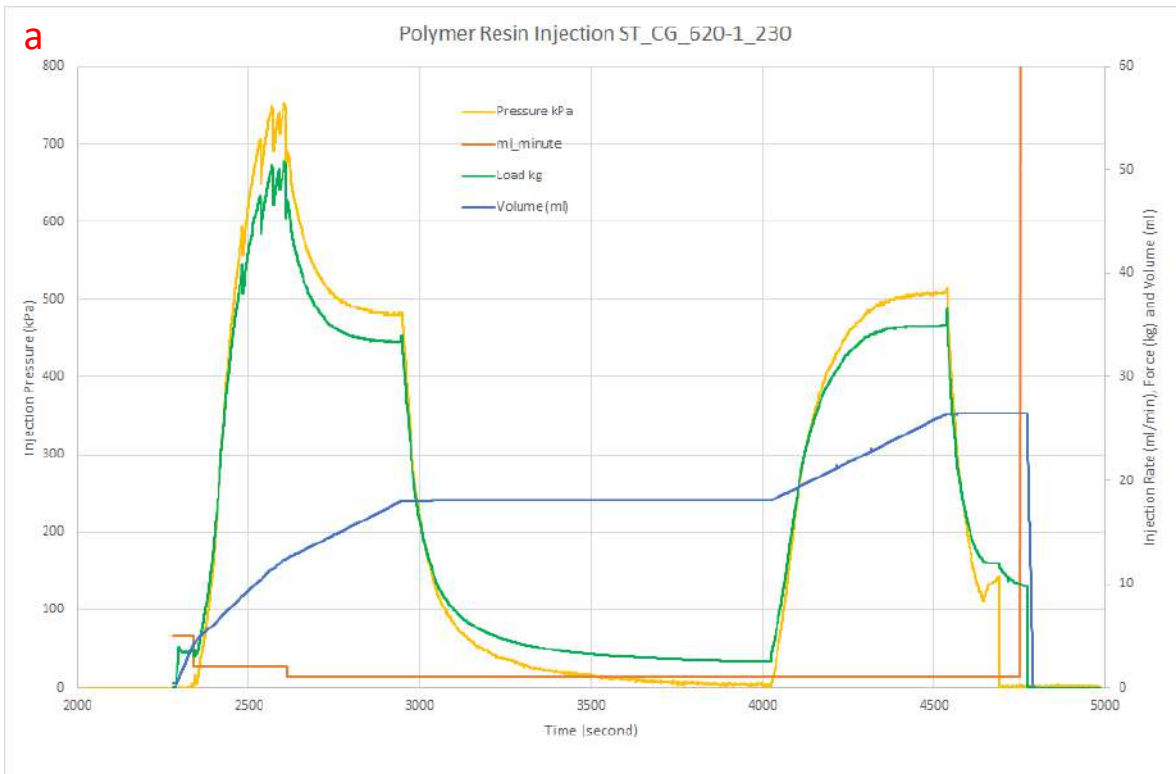


Figure C. 15. Injection test for fracture sample ST_CG_GP_620-1_230, a) Injection pressure, rate, force and volume vs time, and b) Photo of tested sample after shear bonding strength test.

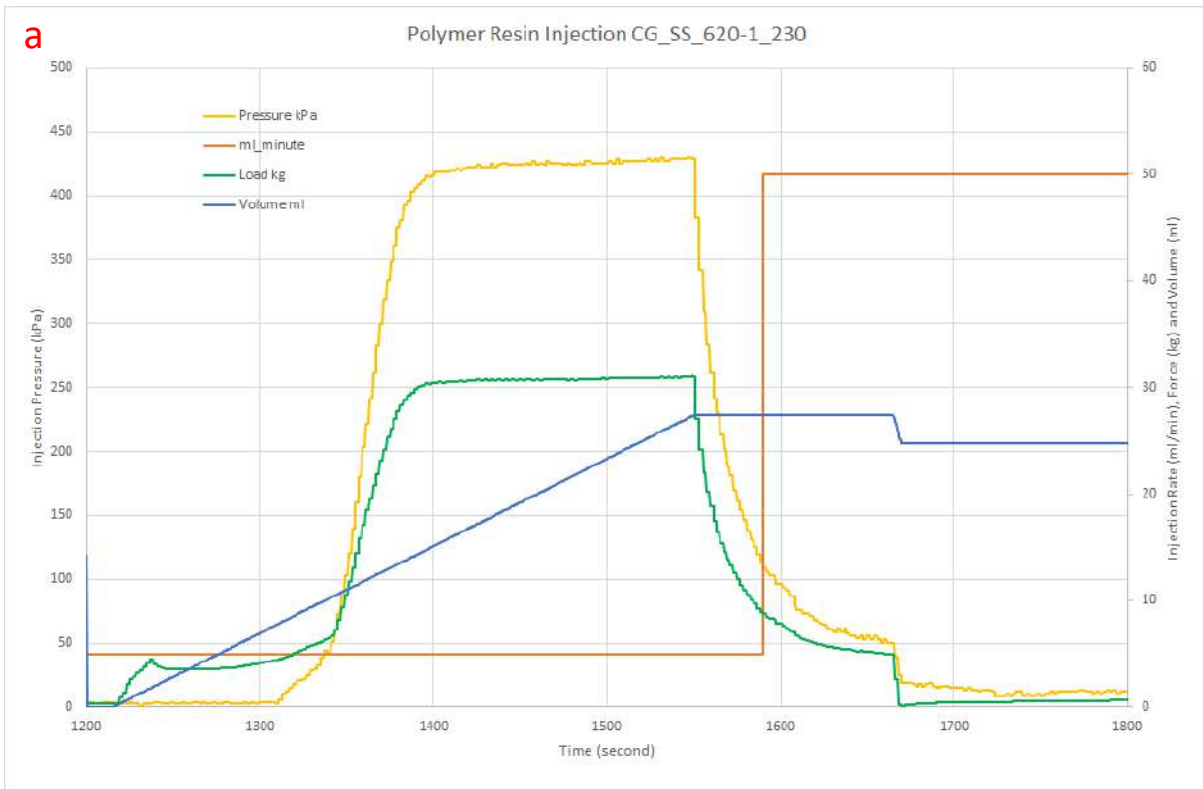


Figure C. 16. Injection test for fracture sample CG_SS_620-1_230, a) Injection pressure, rate, force and volume vs time, and b) Photo of tested sample following shear bonding strength test.

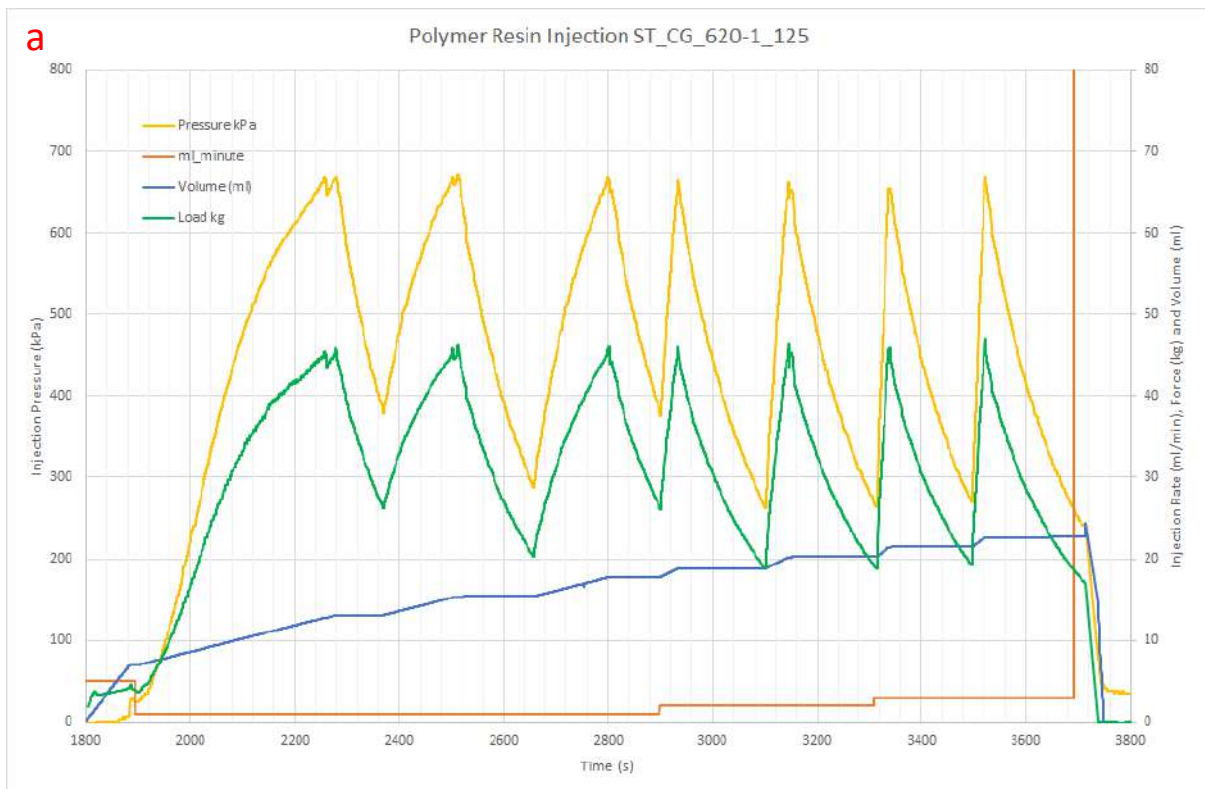


Figure C. 17. Injection test for fracture sample ST_CG_620-1_125, a) Injection pressure, rate, force and volume vs time, and b) Photo of tested sample. Note a layer of plastic tape covered the fracture surface to hold the cement slab together, which was broken following the shear bonding test.

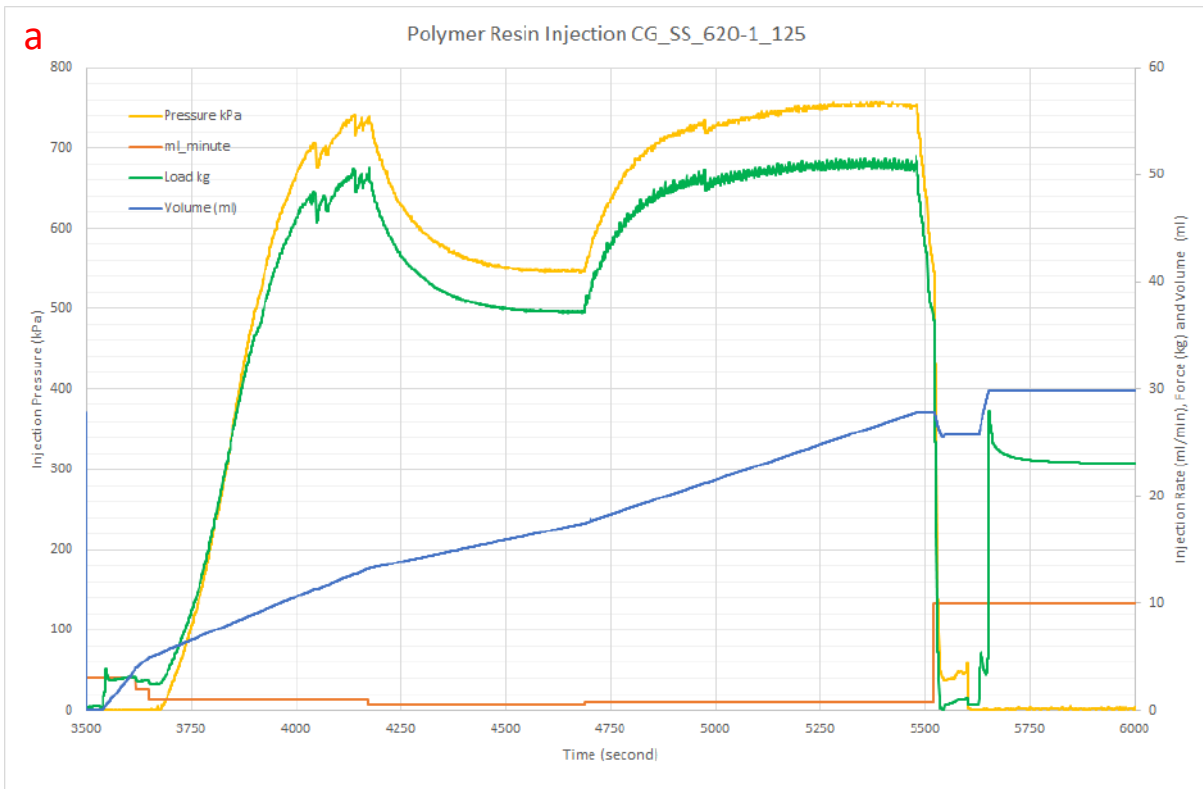


Figure C. 18. Injection test for fracture sample CG_SS_620-1_125, a) Injection pressure, rate, force and volume vs time, and b) Photo of tested sample.

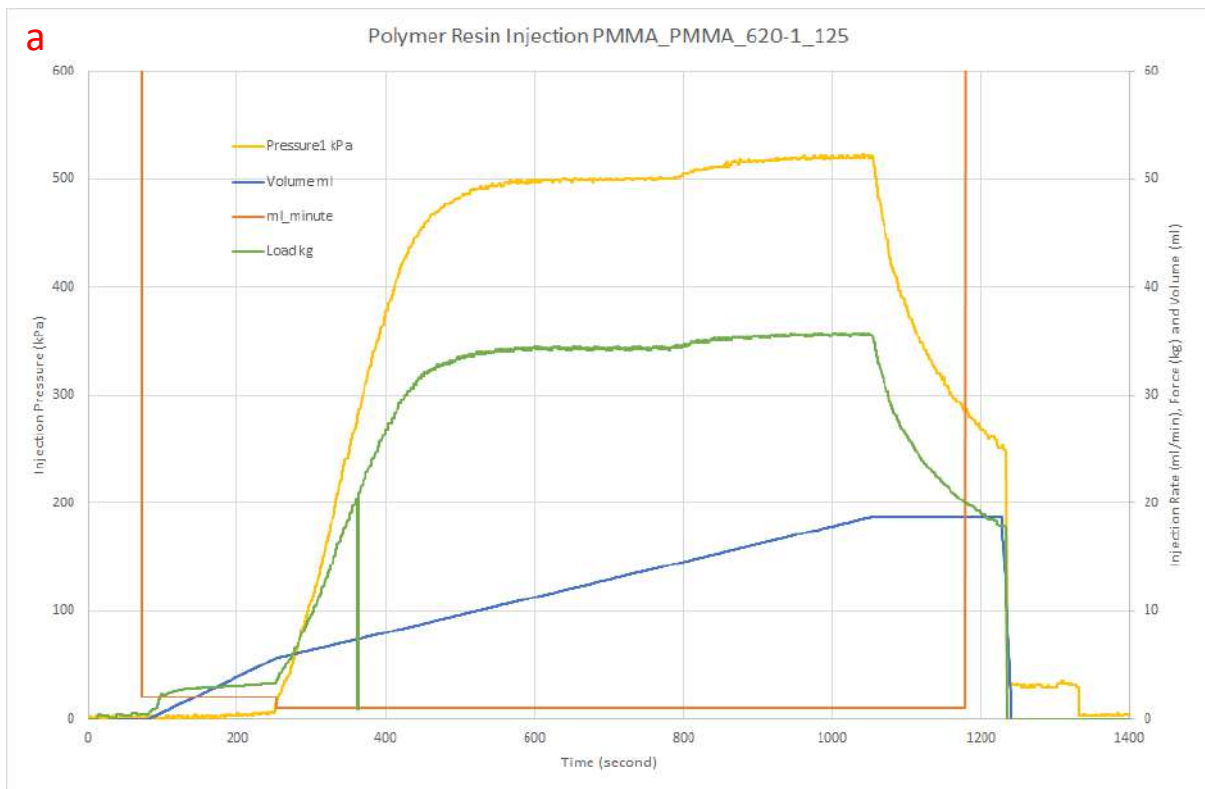


Figure C. 19. Injection test for fracture sample PMMA_PMMA_620-1_125, a) Injection pressure, rate, force and volume vs time, and b) Photo of tested sample.

Polymer Resin 010620-5 Injectivity Tests

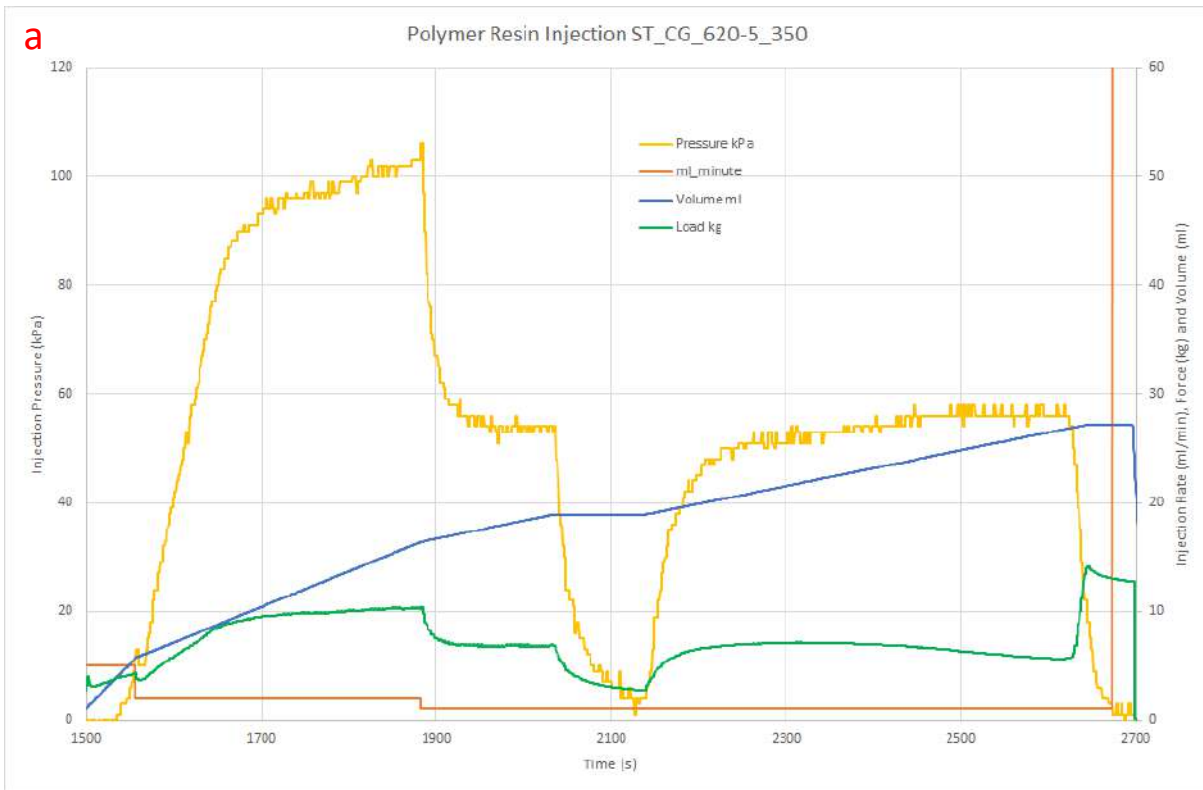


Figure C. 20. Injection test for fracture sample ST_CG_620-5_350, a) Injection pressure, rate, force and volume vs time, and b) Photo of tested sample after shear bonding strength test.

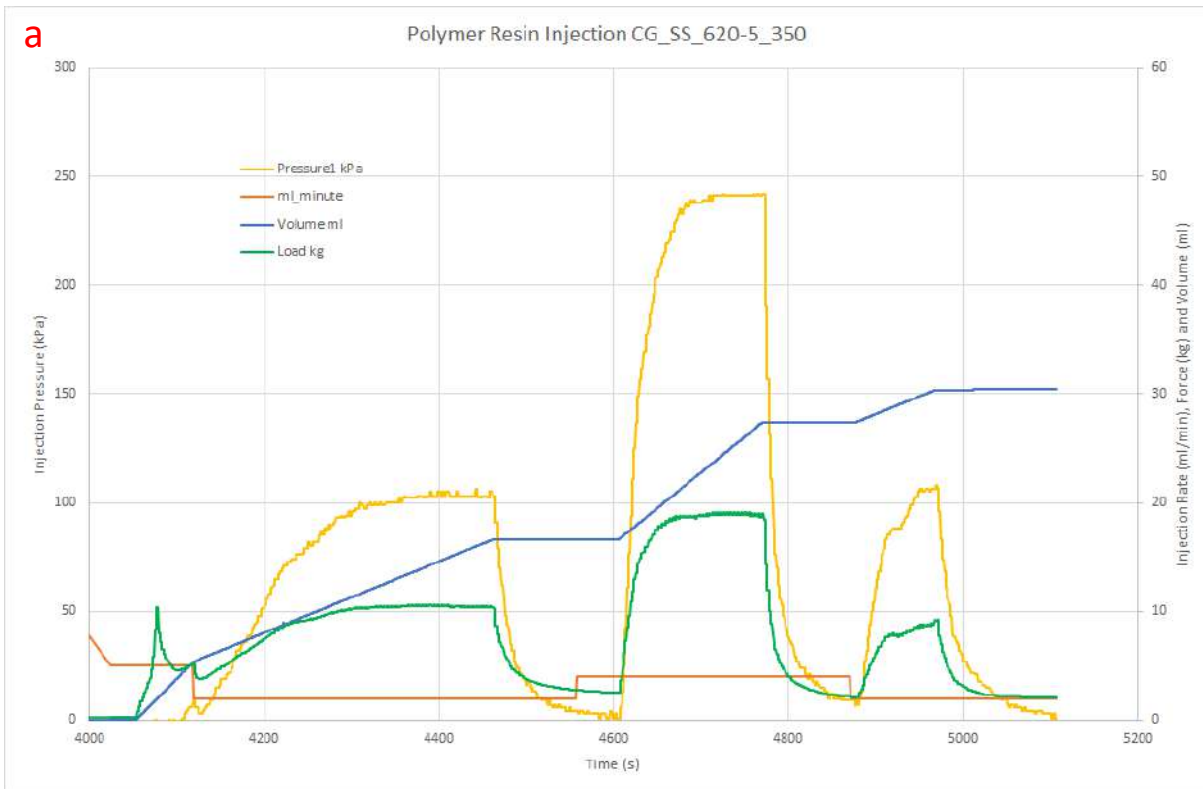


Figure C. 21. Injection test for fracture sample CG_SS_620-5_350, a) Injection pressure, rate, force and volume vs time, and b) Photo of tested sample following shear bonding strength test.

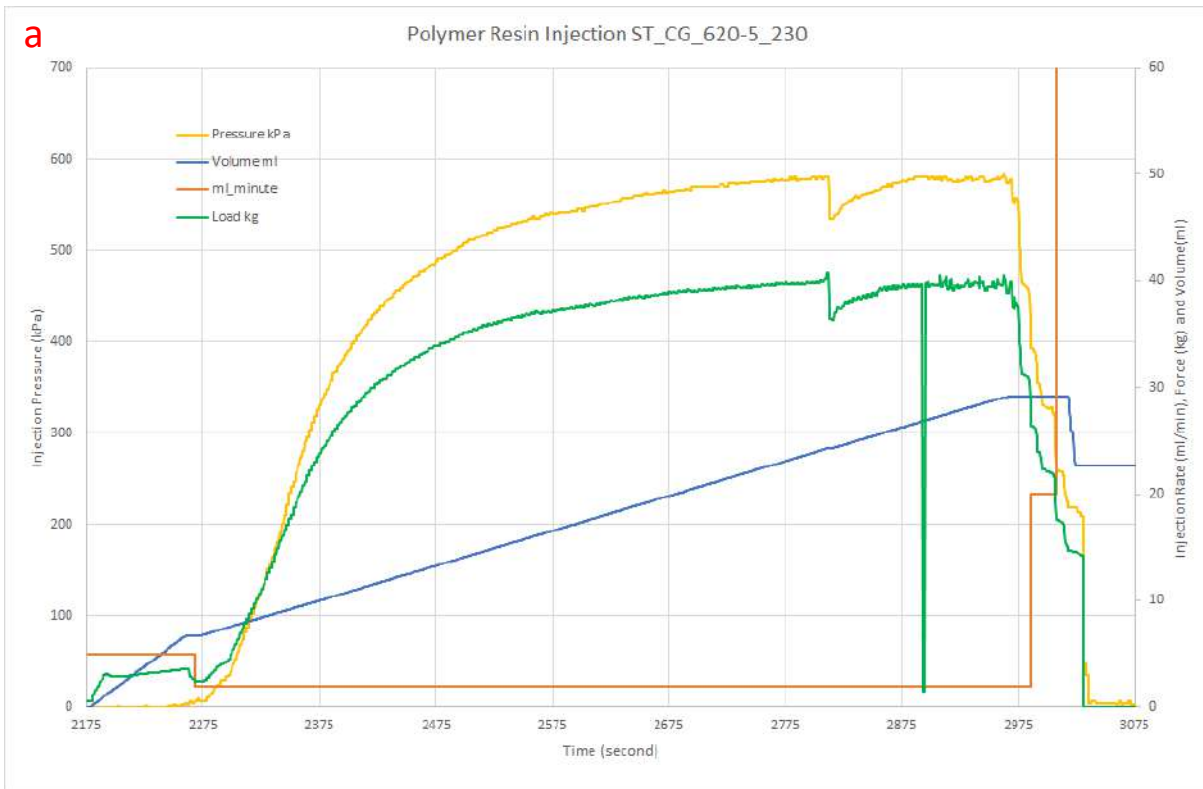


Figure C. 22. Injection test for fracture sample ST_CG_620-5_230, a) Injection pressure, rate, force and volume vs time, and b) Photo of tested sample after shear bonding strength test.

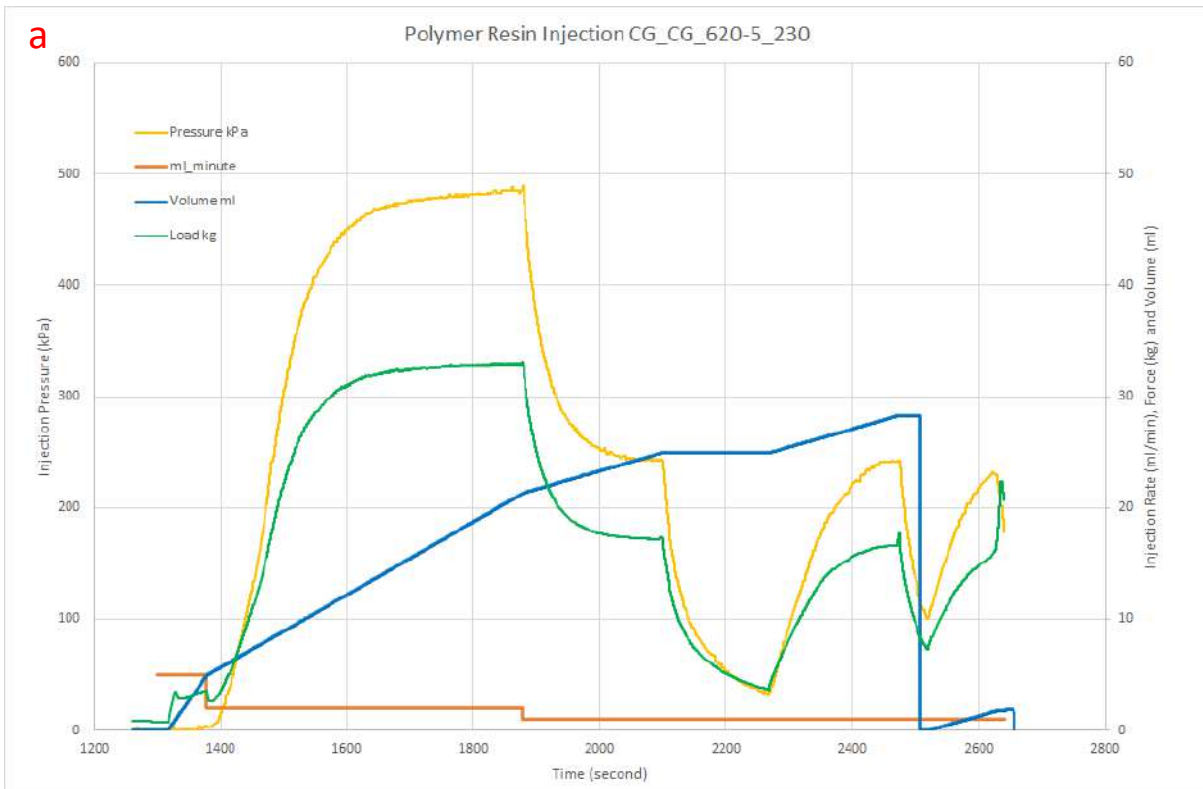


Figure C. 23. Injection test for fracture sample CG_ CG_620-5_230, a) Injection pressure, rate, force and volume vs time, and b) Photo of tested sample.



Figure C. 20. Injection test for fracture sample ST_CG_620-5_350, a) Injection pressure, rate, force and volume vs time, and b) Photo of tested sample after shear bonding strength test.

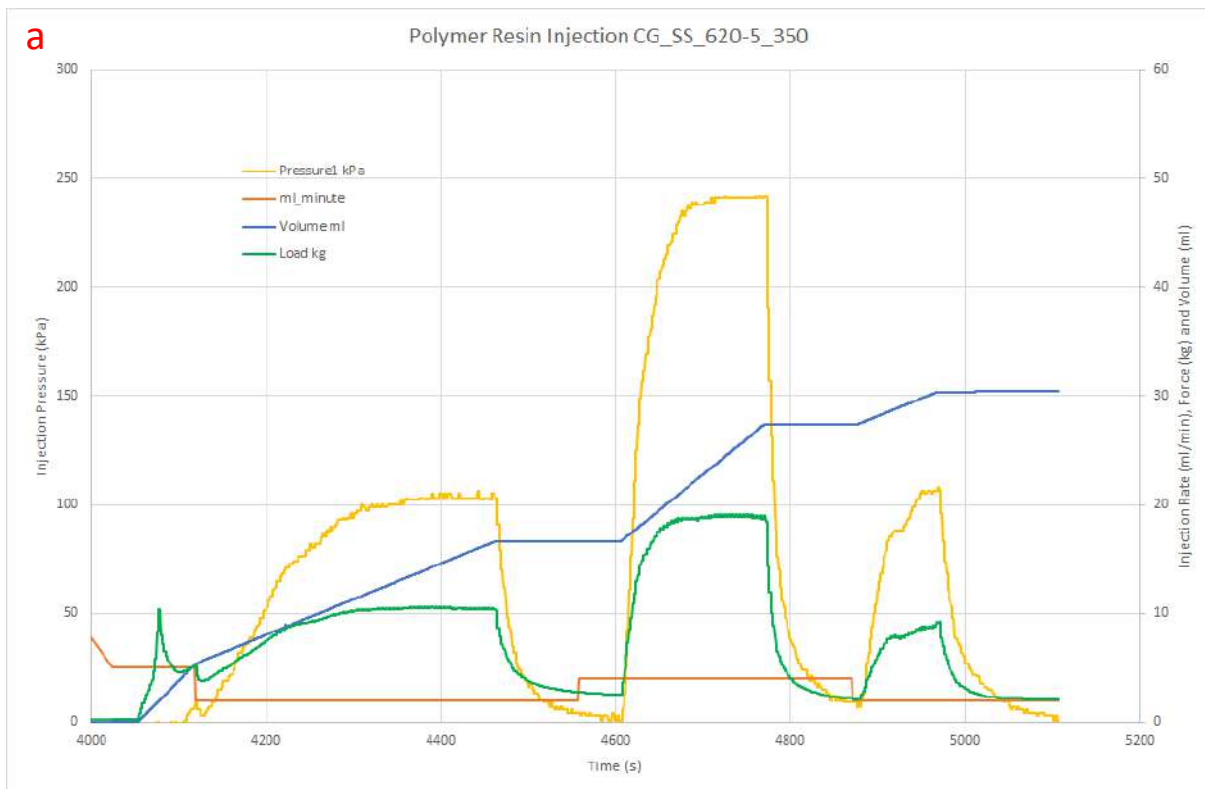


Figure C. 21. Injection test for fracture sample CG_SS_620-5_350, a) Injection pressure, rate, force and volume vs time, and b) Photo of tested sample following shear bonding strength test.



Figure C. 22. Injection test for fracture sample ST_CG_620-5_230, a) Injection pressure, rate, force and volume vs time, and b) Photo of tested sample after shear bonding strength test.

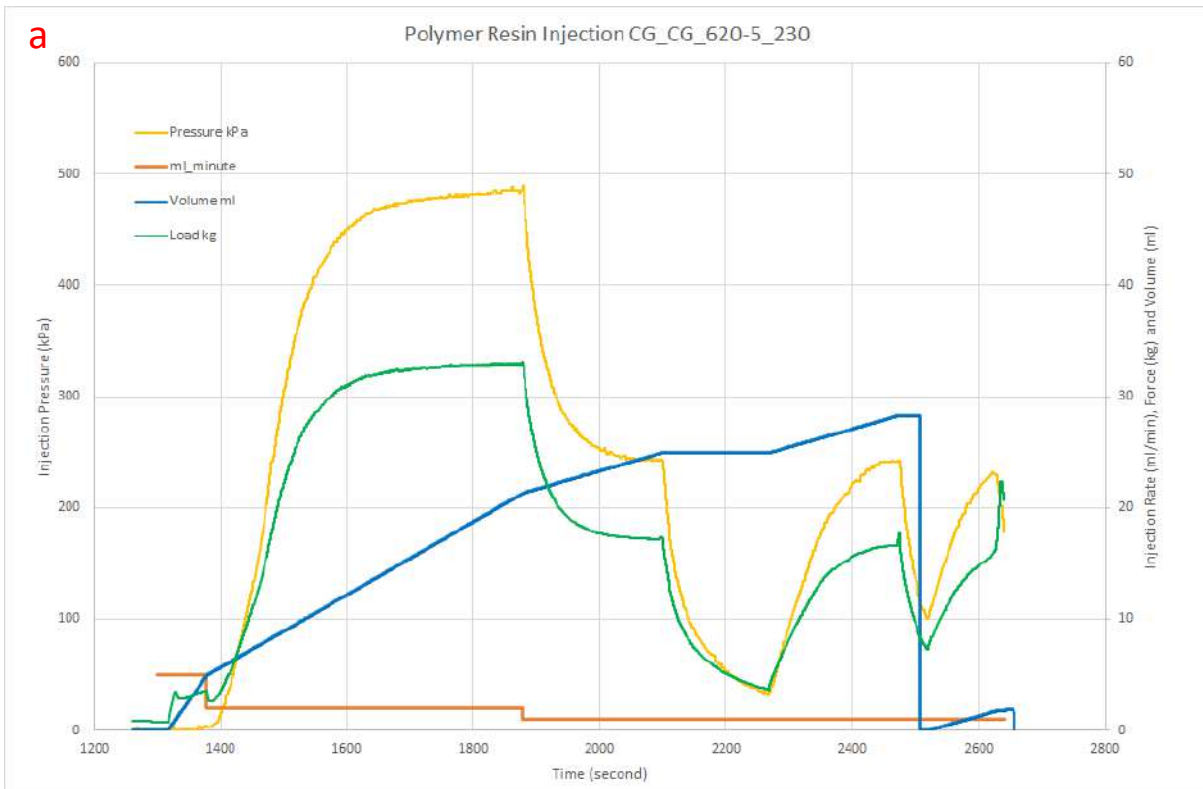


Figure C. 23. Injection test for fracture sample CG_620-5_230, a) Injection pressure, rate, force and volume vs time, and b) Photo of tested sample.

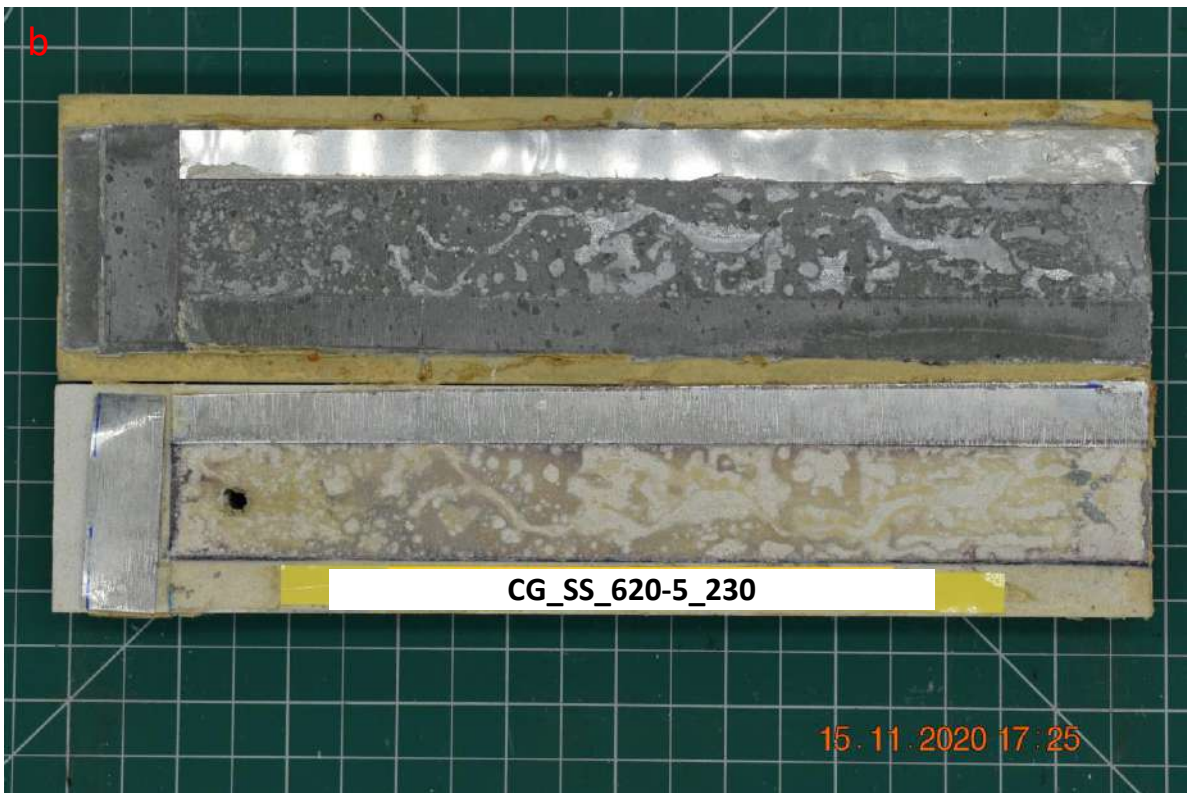
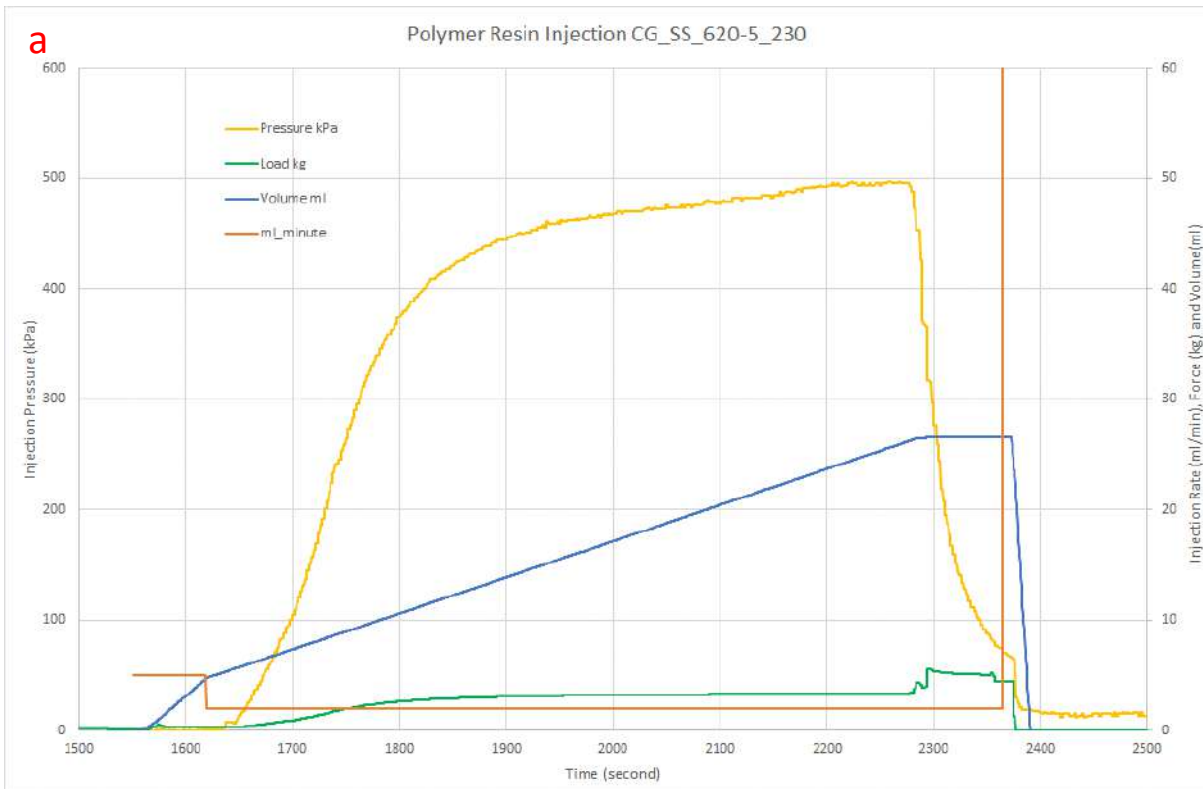


Figure C. 24. Injection test for fracture sample CG_SS_620-5_230, a) Injection pressure, rate, force and volume vs time, and b) Photo of tested sample.

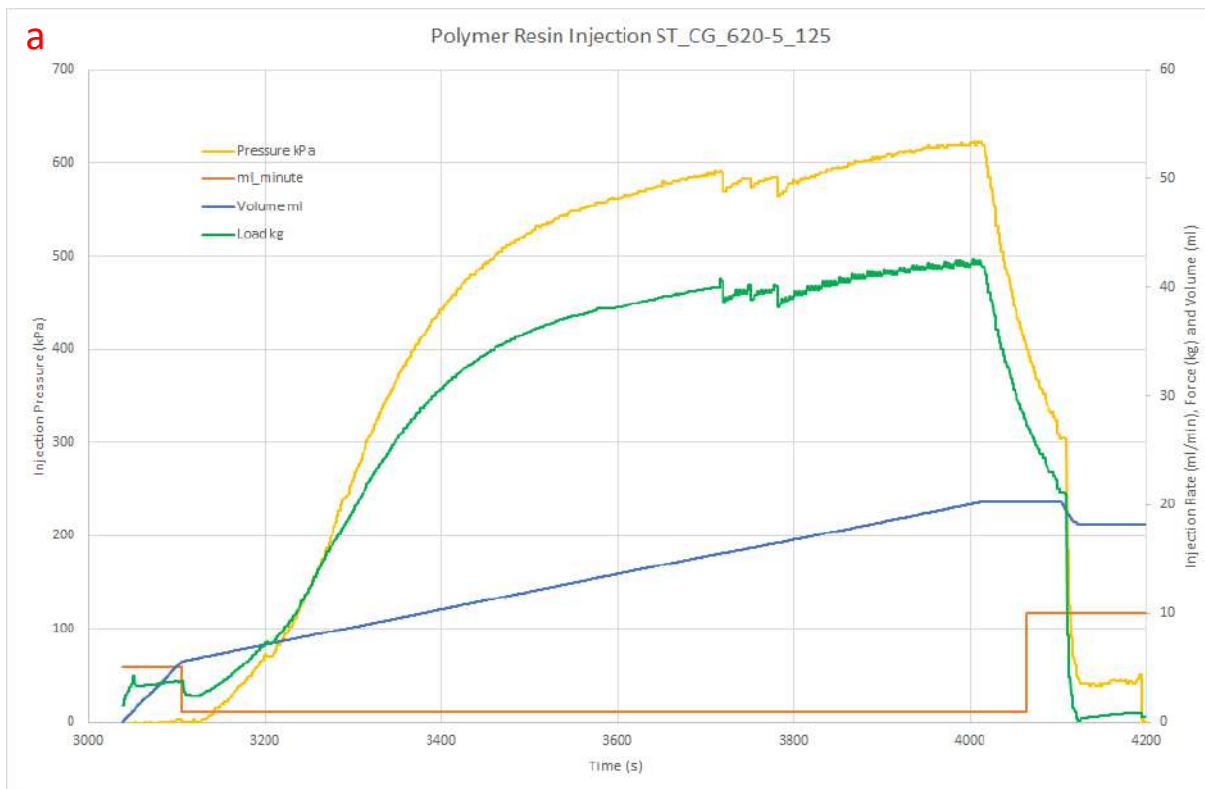


Figure C. 25. Injection test for fracture sample ST_CG_620-5_125, a) Injection pressure, rate, force and volume vs time, and b) Photo of tested sample.

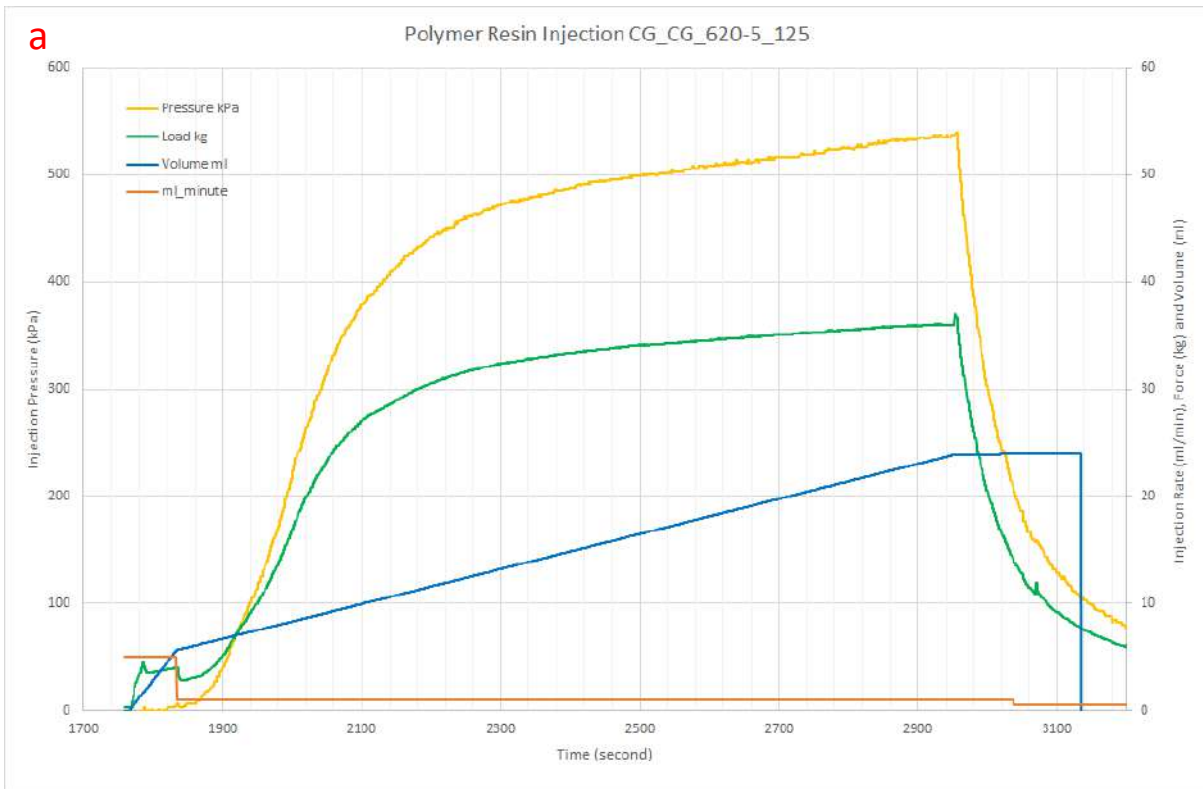


Figure C. 26. Injection test for fracture sample CG_620-5_125, a) Injection pressure, rate, force and volume vs time, and b) Photo of tested sample.

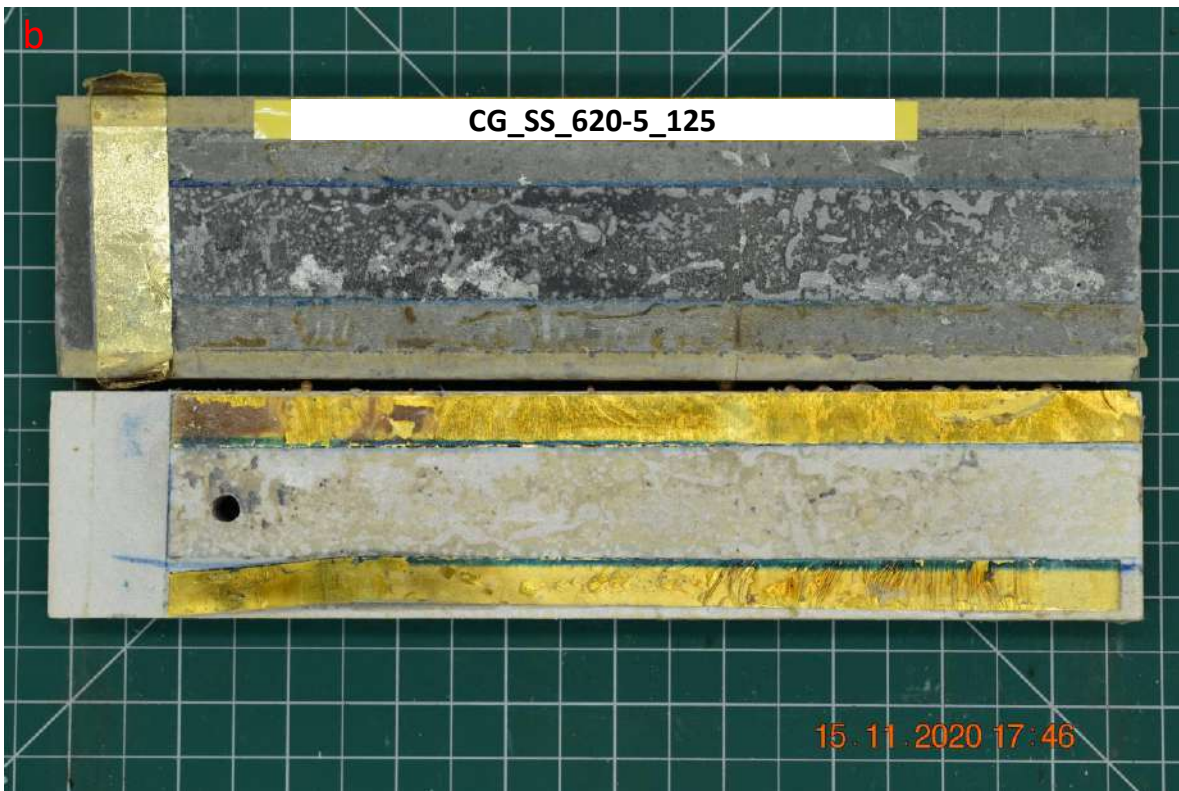
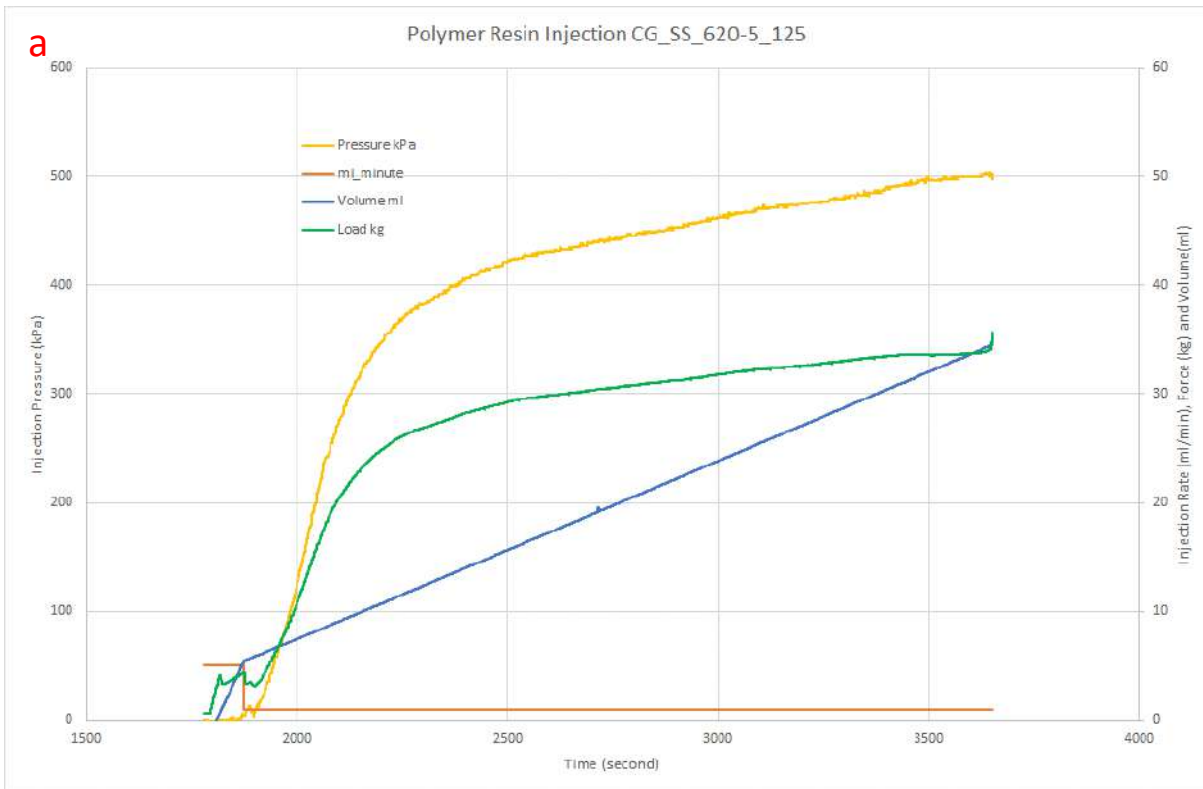


Figure C. 27. Injection test for fracture sample CG_SS_620-5_125, a) Injection pressure, rate, force and volume vs time, and b) Photo of tested sample.

Polymer Resin 020720-3 Injectivity Tests

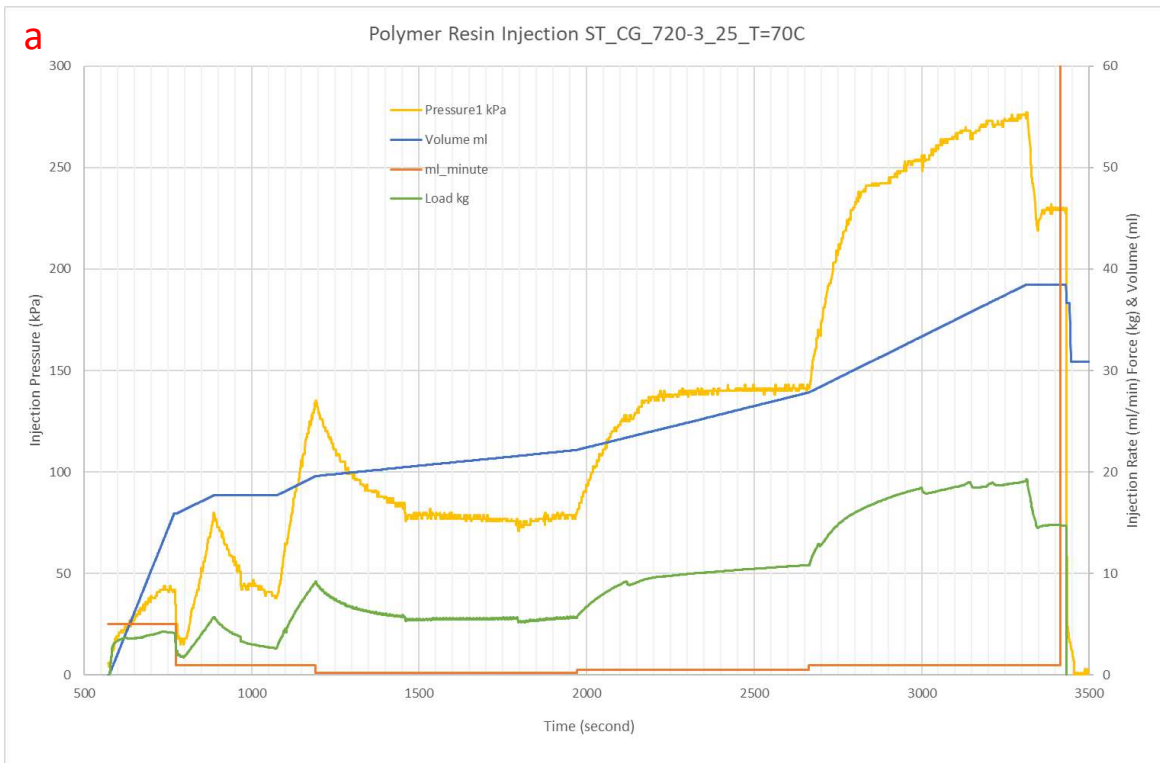


Figure C. 28. Injection test for fracture sample ST_CG_720-3_25_T=70C, a) Injection pressure, rate, force and volume vs time, and b) Photo of tested sample after shear bonding strength test.

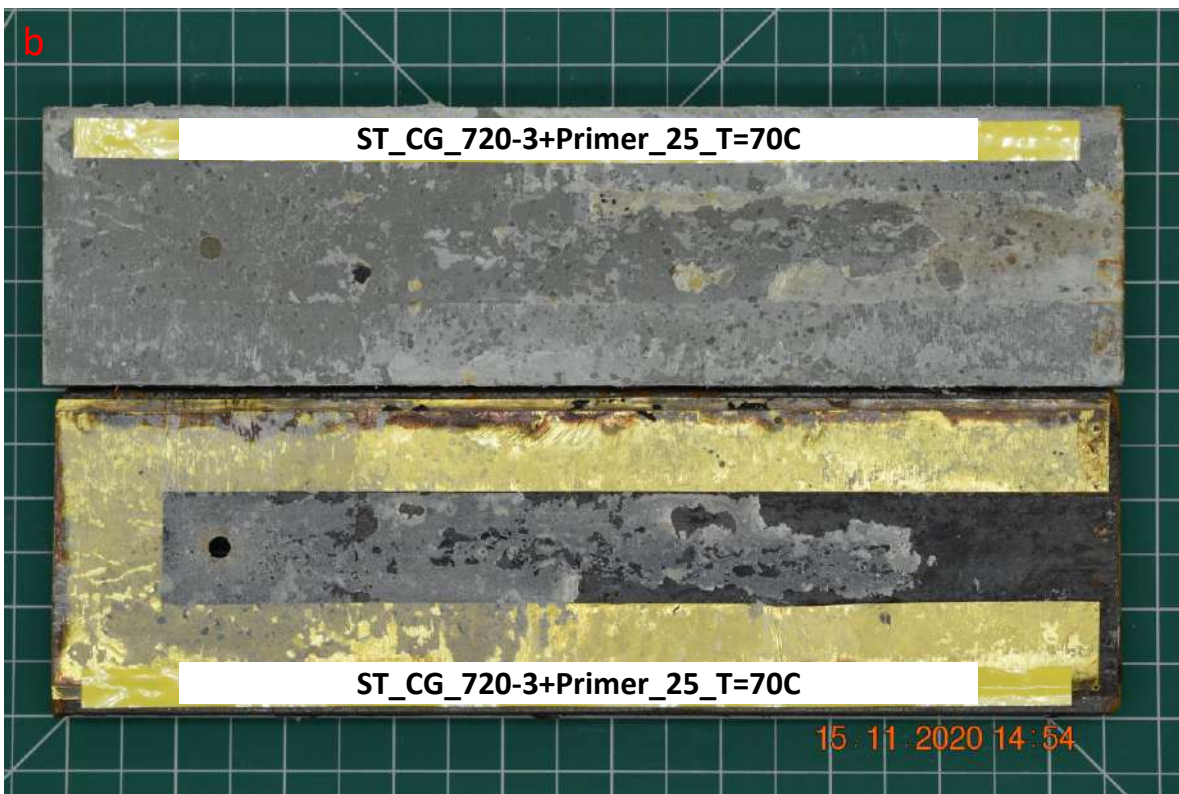
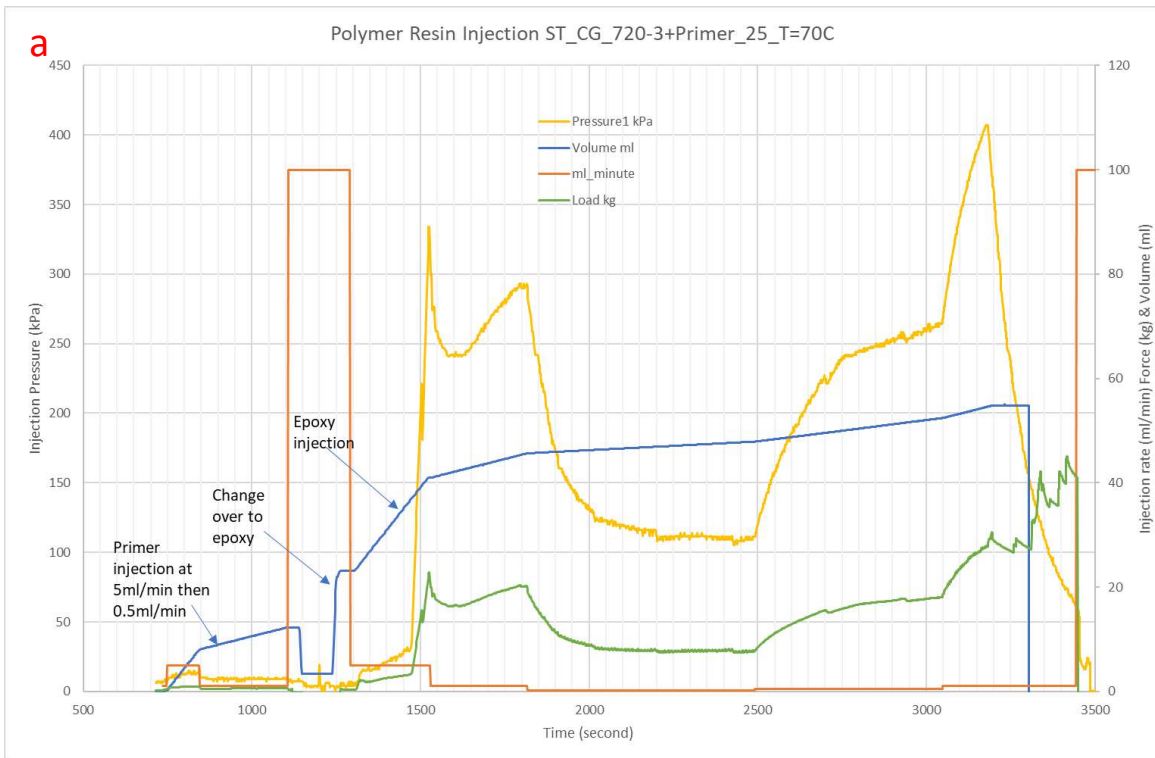


Figure C. 29. Injection test for fracture sample ST_CG_720-3+Primer_25_T=70C, a) Injection pressure, rate, force and volume vs time, and b) Photo of tested sample following shear bonding strength test.

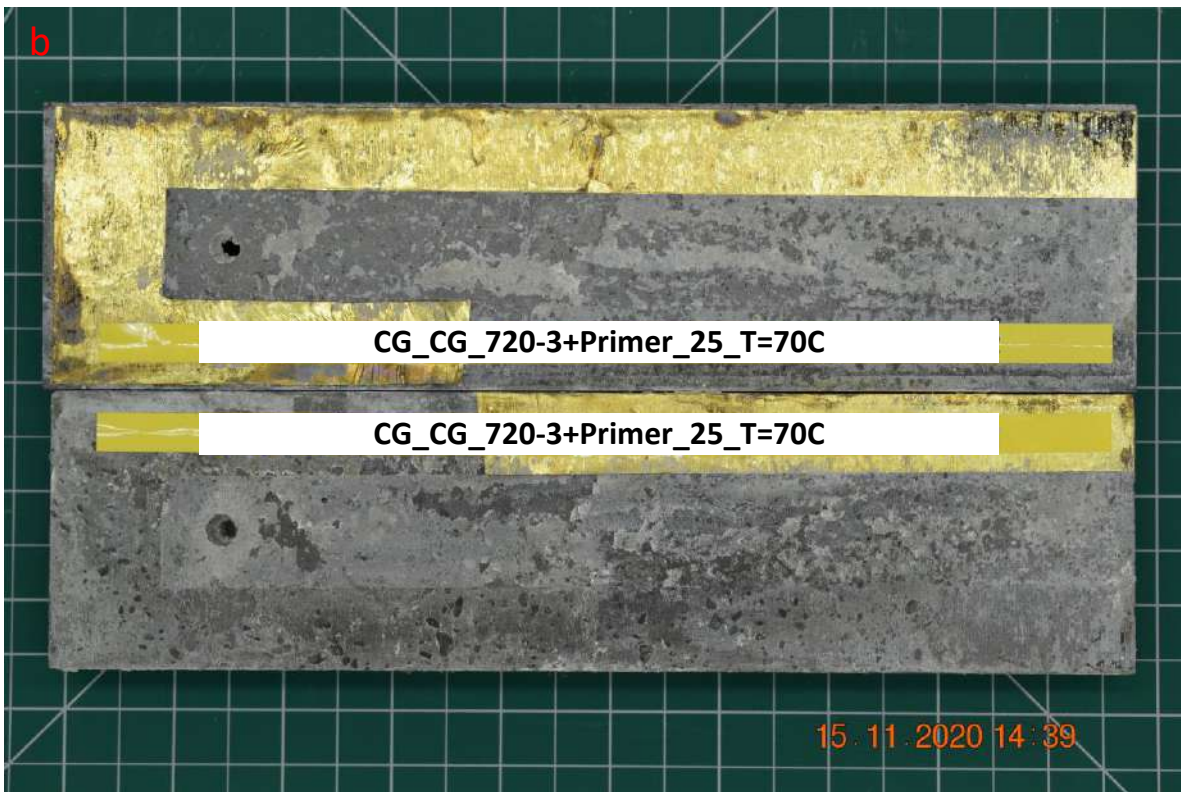
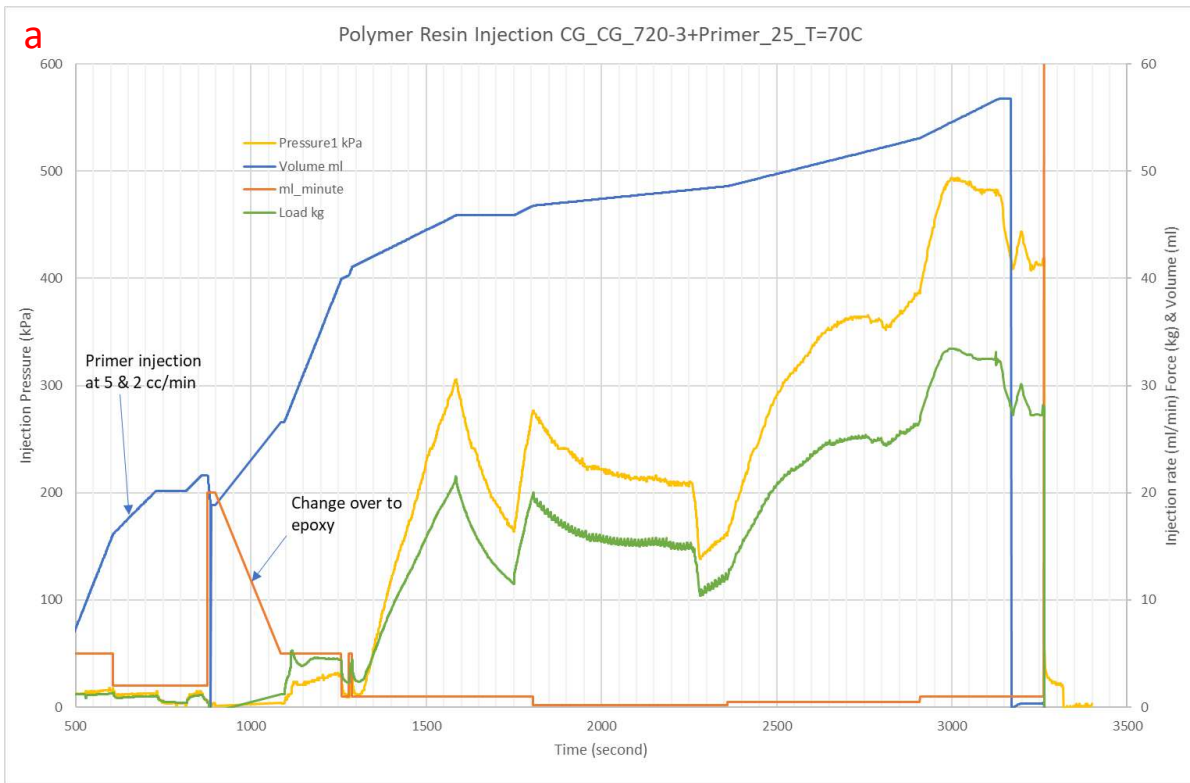


Figure C. 30. Injection test for fracture sample CG.CG_720-3+Primer_25_T=70C, a) Injection pressure, rate, force and volume vs time, and b) Photo of tested sample.

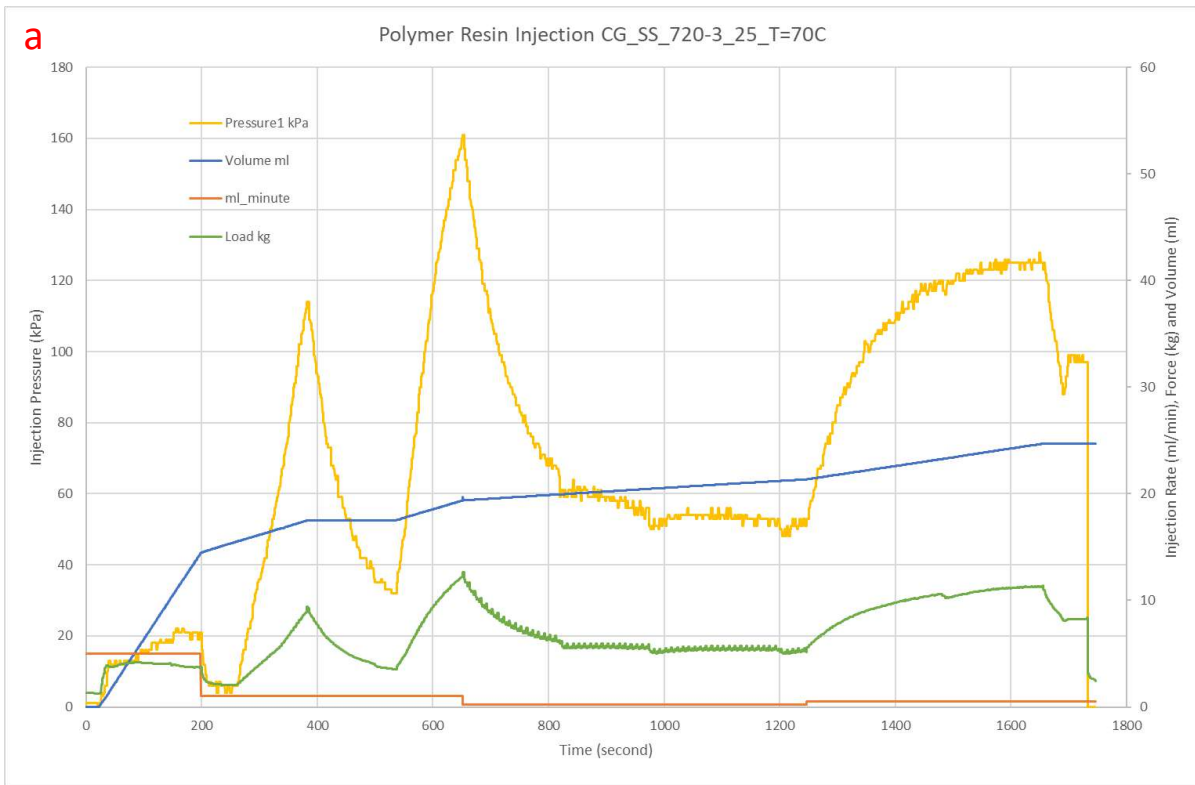


Figure C. 31. Injection test for fracture sample CG_SS_720-3_25_T=70C, a) Injection pressure, rate, force and volume vs time, and b) Photo of tested sample.

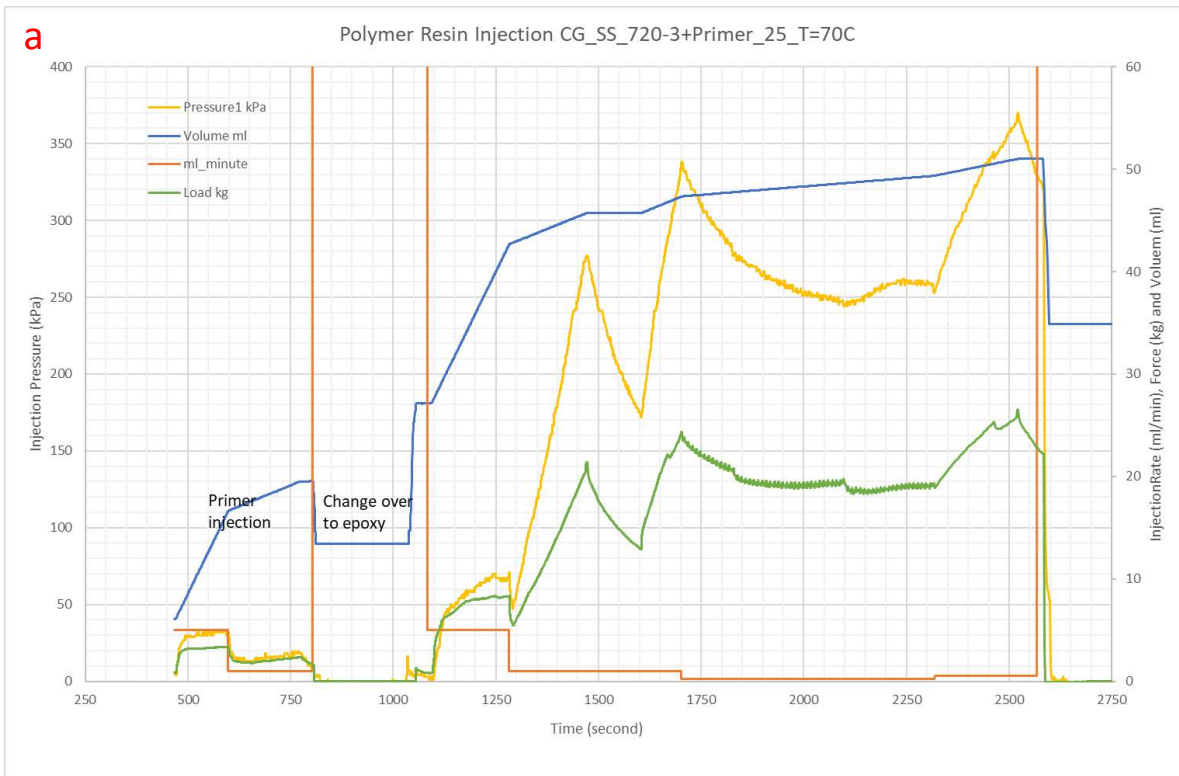


Figure C. 32. Injection test for fracture sample CG_SS_720-3+Primer_25_T=70C, a) Injection pressure, rate, force and volume vs time, and b) Photo of tested sample.

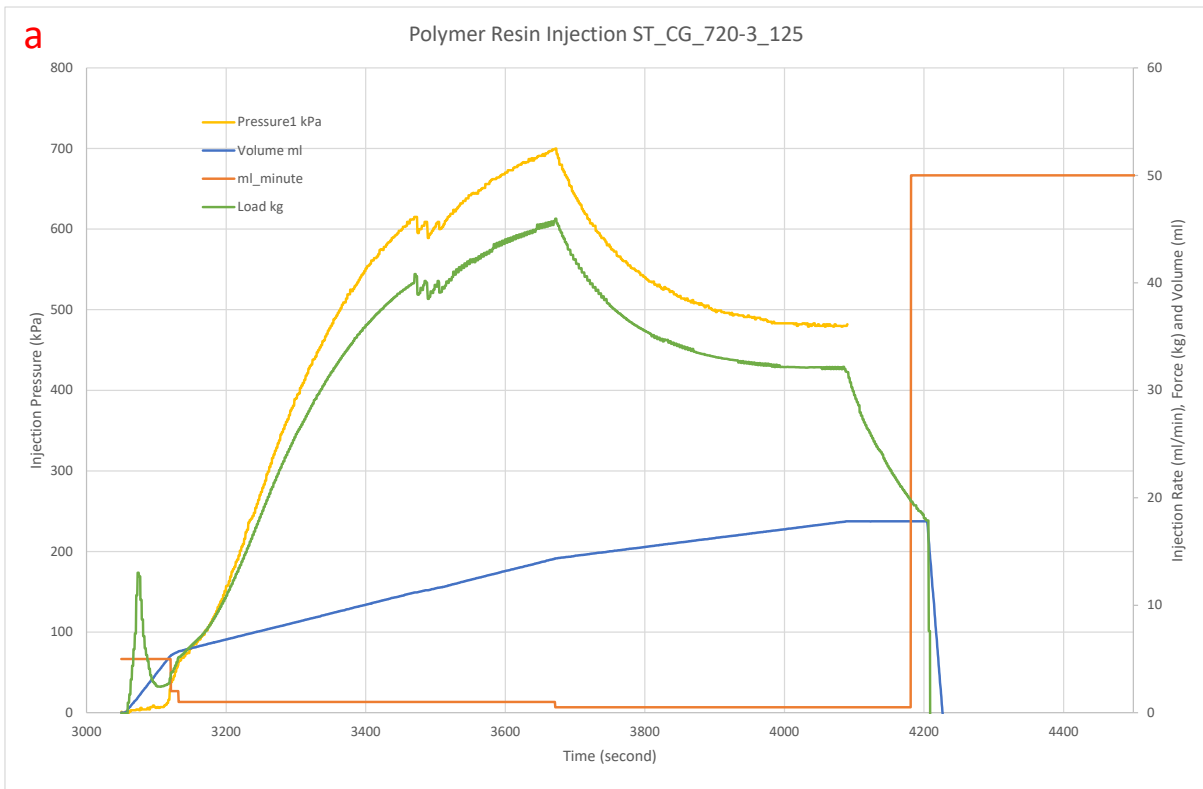


Figure C. 33. Injection test for fracture sample ST_CG_720-3_125, a) Injection pressure, rate, force and volume vs time, and b) Photo of tested sample.

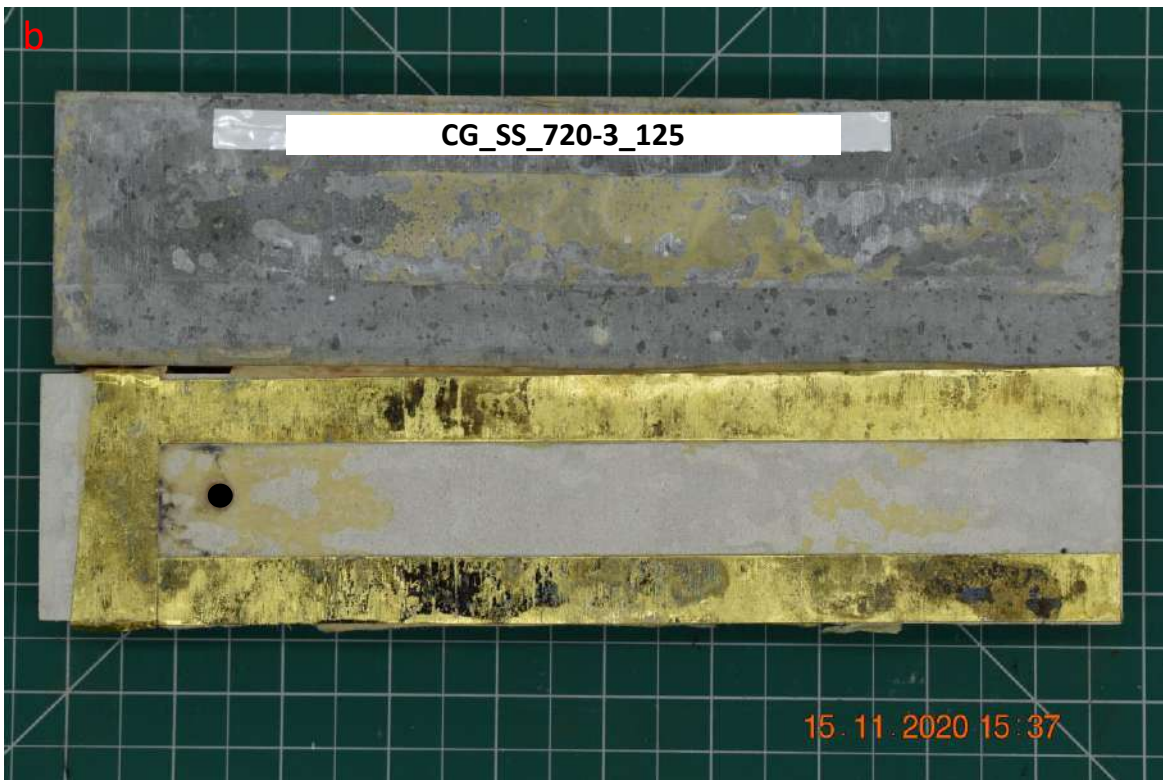
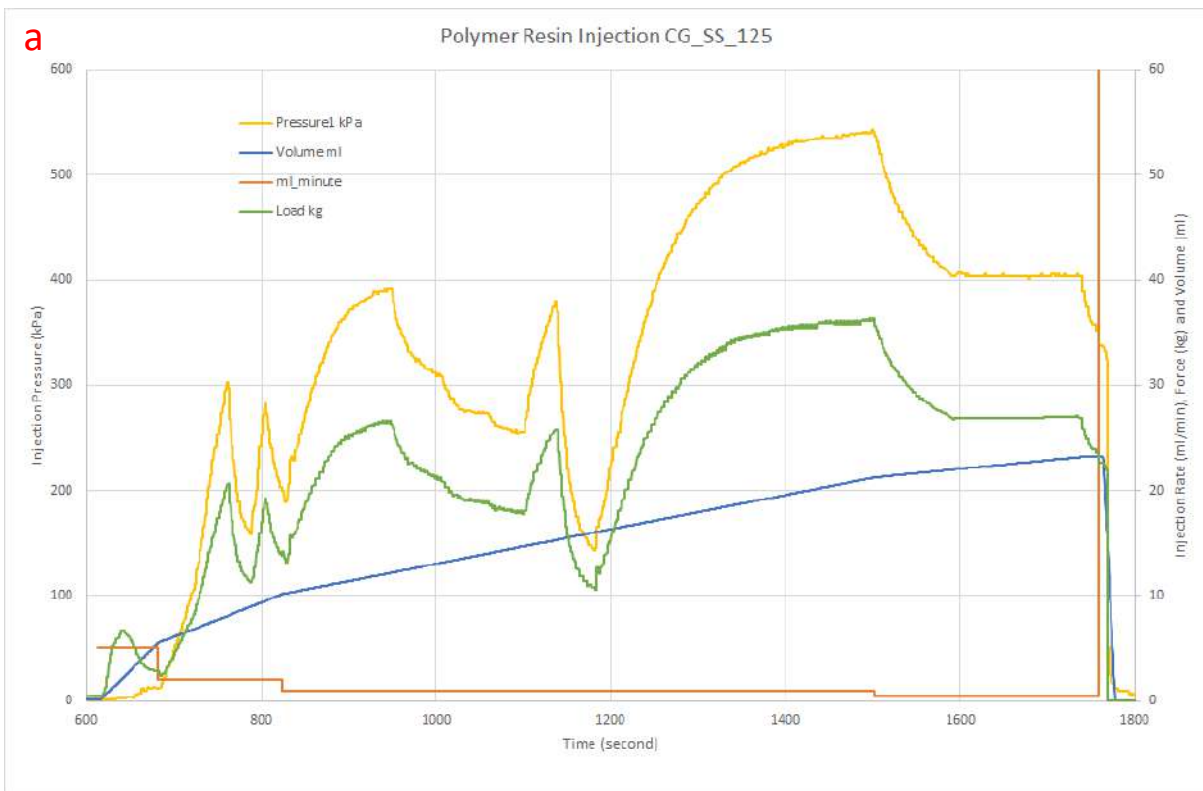


Figure C. 34. Injection test for fracture sample CG_SS_720-3_125, a) Injection pressure, rate, force and volume vs time, and b) Photo of tested sample.

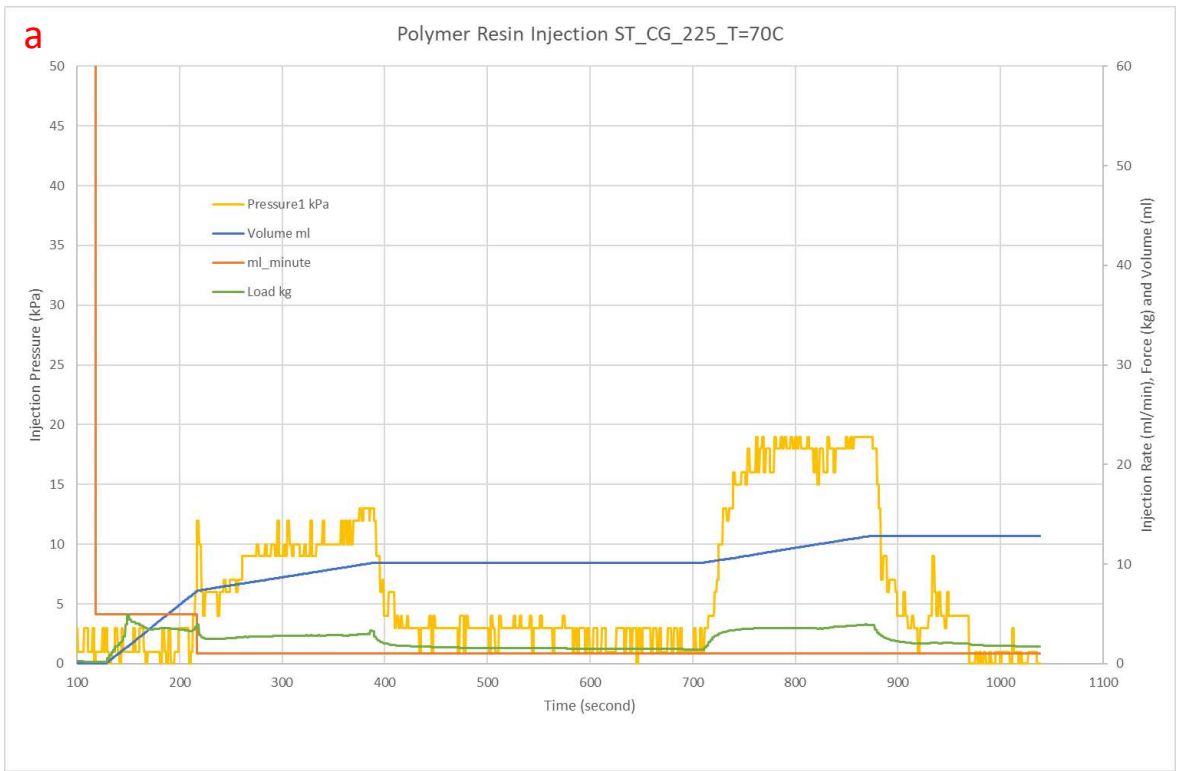


Figure C. 35. Injection test for fracture sample ST_CG_720-3_225_T=70C, a) Injection pressure, rate, force and volume vs time, and b) Photo of tested sample.

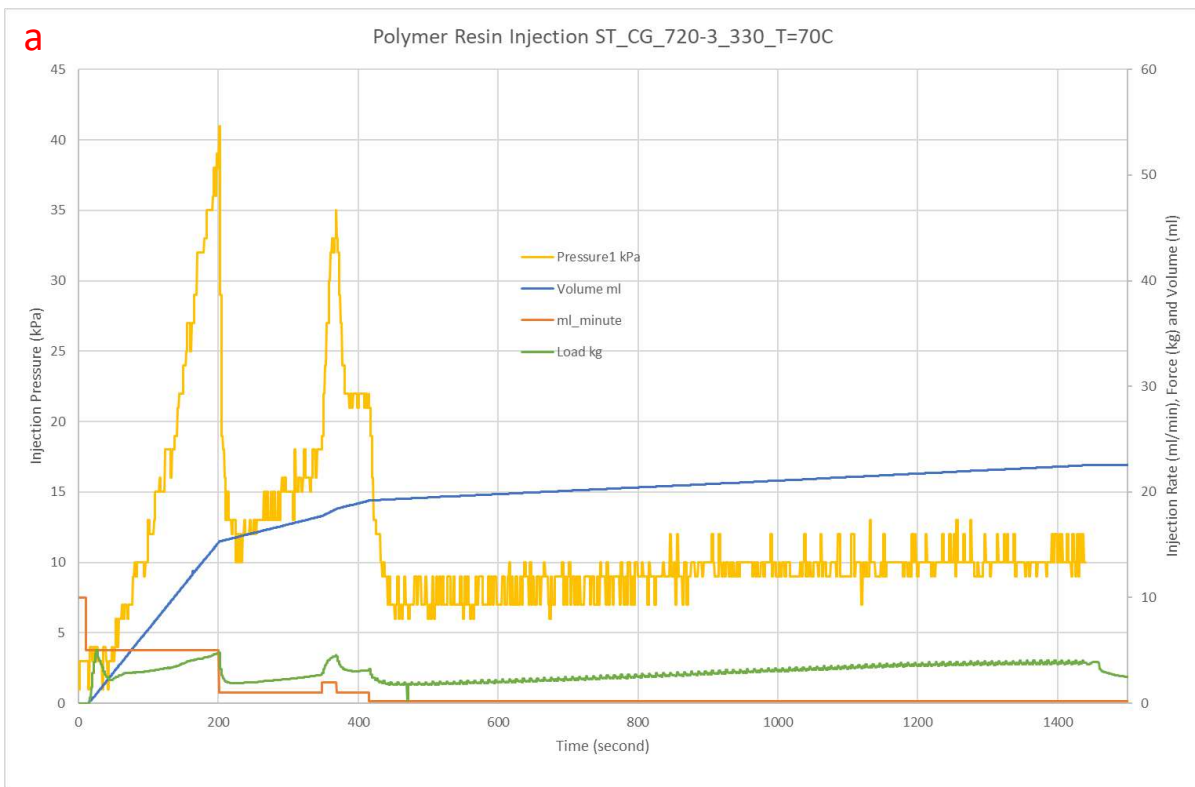


Figure C. 36. Injection test for fracture sample ST_CG_720-3_330_T=70C, a) Injection pressure, rate, force and volume vs time, and b) Photo of tested sample.

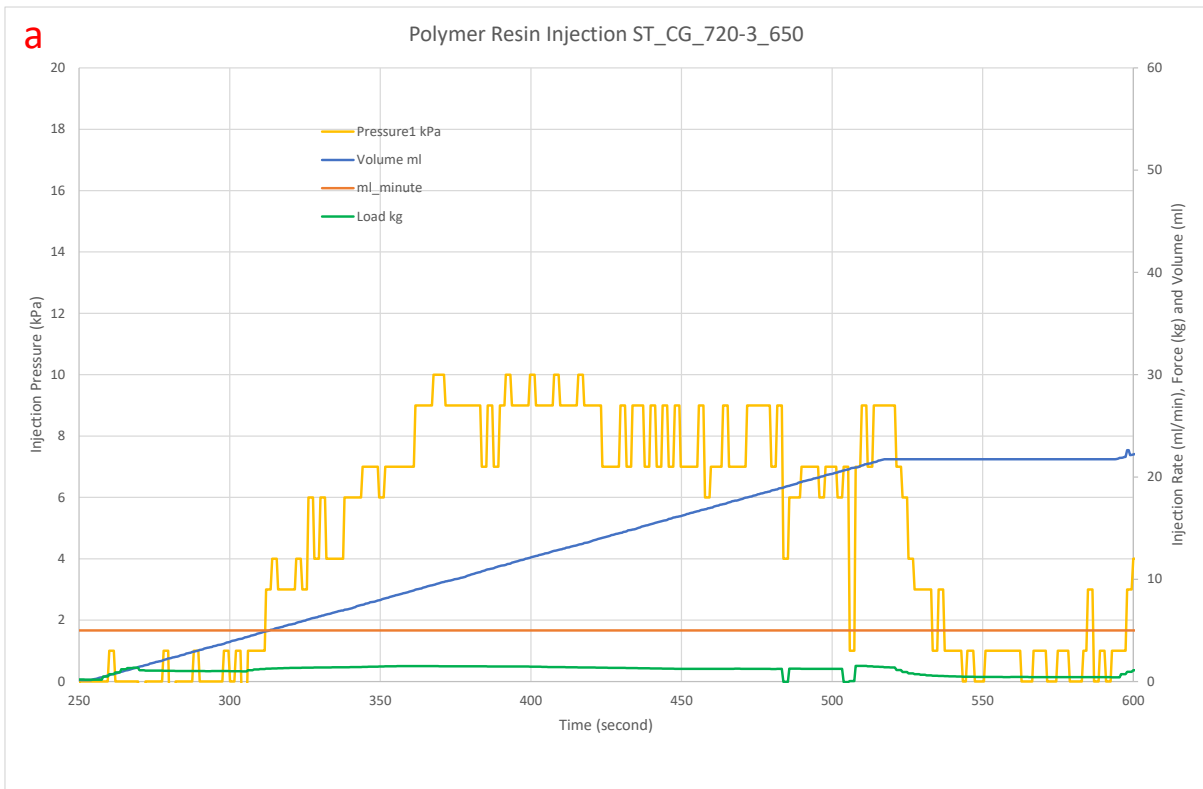


Figure C. 37. Injection test for fracture sample ST_CG_720-3_650, a) Injection pressure, rate, force and volume vs time, and b) Photo of tested sample.

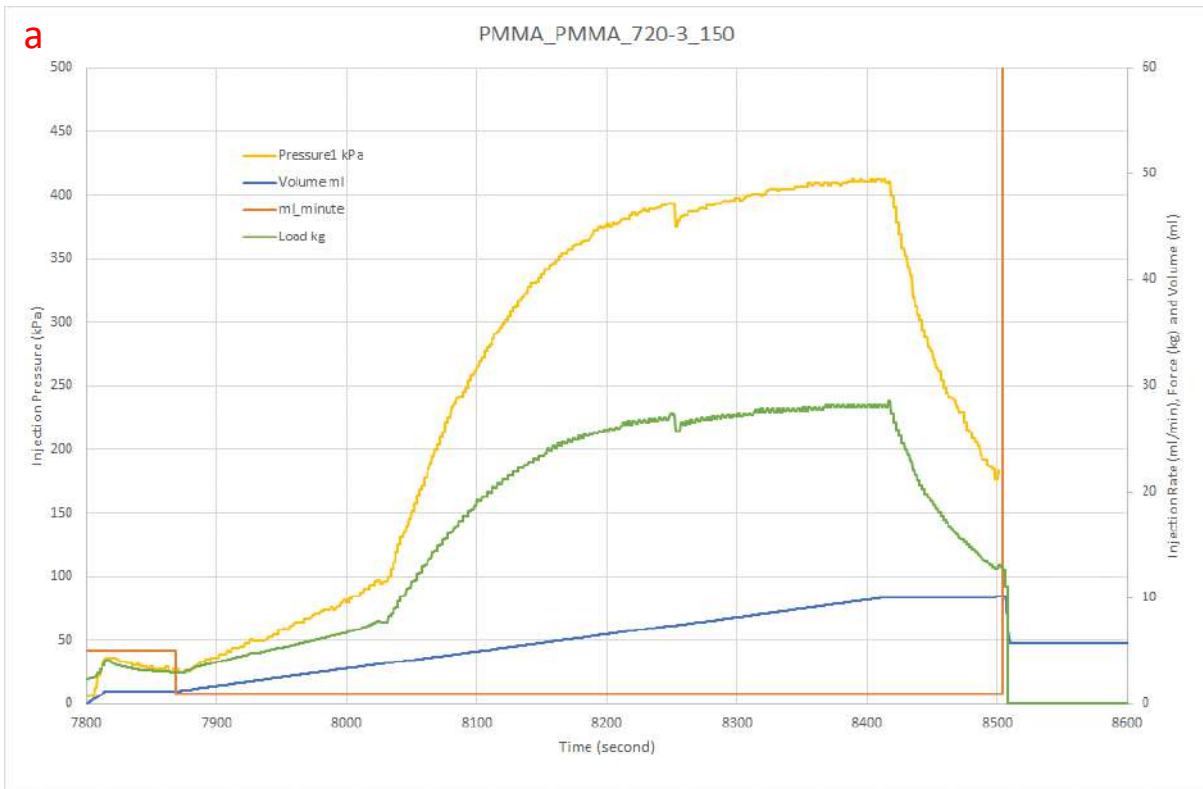


Figure C. 38. Injection test for fracture sample PMMA_PMMA_720-3_150, a) Injection pressure, rate, force and volume vs time, and b) Photo of tested sample. Shear bonding strength testing resulted in cracks in PMMA, not along the fracture.

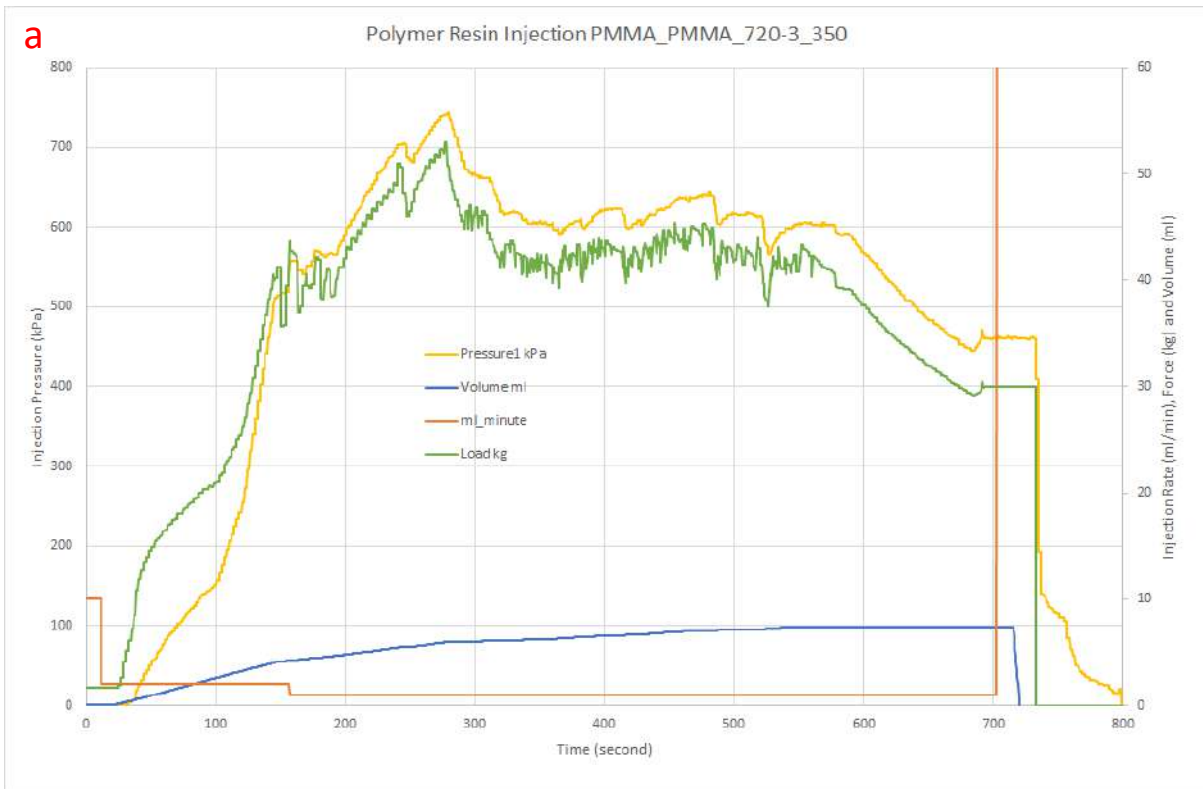


Figure C. 39. Injection test for fracture sample PMMA_PMMA_720-3_350, a) Injection pressure, rate, force and volume vs time, and b) Photo of tested sample. No shear bonding strength test.

Appendix D Ardex P51 Primer Datasheet



ARDEX P 51

Primer and Bonding Concentrate

Floor, wall and ceiling

Safe primer with a wide application range

Primer, bonding agent and water-inhibiting pore closer

Prevents air bubbles rising from the sub-floor when finishing

Solvent-free

ARDEX Australia Pty Ltd
20 Powers Road
Seven Hills NSW 2147
Phone: 1300 788 780
technicalservices@ardexaustralia.com
www.ardexaustralia.com

ARDEX New Zealand Ltd
15 Alfred Street
Onehunga, Auckland 1061
Phone: 0880 227 339
info@ardexnz.com
www.ardex.co.nz

ARDEX P 51

Primer and Bonding Concentrate

DESCRIPTION

ARDEX P 51 is an engineered priming system for use with ARDEX floor levelling cements. It is a solvent-free, blue synthetic resin dispersion, which after drying to a clear film inhibits water penetration.

USE

Water-inhibiting primer, precoat, bonding agent and pore closer.

Priming concrete to take finishing, repairing and levelling compounds.

As a pore closer on concrete and cement screeds

- It prevents air bubbles rising from the substrate in subsequent finishing layers.
- It prevents any mixing water being drained in subsequent finishing layers.

Bonding agent on smooth concrete for gypsum-bound wall finishing compounds.

Protective coat against dust formation on finishing and repairing compounds, which are to serve as wearing surfaces for a short time.

Internal applications only.

DIRECTIONS FOR USE

This product is used diluted with water, to prepare internal surfaces to receive cement-based levelling compounds, adhesives, screeds as well as plaster-based materials, improving adhesion and inhibiting penetration of water. It is used as a pore sealer on floor surfaces to prevent air bubbles rising through subsequently applied subfloor smoothing and levelling compounds.

SUBSTRATE

The substrate must be dry, porous, firm and free from dust and release agents.

APPLICATION

Apply diluted ARDEX P 51 (refer to table) evenly with a soft broom. DO NOT use paint rollers, mops or spray equipment. DO NOT leave any bare spots. Brush off puddles and excess primer. Allow to dry to a clear, thin film (minimum 3 hours, maximum 24 hours). DO NOT install ARDEX floor levelling cements before primer has dried thoroughly. Primer can be applied the day before. Use clean container.

Dilute 1:2 with water as a pore closer for porous concrete sub-floors and ceilings.

Dilute 1:3 with water as a primer and bonding agent on absorbent substrate.

MATERIAL REQUIREMENT

Approximately 100mL in concentrated form at 1:2 with water gives 300mL of diluted ARDEX P 51 per m² as a pore closer on porous concrete and cement screed flooring.

Approximately 50mL in concentrated form at 1:3 with water gives 200mL of diluted ARDEX P 51 per m² as a primer and bonding agent and to bind dust.

Substrate pre-treatment for subsequent finishing, repair and levelling work with products from the ARDEX range can be seen in the table below on the application of primers.

NOTE: Please also refer to the ARDEX P82 and P9 datasheets.

Packaging: Plastic container with 5L and 20L.

Storage: Can be stored for approximately 12 months in originally sealed packaging in a place free from frost.

SUBSTRATE	PRIMER	DILUTION ARDEX P 51: WATER
Smooth and dense substrates such as pre-fabricated concrete floors or particularly compacted cement screeds and wooden particle boards when using finishing and repairing compounds	ARDEX P 9	—
Smooth and dense substrates such as improved anhydrite screed flooring, terrazzo, sandstone, tiles and board coverings when using ARDEX smoothing and levelling compound for other repairing compounds	ARDEX P 82 ARDEX P 9	— —
Porous concrete and sand/cement sub-floors and ceilings	ARDEX P 51	1:2
Very porous concrete lightweight AAC blocks and floors, surfaces.	ARDEX P 51 May require 2nd coat	1:3
	ARDEX P 51	1:1
Smooth concrete walls and ceilings for gypsum-bound finishing compounds	ARDEX P 51	1:3
Gypsum wallboards and gypsum plastering for wall finishing compounds and cement-based thin bed mortar	ARDEX P 82	1:3
Wooden particle board panels when setting tiles with ARDEX S 28 New quick-setting building adhesive improved with ARDEX 90	ARDEX P 9	—
Mastic asphalt, asphalt slab coverings, synthetic coatings, synthetic flooring, metal, wood, varnished, beneath thin bed mortars and repairing compounds	ARDEX P 82	—

NOTE: The information contained herein is to the best of our knowledge true and accurate. No warranty is implied or given as to its completeness or accuracy in describing the performance or suitability of the product application. Users are asked to check that the literature in their possession is the latest issue.

COVERAGE

One litre of ARDEX P 51 diluted with two litres of water will cover 8-10m² depending upon the absorbency of the subfloor.

SAFETY PRECAUTIONS

Wash off skin before drying takes place. Splashes in eyes, mouth or nose should be washed and thoroughly removed with clean fresh water immediately. Safety glasses recommended during use.

GUARANTEE

Ardex Australia Pty Ltd (“we” or “us”) guarantees this product (“our goods”) is free from manufacturing defects and will perform to any applicable specification published by us for 10 years from the date of purchase. Our liability under this guarantee is limited at our option to replacement of the product, repair of any damage to the immediate surface or area of application of the product, or compensation, in each case if we are satisfied loss or damage was due to a breach of this guarantee. This guarantee does not apply if damage or loss is due to failure to follow published instructions or any act or circumstance beyond our control, including shade variations and efflorescence. If you wish to make a claim under this guarantee you must notify us (Ardex Australia Pty Ltd, 20 Powers Road Seven Hills NSW 2147; Toll Free: 1800 224 070; Email: technicalservices@ardexaustralia.com) and provide evidence of your purchase of the product within 30 days of any alleged loss or damage occurring. We reserve the right to ask you for satisfactory evidence of any alleged loss or damage. Any claim under this guarantee is at your cost. This guarantee is in addition to any rights or remedies you may have as a “consumer” under the Australian Consumer Law and to that extent you need to be aware that: “Our goods come with guarantees that cannot be excluded under the Australian Consumer Law. You are entitled to a replacement or refund for a major failure and for compensation for any other reasonably foreseeable loss of damage. You are also entitled to have the goods repaired or replaced if the goods fail to be of acceptable quality and the failure does not amount to a major failure”.

DISCLAIMER

The technical details, recommendations and other information contained in this data sheet are given in good faith and represent the best of our knowledge and experience at the time of printing. It is your responsibility to ensure that our products are used and handled correctly and in accordance with any applicable Australian Standard, our instructions and recommendations and only for the uses they are intended. We also reserve the right to update information without prior notice to you to reflect our ongoing research and development program. Country specific recommendations, depending on local standards, codes of practice, building regulations or industry guidelines, may effect specific installation recommendations. The supply of our products and services is also subject to certain terms, warranties and exclusions, which may have already been disclosed to you in prior dealings or are otherwise available to you on request. You should make yourself familiar with them.

© ARDEX Australia Pty Ltd 2019.

All aforementioned products are the trade marks of ARDEX Australia Pty Ltd, its licensors and affiliates.

Ardex Australia Pty Ltd

20 Powers Road
Seven Hills NSW 2147
Phone: 1300 788 780
Fax: 1300 780 102
technicalservices@ardexaustralia.com
www.ardexaustralia.com


ARDEX New Zealand Ltd

15 Alfred Street
Onehunga, Auckland 1061
Phone: 0800 227 339
Fax: (03) 384 9779
info@ardexnz.com
www.ardex.co.nz

January 2019

References

- Head KH (1982) Manual of soil laboratory testing. Vol 2, Pentech Press. ISBN0-7273-1305-3, p. 448-458.
- Jones SC (1972). A rapid accurate unsteady-state permeameter Klinkenberg permeameter. SPE J. 12 (5), 383-397
- Nelson EB and Guillot D (2006). Well Cementing (2nd Editio). Schlumberger, 225 Schlumberger Drive, Sugar Land, Texas 77478. <https://doi.org/10.1017/CBO9781107415324.004>
- Wu B, Arjomand E, Tian W, Dao B and Yan S (2020) Sealant technologies for remediating cement-related oil and gas well leakage – a state-of-the-art literature review. CSIRO EP201645.
- Zimmerman R and Bodvarsson G (1996). Hydraulic conductivity of rock fractures. Transport in Porous Media Vol 23 (1), p1-30



As Australia's national science agency and innovation catalyst, CSIRO is solving the greatest challenges through innovative science and technology.

CSIRO. Unlocking a better future for everyone.

Contact us

1300 363 400
+61 3 9545 2176
csiroenquiries@csiro.au
www.csiro.au

For further information

CSIRO Energy
Dr Bailin Wu
+61 03 9545 8383
bailin.wu@csiro.au
csiro.au/Energy